Assessing tradeoffs between solar thermal and wind energy integration in an isolated community electrical-thermal grid

By

Keelia LaFreniere

A thesis submitted to the Faculty of Graduate and Postdoctoral Affairs in partial fulfillment of the requirements for the degree of

Master of Applied Science

in

Sustainable Energy Engineering and Policy

Carleton University
Ottawa, Ontario

Abstract

Remote Northern communities in Canada suffer from unreliable access to energy. These largely indigenous communities derive their energy from fossil fuel-powered electricity generators and space heaters. This fuel must be transported long distances, which also contributes to non-renewable energy consumption. Complicated travel logistics throughout the North further compound the issue.

Renewable energy generators powered from sources such as wind and solar can largely address these issues. These generators can provide power on site, partly sidestepping the issue of fuel delivery, and greatly reduce greenhouse gas emissions. By employing a mix of thermal and electrical energy generation powered from wind and solar, a remote community's energy grid can serve the three chief residential energy loads: space heating loads, domestic hot water loads, and plug-in electrical loads.

MoCreebec Eeyoud Istchee is a grid-connected community located on Moose Factory island in Northern Ontario. This thesis uses the case study of the MoCreebec community to determine the benefits of implementing a coupled electrical-thermal grid to serve the residential energy needs of 140 households. The electrical-thermal grid employs a solar thermal array with (and without) heat pump assistance, a wind farm, an electric heater, a district heating grid, and a thermal storage tank.

A model of the proposed energy system is built and simulated in TRNSYS, using a combination of empirical data and estimation methods to determine the community energy loads. An analysis is conducted to investigate how the yearly household energy costs and greenhouse gas emissions of the current grid-connected community fare when compared to a community reliant

entirely on fossil fuel (*i.e.* an off-grid community).

Findings from the study conclude that in most cases the proposed energy system results in higher household energy costs and lower greenhouse gas emissions than the current grid-connected case. However, when compared to a more typical off-grid remote community, there are several instances where the proposed energy system cuts costs and carbon emissions by more than 50%.

Acknowledgements

I would first like to thank my thesis supervisor, Professor Jean Duquette of the Department of Mechanical and Aerospace Engineering at Carleton University. Without his steadfast support and invaluable input, this thesis would never have seen the light of day.

I would also like to thank my thesis co-supervisor, Professor Stephan Schott of the School of Public Policy at Carleton University, for his vital comments on this thesis from a perspective outside that of engineering.

My gratitude goes to those members of the MoCreebec Eeyoud community who partook so wholeheartedly in this research.

Finally and most of all, thank you to Mom, Dad, Conlan, and Jessica. There's no way I could have done this without you.

Table of Contents

List of Tables

List of Illustrations

Nomenclature & Symbols

$\dot{M}$	Mass flow rate [kg/hr]
c	Specific heat [J/kg·K]
C	Cost [$ CAD]
d	Discount rate [%]
M	Mass [kg]
n	Time [years]
η	Efficiency [%]
Q	Heat [kW]
T	Temperature [°C or K]
t	Time [s]
U	Velocity [m/s]
V	Volumetric flow rate [m^3/s]
z	Height [m]
B, ϕ, δ	Angle [°]
compressor	Energy required to run the compressor in the HP
deficit	Energy required to bring the TES up to a maximum of 95°C
excess	Electrical energy left over after servicing system electrical load
FFH supplemental	Energy required to bring DH supply temperature up to 70°C
heat loss	Energy lost in the DH system during fluid transmission
mains	Temperature of local water mains supply
pumping energy	Energy required to run the DH pump for the simulation time step
wind	Energy from WF

Subscripts

STa	Solar thermal array
htf	Heat transfer fluid
i	Inlet
o	Outlet
j	Array index
H	Heating
PL	Part load
e	Electrical
elec load	Electrical portion of energy load

Acronyms & Abbreviations

BaU	Business-as-usual
CC	Capital cost
CHP	Combined heat and power
COP	Coefficient of performance
CT	Cooling tower
DFIG	Doubly fed induction generator
DH	District heating
DHDL	District heating diverter loop
DHW	Domestic hot water
DTC	Differential temperature controller
ECB	Education and Capacity Building grant
EH	Electric heater
FFH	Fossil fuel heater
FIT	Feed-in-tariff
FPC	Flat plate collector
GCU	Grid control unit
GHG	Greenhouse gases
HDH	Heating degree hours
HP	Heat pump
HPA	Heat pump assisted
HPA-ST	Heat pump assisted solar thermal
NCF	Net cash flow
NPV	Net present value
NREL	National Renewable Energy Laboratory
O&M	Operations and Maintenance
OEG	Ontario electricity grid
PLF	Part-load factor
PMAE	Percentage mean absolute error
PME	Percent mean error
PtH	Power-to-heat
ROI	Return on investment
SAT	Solar accumulator tank
SH	Space heating
ST	Solar thermal
STADL	Solar thermal accumulator diverter loop
SxCy	Scenario x Configuration y
TES	Thermal energy storage
TOU	Time of use
TRNSYS	Transient System Simulation Tool
TTP	Two-way Tiered Pricing
WECS	Wind energy conversion system
WF	Wind farm

Foreword

Moose Factory, indicated in Figure 1, is an island Cree community located at the mouth of the Moose River along the James Bay in Northern Ontario. It was established as Moose Fort in 1673 and became known as Moose Factory in 1821. Today, the island community stands at a population of about 2700 [1]. The island hosts two Indigenous groups; that of the Moose Cree, and the MoCreebec Eeyoud Istchee (henceforth, referred to as "MoCreebec"). MoCreebec residents number approximately 1000 [2].

Figure 1: Moose Factory, ON [3]

Unlike most remote communities in Ontario, MoCreebec is connected to the Ontario electricity grid (OEG) via a 115 kV transmission line. The transmission line extends over 150 km of forest from Moose Factory to Otter Rapids, the closest major switching station [4], [5]. Thus, the community has ready access to electricity, whereas most other Indigenous communities in Canada are forced to rely on diesel generator plants for their electrical household needs [6]. Owing

to the existing electricity supply, MoCreebec's residential energy needs were built to rely entirely on electrical energy. According to *Statistics Canada*, the average Ontario household uses 28 MWh of energy in a year [7]. By comparison, a MoCreebec residence uses about 27 MWh of energy in a year. The difference seems negligible until one considers that space heating and domestic hot water (DHW) account for approximately 80% of energy use in an average Ontario home [8]. Typically, these two loads are served primarily with gas-burning appliances [9]. As a result, the average Ontario home only relies on the OEG to supply around a quarter to a third of their total annual energy usage, comprised solely of plug-in appliance loads. Conversely, MoCreebec is fully reliant on the OEG to provide for its DHW, space heating, and plug-in loads. Historically, this has resulted in unaffordable energy bills for community residents.

In an effort to rectify this trend, The MoCreebec council formed a partnership with Carleton University to initiate research regarding the investigation of sustainable, on-site energy generation options with the goal of supplanting the community's current reliance on the OEG. This investigation was subsequently completed under an IESO Education and Capacity Building grant (ECB). The IESO-ECB program "provides funding to support awareness, education, skills, and capacity building initiatives" centered around energy related issues [10]. Three Master's students: Keelia LaFreniere (*i.e.* the author of this thesis), Joshua Russell, and Joseph Coady were hired as research assistants to work on different but complementary aspects of the energy challenges facing the MoCreebec community. While Joshua conducted research on the policy and occupancy behavior related aspects of the project, both Keelia and Joseph were tasked with investigating potential sustainable engineering solutions for the community. Joseph focused on the feasibility of implementing a biomass-powered district heating (DH) grid in the Moose Factory community. Keelia focused on the feasibility of implementing a community electrical-thermal energy grid

powered with wind and solar thermal energy sources.

Chapter 1: Introduction

In Canada, most remote communities are located in the North and have a large proportion of indigenous populations. As these communities are unable to connect to the North American electricity grid, they rely on diesel to generate electricity. Consequently, energy security and affordability are major concerns. Diesel is costly, generates greenhouse gases (GHGs) and local air pollution, causes soil and water contamination, and must be delivered to community sites which limits its availability [6], [11]. Such issues make diesel an undesirable energy source. Many remote communities have therefore expressed increasing interest in the pursuit of alternative energy sources that provide a cheaper, more sustainable, cleaner, and more reliable energy system. Alternative energy systems for remote communities may integrate renewable energy generation and the usage of district heating (DH) systems [12]. A DH system directly supplies buildings with thermal energy through a distribution network made of pipes. The network transports water that has been heated from a plant to various locations on the grid [13].

Many numerical modeling studies have been conducted to assess the impacts of integrating various technological options into energy systems of varying scale. A literature review of studies focusing on district heating systems powered from solar thermal and wind energy is provided in the following section.

1.1 Literature review of numerical modeling studies

The following is a review of the studies currently available that focus on solar thermal and wind powered district energy systems.

1.1.1 Solar thermal district heating systems

In recent years, solar heating has been used with increasing frequency to power DH systems. Solar energy is an intermittent power source. Many heating systems that employ solar thermal (ST)

are small in scale, encompassing anywhere between one to about a dozen homes. These system designs are customized to fit the specific needs and climatic conditions of the location in question. Hsieh, Omu, and Orehounig [14] performed a simulation study focusing on centralized and decentralized solar thermal powered DH networks. An 11-building neighbourhood in suburban Switzerland was used as a case study. This study determined that varying the thermal energy storage (TES) sizing and individual energy load profiles can have a major impact on the resultant system economics and solar fraction (*i.e.* the percentage of total energy load served by solar power). It was determined that building-level long-term TES systems performed the best of the configurations considered. Ampatzi and Knight [15] corroborated this finding with their building-level study of twelve Welsh dwellings being served by a solar thermal combisystem. A combisystem is a solar thermal system that serves both space heating and domestic hot water (DHW) needs [16]. Simulations were run using the TRaNsient System Simulations tool (TRNSYS). These simulations focused on the effects of weather data, electrical energy needs, and thermal comfort requirements on the solar thermal combisystem's effectiveness. It was noted in the study that the higher the resolution of the load profile data, the more accurate and useful the economic results of the simulations became. Moreover, to design a robust and efficient system, the energy usage trends, housing insulation, physical dwelling layout, and other such parameters must be accounted for in great detail [15].

Due to this high level of customization required in solar thermal system designs, there exist many validated solar thermal system models built to supply space heating and DHW needs. Ayompe et al. [17] designed two systems in TRNSYS to serve DHW loads in a typical European household; one that employed a flat plate solar collector, and one that employed an evacuated tube collector. The DHW loads were served using forced water circulation. It was found that TRNSYS

routinely overestimated the heat collected by the flat plate solar thermal collectors as well as that delivered to the load by roughly 7%. In the case of the evacuated tube collector, TRNSYS overestimated these parameters by 12% and 8%, respectively. Banister et al. [18] designed a similar solar thermal system. This system was also modeled in TRNSYS and was designed to serve DHW loads. However, this system used heat pump-assisted solar thermal (HPA-ST) to serve the DHW load for a single household based in Ottawa, ON, Canada. The addition of a heat pump boosts the amount of useful energy that can be extracted from the solar thermal system as compared to a system charged through only a solar thermal collector. It accomplishes this by enhancing the input low-grade energy to high grade energy through the addition of electrical energy [19]. Banister's study compared the TRNSYS system simulation to a two-day experimental trial using a purpose-built apparatus for the study. The comparison found the results to be in 'excellent agreement' [18], proving TRNSYS to be an effective tool in the analysis of such systems.

Larger scale district heating systems are the subject of many studies as well. A study of 6 simulated households and 3 schools in the climatic conditions of Naples, Italy was conducted using TRNSYS over a 5-year period by Rosato et al [20]. Performance of solar thermal heating in combination with short-term TES and borehole TES solutions was investigated. Backup heating was provided by one of three systems; an electric heat pump, a natural gas-fired boiler, and an engine-based micro-cogeneration unit. The simulations that employed the electric heat pump had a reduction in primary energy consumption of 8.5%, the largest reduction of the systems considered.

A study of similar scope performed by Wang et al. [21] investigated a solar thermal district heating system employing a natural gas boiler as the supplemental heat source. A simulation was built in Matlab and applied to a theoretical case study of 20 buildings. As in Rosato et al. [20], the

building stock used in this study was mixed. It was comprised of both residential and office buildings. The simulations showed that when the area of solar thermal collectors equaled the area of the roof space of the buildings considered, the solar fraction of the system reached 15%. It was further shown that the DH system thermal losses decreased as the amount of decentralized solar thermal arrays was increased. Consequently, system pumping power also increased [21].

Denmark has the largest share of the world's solar thermal DH systems; more than 70% [22]. The country typically employs ground-mounted flat plate solar thermal collectors to power these DH systems, to which 64% of all Danish households are connected. The 111 large-scale ST DH networks in Denmark commonly employ electric heaters, gas boilers, heat pumps, and in one system, a biomass boiler, as secondary heat sources. The Danish ST DH systems are approximately 40% efficient.

To increase this efficiency, thermal energy delivery via DH systems may also be supplied by methods other than direct thermal energy transfer. The next section of this thesis explores the potential of integrating wind power in DH systems.

1.1.2 Wind power-to-heat for district heating

The use of electrical wind power in thermal applications has been employed to address the issue of curtailment. Curtailment is a blanket term for using only a portion of the power made available by an energy source [23]. With regards to wind power, curtailment means mechanically reducing a wind turbine's output in order to produce less energy than is technically available at that moment [24] (see Section 2.3 for more information on curtailment). A 2018 study by Hailong et al. [25] examined the effectiveness of using a standalone wind turbine to power a HP, thereby providing space heating to a residence. The system used a battery bank to store electricity at times when the wind was blowing and no thermal load was present. It was found that while increasing

the battery bank size improved the system's ability to serve the thermal load, further increasing the capacity of the wind turbine had comparatively no effect. During times of high thermal load, wind intermittency was incompatible with consistent heat pump operation.

Böttger et al. [26] conducted a study in 2014 into the feasibility of using power-to-heat (PtH) technology in DH grids located in Germany. The concept was found to be particularly attractive when considering intermittent renewable PtH integration with existing combined heat and power (CHP) systems, which is a relatively simple upgrade. However, the economic utility of selling back extra power generation to the grid was determined to be unfavourable. This conclusion was owed to current German regulations, which include a feed-in-tariff program that pays electricity producers for excess electricity. This precludes this excess electricity from use in a PtH application. However, these policies are subject to change (feed-in-tariffs are set to expire for German renewable installations starting in 2021 [27]), and the study may therefore become economically viable in the future. This study also found that the theoretical maximum potential to convert thermal energy to electrical energy through the proposed PtH systems in Germany was 32 GW_e.

A similar study, conducted in 2017 by Schweiger et al. [28], examined the potential for PtH integration into Swedish DH systems via electric heaters. Although the estimations on the PtH heating potentials varied greatly (0.2-8.6 TWh per year), the study determined that the addition of TES systems increased the viability of PtH integration. Additionally, system economics became more appealing as the cost of electricity decreased. Notably, this study claimed that wind and solar energy are highly compatible with PtH technologies [28].

Yilmaz et al.'s [29] analysis of the PtH potential in the European energy system corroborates these findings. The study analyzed the potential to integrate PtH converters into the existing European DH grids using existing hourly residual load and heat load data. It was found that the

total potential capacity for PtH in Denmark, Germany, Austria, the Netherlands, France, and Italy combined will be approximately 20 GW in 2030. The study confirmed that there exists significant potential to integrate renewably sourced PtH converters into heating grids, but electricity prices make generating more energy than required to serve thermal loads an economically unsound approach. Chen et al. [30] examined increasing Chinese CHP system flexibility to allow for additional integration of wind power that would otherwise be curtailed. The CHP system was made more 'flexible' by increasing the availability of electric heaters and TES solutions to convert and store the otherwise-curtailed wind power. The study used a linear optimization model that prioritized the use of wind energy in the CHP system serving each of the Chinese heating districts considered. It was determined that integrating wind power with PtH technologies into Chinese CHP systems in this way was technically viable as well. The study found that 0.19 tonnes of coal combustion was displaced for every MWh of curtailed wind power used in these improved CHP systems.

Like electric heaters, the use of heat pumps in tandem with wind power in order to provide PtH generation has been previously investigated. Both Meibom et al. [31] and Blarke [32] have demonstrated the potential for heat pumps to reduce both wind energy curtailment and reduce fossil fuel usage in existing thermal systems. Meibom employed a stochastic wind power model within the Northern European energy system. The study found that wind power curtailment was reduced by 13% when using heat pumps, and 20% when using electric heaters [31]. Blarke modelled an existing natural gas-fired 5 MW_e CHP plant with reference data collected from 2003 to 2010. Using COMPOSE, a techno-economic optimization program used for the analysis of CHP systems, Blarke examined the benefits of adding heat pumps and electric heaters to the operation of this plant. The study focused on maximizing intermittency-friendliness and minimizing plant operating

costs. The results yielded a 21-33% operational cost reduction for the plant with a heat pump utilizing flue gas heat. The same plant with an electric heater reduced operational costs by less than 1%. The electric heater increased intermittency-friendliness by approximately 5-10%, whereas the addition of the heat pump was found to both improve and worsen intermittency friendliness from year to year, by roughly 10% in either direction [32].

1.1.3 Research Gaps

The studies described in Sections 1.1.1 and 1.1.2 discuss the potential technical benefits of integrating solar thermal and wind technologies in district heating systems. The impacts of introducing various components to improve system efficiencies were also examined, chiefly the effect of TES systems and PtH technologies such as heat pumps and electric heaters. Residential load profiles, both estimated and derived from empirical data, were used to assess the efficacity of these systems. Worth mentioning is the recurring theme that these renewably sourced heating systems are sensitive to a wide and sometimes unpredictable array of parameters, requiring that each design be heavily tailored to the current technological, climatic, and political landscape of the region in question.

Although both solar thermal and wind were shown to be viable sources worth integrating in electrical-thermal grids via PtH technologies, the studies found in the literature tended to focus on the integration of a single source of renewable energy into these energy systems. Multiple intermittent renewable energy sources being fed into the same heating grid was not explored. As such, the effect of varying the installed capacity of a single renewable energy source in an energy system comprised of multiple sources is still not well understood. The evaluation of a HPA-ST driven district heating system, wherein the heat pump is powered purely by a wind turbine, is also

markedly absent.

Finally, while there have been grid-connected and off-grid studies of each of the systems mentioned above, no studies investigate how the functionality of a single solar thermal/wind driven district heating system would fare in a grid-connected versus off-grid environment.

1.2 Objectives

The primary objective of this thesis is to assess the impacts of integrating both wind and solar thermal energy in a coupled electrical-thermal grid (integrating electrical and thermal energy use in a single system) relative to a conventional fossil fuel-based energy system.

The two sub-objectives of this thesis are:

1) To investigate the potential benefits of using a HPA-ST system versus a direct ST system, and;
2) To assess the impacts of implementing the proposed system in both grid-connected and off-grid communities.

The MoCreebec community is used as the grid-connected case study in this research. An off-grid community sharing the same energy profile as MoCreebec is developed and used to assess the proposed energy system performance when operating off-grid.

1.3 Organization of the thesis

The main body of this thesis contains six chapters. Chapter 2 is an overview of the basic engineering principles related to the technologies discussed in this thesis. The principles covered include those of solar heating plants, DH grids, wind energy, and coupled electrical-thermal grids.

Chapter 3 describes the methodology applied to the research. The modelling tool, and the case study location and energy profile are discussed. This chapter also describes the energy estimation methods utilized to develop the energy models and underlying scenarios. Finally, model

assumptions, inputs, costing data, and carbon analysis parameters are provided.

Chapter 4 presents the simulation results for all proposed energy system models. These simulation results span grid-connected, off-grid, HPA-ST, and direct solar thermal models. Simulation energy outputs, carbon footprint comparisons, and economic analyses are presented. A sensitivity analysis assessing the effect that altering several different costing variables has on the system economic results is included.

Chapter 5 provides an analysis of the simulation results, in which eight key findings of this research are outlined and discussed.

Finally, in Chapter 6, recommendations regarding next steps towards the proposed energy system implementation are made. These recommendations include areas for further research and recommended actions to be undertaken by the MoCreebec community. These actions account for current provincial policies, community preferences, and simulation results.

Chapter 2: Background

In the interest of generating clean thermal energy, many cities and industries have been turning to district heating (DH) systems powered by renewable sources. These systems can vary greatly in size, from servicing an individual building to entire cities. It is estimated that worldwide, there are currently more than 80,000 district heating systems in use [13]. Many of these systems use technologies such as thermal energy storage (TES), solar thermal (ST) (with and without heat pump assistance [HPA]), and power-to-heat (PtH) plants to convert excess intermittent renewable energy to useful heat.

TES systems are used in conjunction with district heating systems to further increase DH system effectiveness. In Canada, domestic hot water (DHW) and space heating loads are responsible for an estimated 80% of residential energy use [33], [16]. The advantage of TES systems is that they can be charged from temporally fluctuating renewable sources such as solar thermal energy at times when excess energy is available and discharged at times when energy is required. The use of a TES-based energy grid can increase the penetration of these renewable energy sources in a thermal system [34], [14]. This captured sensible heat can be stored in many mediums, including but not limited to water, rock or gravel beds, soil, and chemical storage systems. Due to its high heat capacity, its low cost, and ready availability, water remains a standard storage medium for solar thermal-powered TES installations [33].

Heat pump-assisted solar thermal (HPA-ST) systems have been in use for decades now. They have been determined to be a technically viable alternative to traditional fossil fuel powered heating systems, and as such hold great appeal as a more sustainable space heating alternative. HPA-ST systems share a key characteristic in common with direct solar thermal set-ups: each system is tailor-made for the installation's regional energy needs and climate. The systems are so

highly specialized for their individual installations that a defining characteristic for one system can be disregarded altogether in another [35].

In addition to being constructed in step with a new district heating system installation, solar thermal systems, HPA or otherwise, may be retroactively installed into existing heating grids. One study suggests that modestly (in comparison to the capacity of the original system) sized solar arrays may be installed into existing DH grids to achieve solar fractions of up to 15% [36].

DH systems can also be charged with electrical generation through PtH technologies. Electricity that would otherwise be curtailed from a wind farm (WF) can be sent to an electric heater (EH) to be converted to thermal energy for use in a DH. Alternatively, this otherwise curtailed electricity can be used to operate a heat pump to extract heat from the air, ground, or ST systems [37].

The technologies mentioned above (and their underlying engineering principles) are described in more detail in the following sections.

2.1 Solar heating plant principles

A ST collector is a device that absorbs incoming solar radiation, then transfers the amassed heat through a heat transfer medium. This medium is usually air, water, or oil. The thermal energy can then be used for a variety of purposes, such as DHW or space heating, depending on the supply temperature provided by the ST collectors [38], [39].

A flat-plate collector (FPC) is a simple collector model, which consists of six key components. Figure 2 shows the location of these components in an assembled FPC. A glazing layer permits radiation to enter the collector. Fluid passageways permit heat transfer fluids to flow from the collector inlet to outlet. These passageways can be built using a header pipe that is fed by many riser pipes spanning the length of the collector. The passageway may also be a single tube

that runs back and forth across the collector in a serpentine fashion. Headers serve as the inlets and outlets through which heat transfer fluid is admitted and discharged from the collector. Insulation is installed to minimize heat loss. Finally, the collector is assembled inside of a casing in order to protect all components from environmental damage [39].

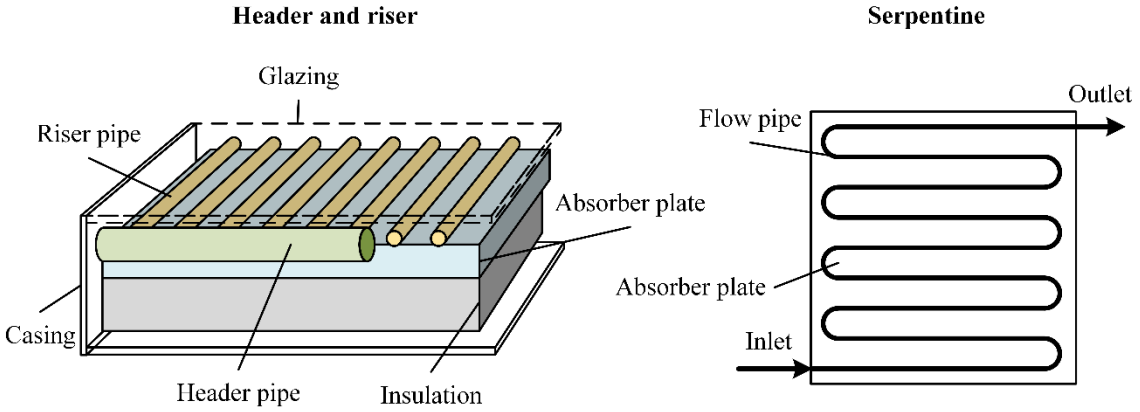

Figure 2: Schematic of flat plate solar thermal collector assembly (adapted from [37])

Solar thermal systems are sized according to the desired energy system functionality at the point of use. For example, a solar thermal array being installed in a preexisting grid can be sized to minimize system installation costs while maximizing fractional energy savings. Conversely, a system could instead be sized to produce the largest energy output for the available installation area, regardless of cost.

A simple solar thermal system can be controlled using a differential temperature controller (DTC), as shown in Figure 3. In this diagram, two temperature sensors (one at the ST array outlet, and one at the storage tank inlet) are read by a DTC. The temperature at the outlet of the ST array is read and compared to the temperature at the storage tank inlet. If the ST array outlet temperature is above that of the storage tank, then the system is set to charge the tank with the heat transfer fluid via a heat exchanger using a solar pump. If not, then the heat transfer fluid continues to circulate through the ST collector until it reaches a temperature suitable to charge the TES. The

solar pump remains off until this time.

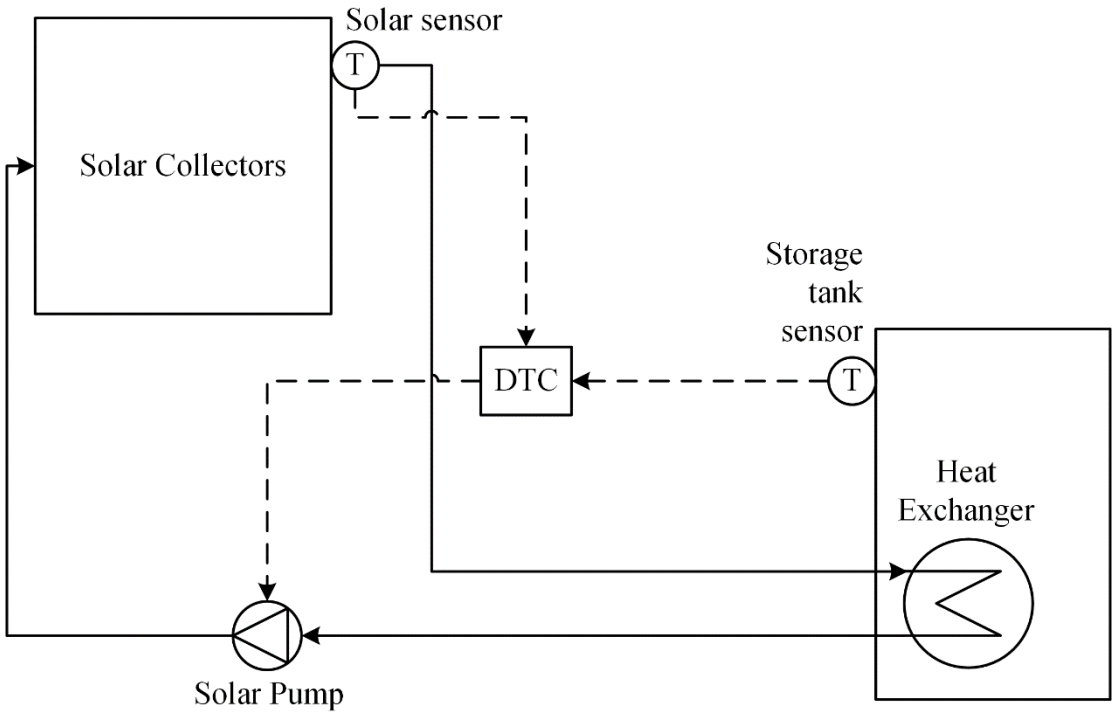

Figure 3: Solar thermal array simple control scheme (adapted from [37])

ST systems may also employ heat pumps to increase the amount of useful energy extracted from the ST array. Figure 4 shows a simple diagram of such a system. The solar collector feeds a DHW storage tank. There is a secondary storage tank, called the buffer storage tank, from which a HP draws thermal energy in order to heat fluid that was otherwise too cool to be stored in the DHW tank directly. This fluid is then sent to the DHW tank (or through a supplementary heating circuit, if necessary) to serve the DHW load.

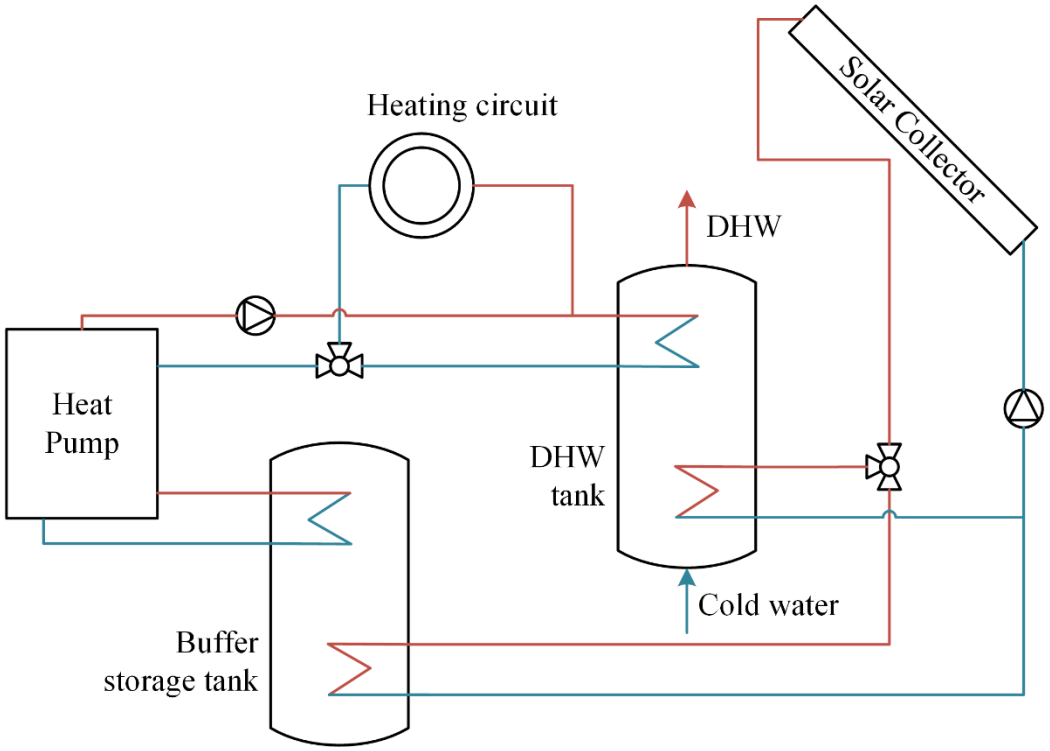

Figure 4: Heat pump-assisted solar thermal water heating system diagram (adapted from [38])

The energy collected by ST arrays can be used directly in a DH system. Collectors can be arranged in arrays, with combinations of collectors connected in series and in parallel. Sometimes specific manufacturer instructions dictate the array connections to ensure the highest heat transfer through the system [41]. A solar district heating system at its most basic includes a solar thermal array, a heat exchanger, a storage system, a backup system, a piping network, and a load to serve [42].

The following section discusses the basic engineering principles for renewably-powered district heating systems.

2.2 District heating grid principles

A simple DH system comprises a production plant, a transmission/distribution system, and in-building heating equipment. Figure 5 displays the layout of this simple system. The production plant serves as the heat source for the system, and can take the form of a boiler, an incinerator, a

heat exchanger, or a chiller. The fuel used in the production plant may be renewable or non-renewable. The transmission and distribution system then sends heated fluid through the network, delivering thermal energy to all points on the grid and directing cooled fluid back to the production plant to be reheated. The in-building equipment may be used to serve the DHW load, space heating load, or other such applications [43].

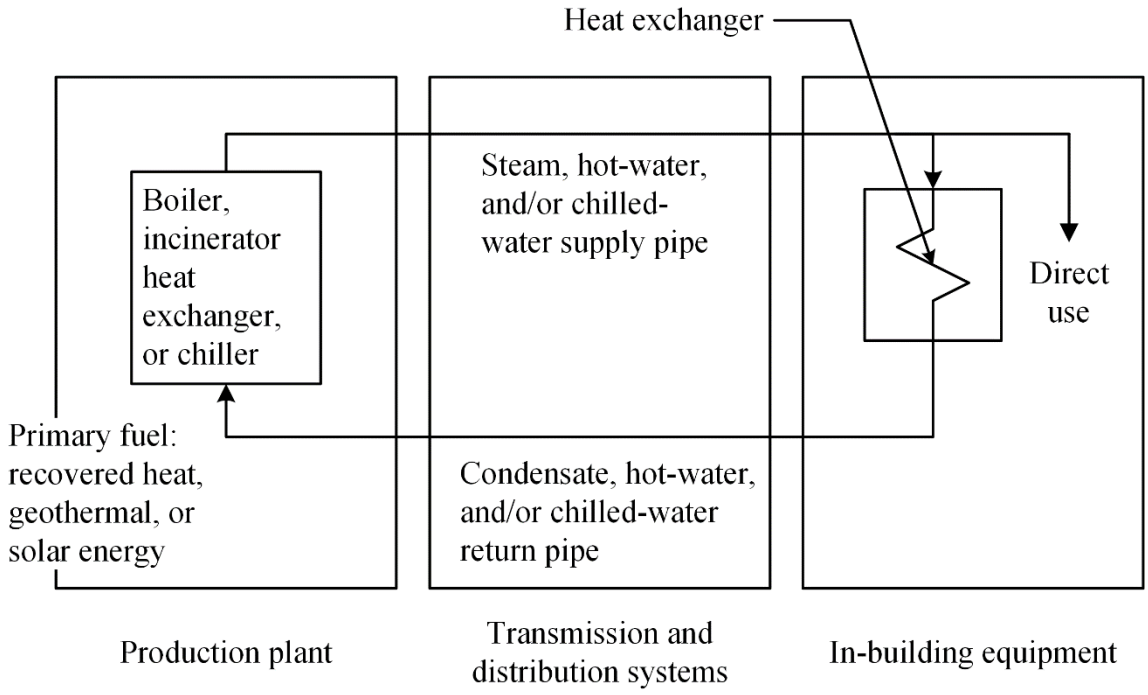

Figure 5: Layout of a simple district heating system (adapted from [41])

According to Kavvadias et al. [44], combined heat and power (CHP) based DH systems are most commonly controlled according to one of the five strategies, as outlined in Table 1. “Heat demand following” serves the heating load first, and the electrical load second. “Electricity demand following” does the opposite. “Continuous operation” has the system operating for a given amount of time, regardless of electrical or thermal energy demand. “Peak shaving” operates strategically in order to serve part of the electrical and thermal load during peak hours. Finally, “base load operation” sets the DH system to serve a constant portion of the energy load and lets other

dispatchable energy systems take care of peaking energy loads.

Table 1: Typical district heating system control strategies [44]

Strategy	Method
Heat demand following	Serve heat load first, then buy or sell electricity as required
Electricity demand following	Serve electrical load first, use via an auxiliary boiler or waste generated thermal energy as required
Continuous operation	System operates for a given amount of time, regardless of energy demand
Peak shaving	System operates for limited time to serve part of the load during peak hours
Base load operation	System operates to provide a constant energy load

The following section discusses wind energy intermittency, and the strategies employed to overcome it.

2.3 Wind energy and intermittency

Wind energy is harnessed through wind turbines. When multiple turbines are installed at a single location, this is referred to as a WF. A simple diagram of a wind turbine energy system is shown in Figure 6. When the wind blows through a turbine, it turns the blades, which rotates the rotor. The rotational energy in the rotor is transferred through a gear system to power an electrical generator. The generated electricity is fed into a power grid for use by consumers. A controller operates the gear system and the generator, ensuring such things as a constant voltage output and that the turbine does not spin too quickly in heavy winds [45].

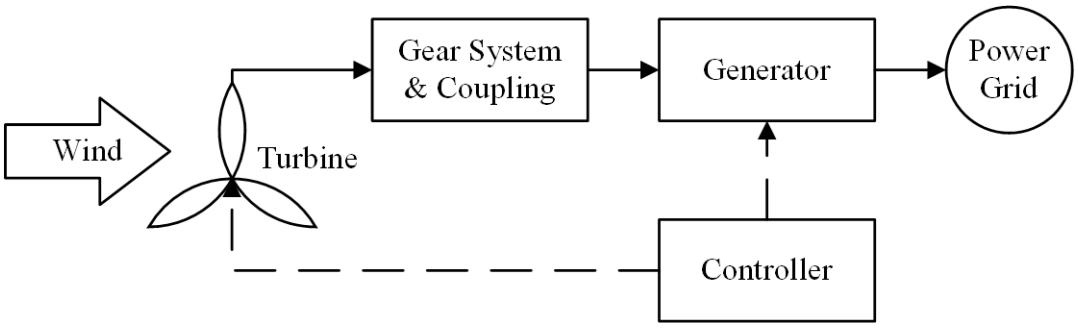

Figure 6: Basic wind turbine components (adapted from [45])

Wind energy is by its nature unpredictable and therefore presents issues when trying to integrate into an existing power system. Wind turbines disconnect and reconnect regularly to the power grid during periods of limited or excessive wind speeds, causing transient grid instability issues [46], [47]. Even wind variations on a scale too small to stop energy production can cause voltage fluctuations on the grid, which manifest themselves most notably as flickering lights [47].

The more common method of preventing these intermittency issues is to curtail the wind power output based on the load served by the local electrical grid. A report from the Risø National Library [48] suggests that the instantaneous penetration of wind power should be approximately 25-35% of the momentary energy demand to ensure grid stability. In a study regarding the integration of renewable electricity into remote Northern Ontario communities, instantaneous penetration from renewables was kept between 20 and 50% for these reasons [49].

Off-grid systems most commonly use both wind energy and a diesel generator plant in tandem. This ensures a constant source of electricity for remote communities [50]. Wind energy penetration is typically kept below 40% in these systems, as further penetration results in a reduction of power quality [47].

Curtailment presents another issue. In assuring the stability of the grid, potential electrical generation is sacrificed. China, one of the world's largest producers of wind power, curtails an annual average of 10-20% of their wind power [23]. To reclaim this wasted energy, district PtH technologies may be employed. This technology is explained in detail in the following section.

2.4 Benefits of district power-to-heat technologies for addressing intermittency

PtH technologies provide flexibility to an existing electrical grid when intermittent renewable energy generators are introduced. It has been established that renewable energy availability does not necessarily correlate with energy demand. With PtH systems, excess electricity generated during off-peak energy usage times can be converted to useful thermal energy and subsequently stored or immediately employed [37], [51].

PtH applications are varied, and therefore so are the technologies developed to employ them. Bloess et al. [37] divides PtH technologies into two groups; centralized and decentralized. Of interest in this study is the DH system, which utilizes a centralized PtH approach. DH systems can be fed by heat pumps, which may be ground-sourced or utilize waste heat from other industrial processes. Electrically driven heat pumps can utilize electricity generated from renewable sources that would otherwise be curtailed.

This excess electricity may also be used to run an electrical boiler, which directly heats fluid that can then be fed into a DH system. This technology can be applied to both on and off-grid systems, especially when paired with a TES system to stockpile excess thermal energy during periods of high electrical production and low electrical demand.

A study conducted on Helsinki, Finland found that the application of PtH technologies can potentially reduce the amount of surplus (*i.e.* wasted) electricity generated by the current energy grid by up to 35%. Adding a TES component to the PtH units further reduces this amount by approximately 3-6%, and load shifting was found to reduce it about another 2-5% [52]. In addition to technological benefits, PtH technologies also have a positive effect on renewable energy system economics, which results in fewer subsidies required to increase the market penetration of renewable energy generation [51].

Chapter 3: Methodology

3.1 Case study: The MoCreebec community

The MoCreebec community, located in Moose Factory, ON, is used as the case study in this research. Researchers from Carleton University travelled to Moose Factory on two separate occasions; once for 3 weeks in 2018, then again for 5 days in 2019. Researchers gathered data on the local renewable energy supplies, local climate and topology, and community sensitivities towards these proposed technologies through meetings, workshops, focus groups, and the administering of surveys. This information proved invaluable, as local knowledge nullified data previously found through the Government of Canada's website. This local knowledge is the reason why hydro power was removed as a possible renewable energy source, due to poor suitability despite high local hydro potential. Concern regarding the continued maintenance of a solar photovoltaic electrical system by community residents contributed to the decision to disregard solar photovoltaics as an energy source.

Climate data from Moosonee, ON is utilized as there is no data available specifically for Moose Factory. Moosonee is located approximately three kilometers from Moose Factory Island, on the mainland. 2016 is the most recent year data is available for the Moosonee/Moose Factory area [53].

Figure 7 shows the wind speeds recorded in Moosonee in 2016. There is a good, consistent wind resource present in the area, providing potential for the installation of a wind farm (WF). In Figure 7, Figure 8, and Figure 9, hour 1 represents January 1st at midnight, and hour 8760 represents December 31st at 11pm.

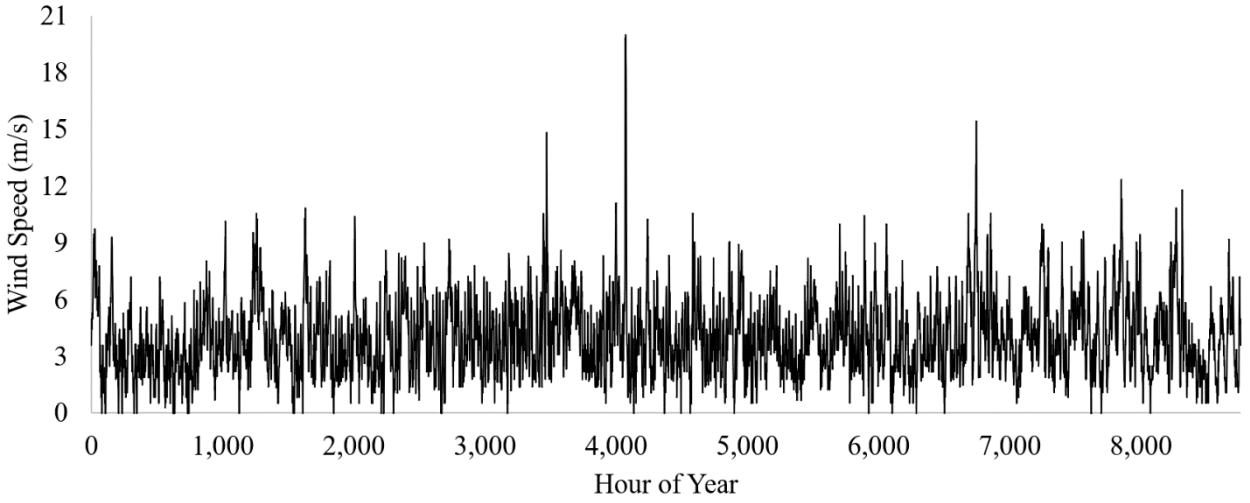

Figure 7: Moosonee 2016 wind speed [53]

Figure 8 shows the 2016 daily average incident insolation present in Moosonee. The area gets significantly less insolation during fall and winter months. However, it has high levels of insolation during the spring and summer. Solar thermal is therefore a viable renewable energy source for the region.

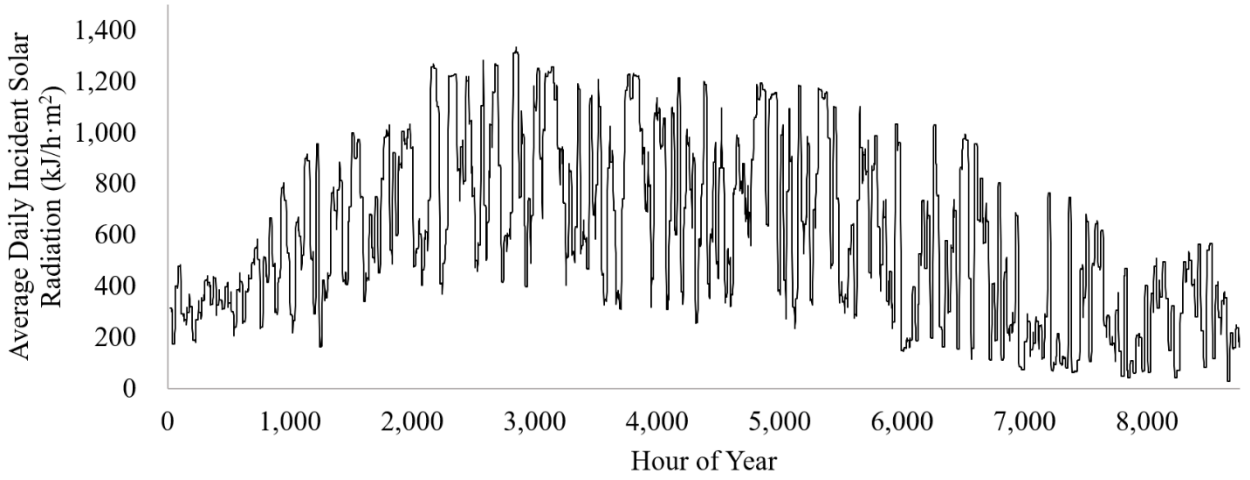

Figure 8: Moosonee 2016 solar radiation [53]

Figure 9 shows the 2016 ambient outdoor temperature in Moosonee. The coldest temperatures correspond with the periods of lowest insolation shown in Figure 8 below. The low temperature in the area corresponds with high space heating needs for residents.

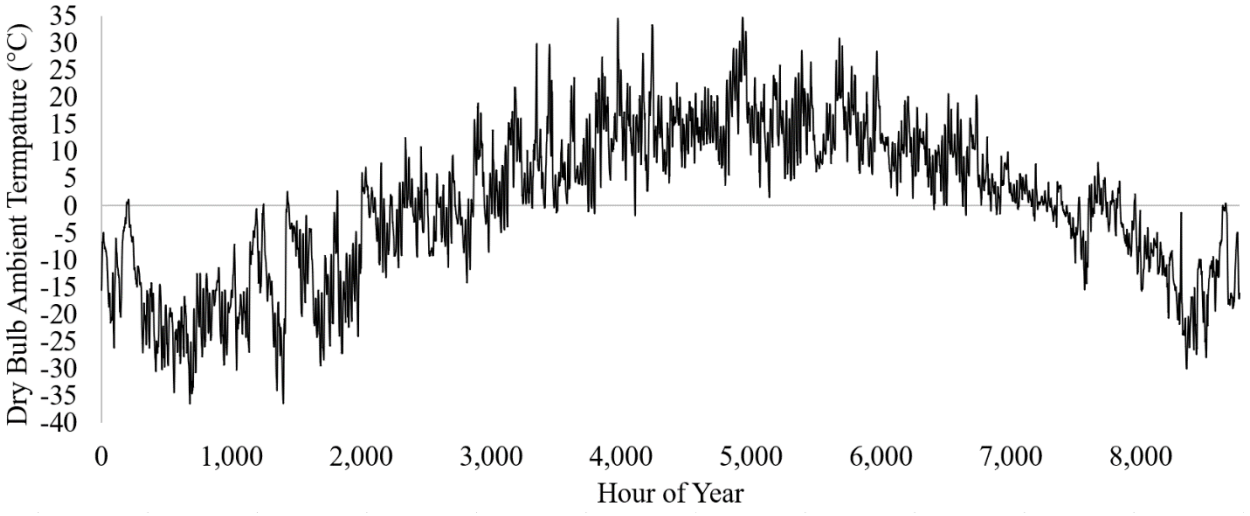

Figure 9: Moosonee 2016 ambient outdoor temperature [53]

3.1.1 Energy profile

The MoCreebec community has approximately 1000 residents [1]. The community building stock comprises the homes for these residents, as well as several other commercial centres such as the hospital, the public school, and the Cree Village Ecolodge (a 20-room hotel) [55]. All of MoCreebec's residences and other buildings reside on the off-reserve segment of the island [1]. For the purposes of this study, only the energy profile of the residential buildings is considered. This is owing to the difficulty encountered when searching for reliable statistics on energy usage in the larger commercial buildings.

Apart from their electrical plug-in loads, MoCreebec currently uses electricity to serve nearly 100% of their space heating and domestic hot water (DHW) needs. Figure 10 shows that space heating and DHW heating combined comprise approximately 61% of the MoCreebec community's annual residential energy load. This high electricity usage has resulted in a complete dependence on the Ontario electricity grid (OEG) for their energy supply.

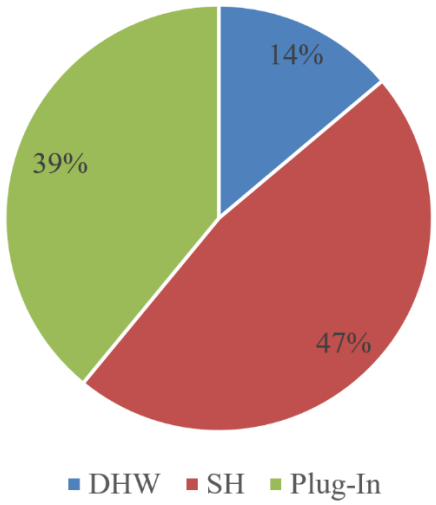

Figure 10: MoCreebec Residential Energy End-Use Distribution

3.1.2 Energy model description

The energy system combinations proposed in this thesis use a district heating (DH) grid to serve both the DHW and space heating loads of the community, supplanting the current fully electrically heated system. This significantly reduces the community's reliance on third party providers for their energy security.

Two model scenarios are considered in this study. Scenario 1 and scenario 2 are representative of a grid-connected system and an off-grid system, respectively. For each scenario, two alternative energy system configurations are considered. Configuration 1 represents a single thermal energy storage (TES) tank system with a heat exchanger located between the tank and the solar thermal (ST) array (henceforth referred to as direct ST), and includes a WF. Configuration 2 is distinct from configuration 1 in that two TES tanks are utilized instead of one, and the system employs a heat pump-assissted solar thermal (HPA-ST) system. Configuration 2 also includes a WF. These energy system models and configurations are described in Table 2.

Table 2: Energy system scenarios and configurations

Scenario	Configuration	Abbreviation	System description
1	**1**	S1C1	Grid-connected with thermal storage, wind power, and direct ST
	2	S1C2	Grid-connected with thermal storage, wind power, and HPA-ST
2	**1**	S2C1	Off-grid with thermal storage, wind power, and direct ST
	2	S2C2	Off-grid with thermal storage, wind power, and HPA-ST

The model configurations are decided upon after many iterations. Different renewable energy systems are considered and discarded based on MoCreebec local testimony and available resource data. The system is reconfigured several times over to find the simplest version that is able to account for all system needs; *i.e.* system overheat, thermal energy deficits, maximized energy extraction, and maintenance on minimum temperature requirements.

Energy system configurations 1 and 2 (each depicting grid-connected and off-grid scenarios) are shown schematically in Figure 11 and Figure 12, respectively. Both grid-connected and off-grid scenarios govern the transfer of electricity from the WF throughout the rest of the proposed energy system through a grid control unit (GCU). Both scenarios utilize an electric heater (EH) to convert excess electricity into thermal energy that can be used by the DH system. The TES tanks of both configurations are connected to a cooling tower (CT) that provides an outlet for excess thermal generation that can neither be deployed in the DH grid nor stored in the TES. The TES tanks operate with an upper temperature limit of 95°C. Factoring in heat losses in the DH system and assuming the use of tempering valves at DHW taps along the DH grid to lower the water temperature and eliminate scalding [56], a minimum DH supply temperature of 70°C is selected (maintained through the use of a fossil fuel heater [FFH] should the DH supply temperature fall below 70°C). The upper temperature limit of 95°C is selected as it is assumed to be the highest

safe temperature at which water can be stored without risk of water vaporization. Both configurations operate the ST array with a glycol loop. The working fluid of the loop is 75% ethylene glycol by volume to prevent freezing of the fluid during periods of low ambient temperature [57].

The direct ST configuration (C1) employs the use of a single TES, whereas the HPA-ST configuration (C2) uses two TES tanks (a large TES and a small solar accumulator tank [SAT]) to permit the addition of the HPA-ST system.

The grid-connected scenario (S1) dumps excess electricity generated by the WF (*i.e.* electricity that cannot be utilized in the community energy system) to the OEG and draws electricity from the OEG during periods of high electricity load and low wind availability. The off-grid scenario (S2) uses a diesel generator plant to provide supplemental electricity as required. As there is no larger electrical grid into which to feed excess electrical generation in S2, all excess electricity is used to power the HPA-ST (in C2), or converted to thermal energy and either stored in the TES or vented through the CT as required.

The specifics of the simulation parameter selections employed in this research are discussed in detail in Section 3.2.3. The dispatch strategies governing the operation of the proposed energy systems illustrated in Figure 11 and Figure 12 are discussed in Section 3.2.4

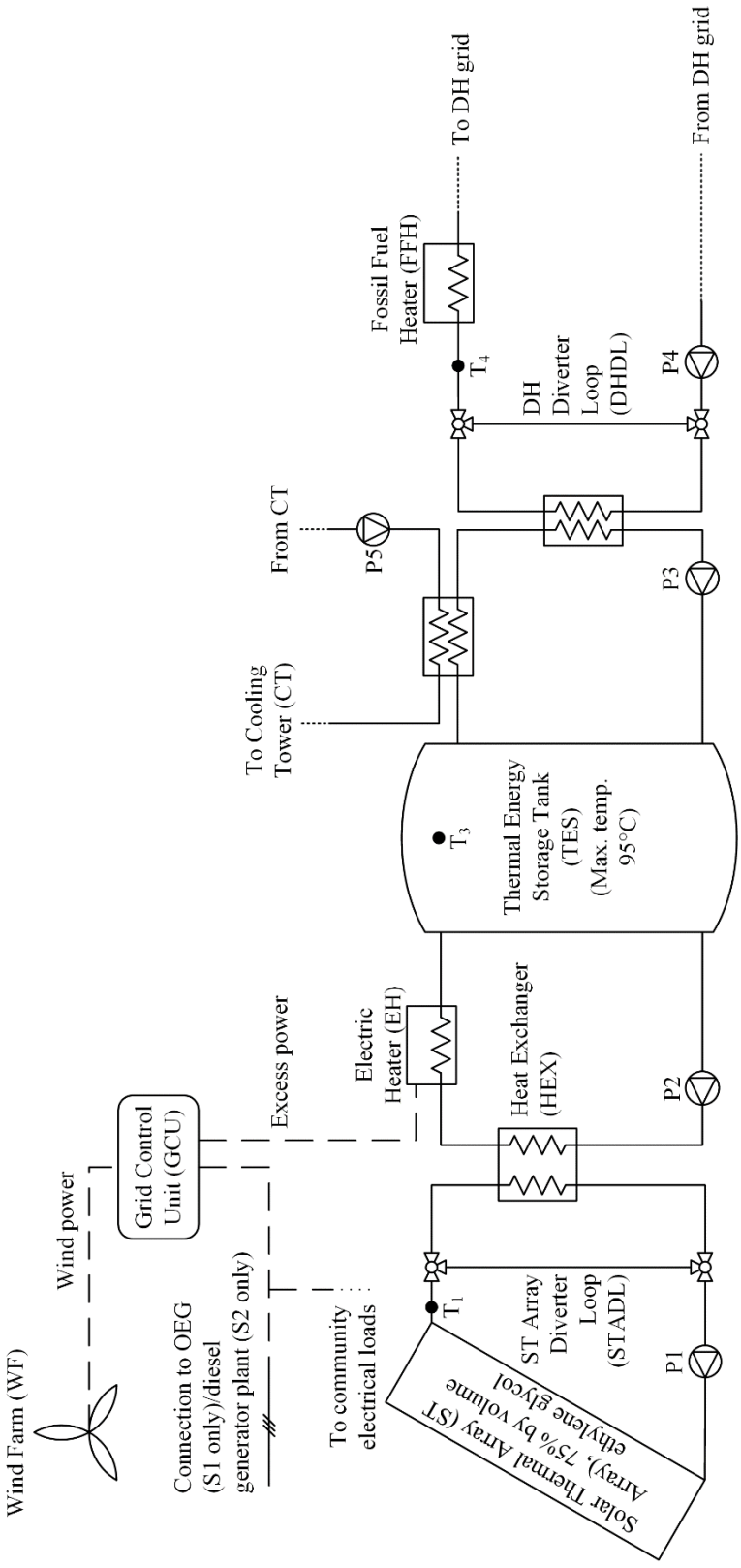

Figure 11: Schematic representation of Configuration 1 (C1) – wind power combined with direct ST system

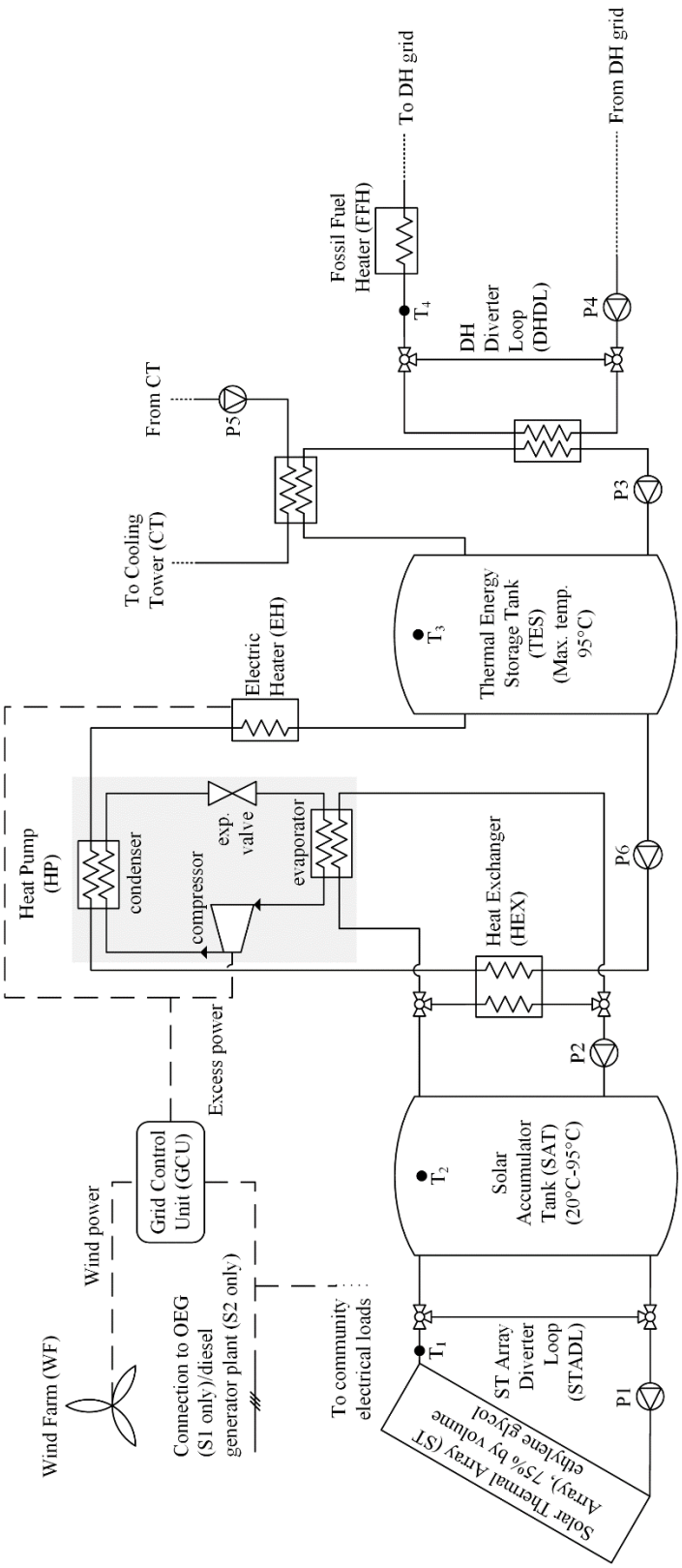

Figure 12: Schematic representation of Configuration 2 (C2) – wind power combined with heat pump-assisted solar thermal (HPA-ST) system

3.2 The Transient Systems Simulation Tool (TRNSYS)

The transient systems simulation tool, TRNSYS, is used to develop the models and perform the simulations presented in this research. TRNSYS provides a numerical environment for the transient simulation of energy systems. The tool focuses on the simulation of solar systems, low energy buildings, renewable energy systems, and cogeneration-based systems. To run simulations, users connect individual component models (referred to in TRNSYS as 'types') together to form their system model. The source code governing these types is made available to users, permitting the alteration of existing types or the creation of new types in order to suit the users' purposes [58]. TRNSYS is an equation solving program, and as such, the mathematics governing each type can be found and verified through the Mathematical Reference that is provided with each version of the program [59]. This makes model validation a straightforward process. There exist many papers with validations of individual types and components- too many to be mentioned here. A lengthy list of journal and conference publications that make reference to TRNSYS may be found on the *papers and validation* page of the University of Madison-Wisconsin website [60].

3.2.1 TRNSYS types used to simulate energy model components & model assumptions

The TRNSYS models developed for this research all share the same elements. The model runs the simulation in one-hour time steps for the duration of one year. A list of the key components employed and the functions they serve is included in Table 3.

Table 3: TRNSYS component types used to develop models, and their associated functionalities

TRNSYS Component Names	TRNSYS Type	Purpose in Simulation
Solar thermal flat plate collector	942	Flat plate solar thermal collector operating under steady state conditions [61]. The parameter values used in this type are determined using a method outlined by Duffie and Beckman [62]
Wind energy conversion system (WECS)	90	Wind turbine generating power per climatic inputs and user inputs for wind turbine parameters, assuming operation at the Betz limit [63]
TES tank	534	Vertical cylindrical constant volume fluid-filled storage tank with up to 5 inlets/outlets through which to pass fluid [64]
Auxiliary heater	659	Heats fluid stream passing through the component; serves as the FFH [65]. The FFH operates with 95% efficiency [66]
Auxiliary cooler	1246	Cools fluid stream passing through the component; serves as the CT. The auxiliary cooler operates with 100% efficiency [65]
Electrical boiler	700	Serves as the PtH electrical heater for excess wind energy production and converts electrical energy to thermal energy, operates with 100% efficiency [65]
Pump	114	Single, constant speed pump controlled by a binary input control signal, operates with 100% efficiency [67]. Used in the heating plant
Variable speed pump	110	Variable speed pump (VSP) serving as the DH grid supply pump using direct values from Coady [68] for pumping flowrates. Efficiency of the pump was assumed to be 80%
Heat exchanger	91	Zero capacitance, constant effectiveness heat exchanger with an effectiveness of one (idealized) used to transfer energy to and from different flow streams [67]
Pipe	31	Included in order to encourage numerical stability of simulations. Without it, the lack of energy capacitance causes numerical oscillation issues which prevent system convergence [69]

Several components of the proposed energy system model are implemented in TRNSYS using simplified methods. The CT, which is present in all scenarios and configurations, is modeled in TRNSYS as an auxiliary cooler to remove excess thermal energy from the flow stream directly. Similarly, the FFH (also present in all scenarios and configurations) is modeled using an auxiliary heater with 95% combustion efficiency [66].

Energy required from the diesel generator plant is assumed to be the difference between the available WF electricity and the plug-in load for the current time step. The generator plant is only activated when there is insufficient electrical energy being generated by the WF. The diesel generator plant is assumed to have an average electrical conversion efficiency of 42.5% [70].

The HP is modeled using an auxiliary heater and auxiliary cooler to directly add and remove the energy from the load and supply flow streams, respectively. An idealized heat exchanger passes this energy to the TES. See Section 3.2.3 for a more detailed description of the HP implementation.

TRNSYS Model Assumptions

The following assumptions are applied to the models used in this study:

1. The infrastructure for diesel generator plants, municipal electricity distribution, and a connection to the provincial power grid are already in place.

   This assumption is made because the provincial power grid connection is already in place in MoCreebec. Additionally, off-grid communities that rely on diesel have preexisting generation and distribution infrastructure.

2. The wind farm is always generating power if the wind is blowing.

   This assumption is made for the sake of simplicity in the model. The TRNSYS wind turbine type in the model is highly generalized, so it is deemed reasonable to ignore cut-out speed limitations.

3. All pumps operate with no losses and require no energy input to operate.

The pump supplying the DH distribution network of pipes is the single largest pumping load in the system. The DH pumping energy is found to be less than one quarter of a percent of the yearly electrical energy load [68]. Since the largest pump represented such a small portion of the yearly energy load, it is decided that the pumping energy for all pumps will be neglected for simplicity.

4. All heat exchangers operate at 100% effectiveness.

This assumption is made for the sake of simplicity in the model.

5. All storage tanks have an edge loss coefficient of 5 kJ/h·m^2·K.

This is an average value for a storage tank edge loss coefficient acquired from Wills' work with water-based TES systems [69].

6. The CT uses no electricity.

This assumption is made for the sake of simplicity in the model, in part due to the infrequency with which the CT is employed.

7. System thermal and pumping energy losses occur only in the DH grid.

This assumption is made since the model is meant to be implemented in a very compact area. Transmission losses are therefore limited to the more widespread DH distribution network.

3.2.2 Load distribution of proposed energy system

The MoCreebec energy model comprises a total of 140 houses, which are broken down into 2, 3, 4, and 5-bedroom houses, shown in Table 4. There are approximately 30 houses with 2 bedrooms, 60 houses with 3 bedrooms, 30 houses with 4 bedrooms, and 20 houses with 5 bedrooms.

Table 4: Distribution of MoCreebec housing stock used in model combinations

Number of Bedrooms per House	Number of Houses
2	30
3	60
4	30
5	20

Figure 13 shows a stacked graph of the estimated yearly energy usage for these 140 houses, divided into the following three load categories: space heating, DHW, and plug-in loads. Currently, the space heating load is estimated based on measured electrical load data for the years 2016, 2017, and 2018. To determine the true magnitude of space heating in these houses, it is assumed that an additional load equivalent to approximately 5% of the space heating load is added to the estimated yearly energy usage to account for the use of wood-burning stoves in the community. This estimation is based on the percentage of homes in the MoCreebec community that have a wood-burning stove in addition to their electric baseboard heaters [71].

The space heating load comprises the bulk of the yearly energy load. No space cooling load is assumed for this study. In Ontario, an average of 5% of yearly energy load is used for space cooling. MoCreebec residents use space cooling less than the typical Ontarian [72]. Thus, space cooling is assumed to be sufficiently small as to be neglected. DHW loads are estimated using a stochastic numerical tool developed by NREL [73]. Details regarding the methods used to estimate electrical and heating loads are described in Section 3.2.5.

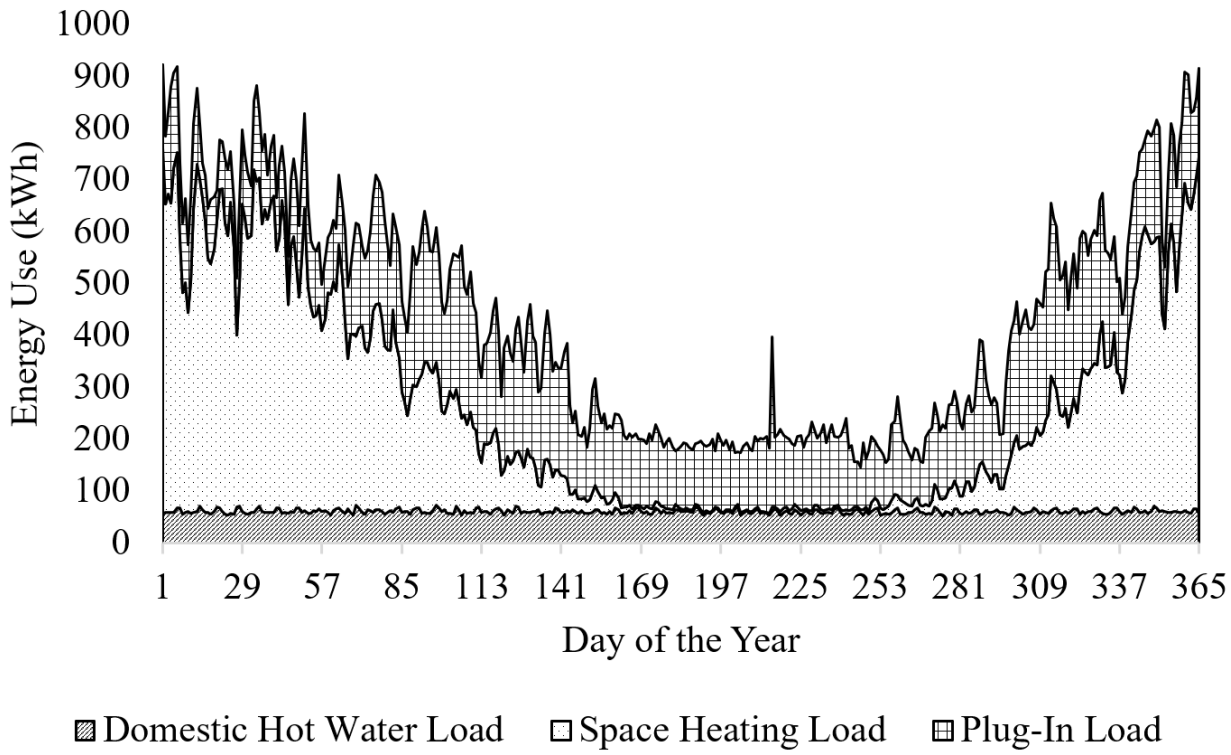

Figure 13: MoCreebec community yearly load distribution (constructed from combination of measured data and estimation methods)

3.2.3 Component specifications for combinations

A total of 140 combinations of the proposed energy system are run in TRNSYS. Each of the 140 combinations is a different permutation of the following parameters: the size of the ST array, the number of turbines in the WF, grid-connected or off-grid, and the proposed energy system configuration.

Table 5 shows a summary of the variations in component sizes used with the combinations assessed in this study. These components include the ST array surface area, the SAT and TES volumes, and the number of wind turbines in the WF. Variations of these key components are determined separately for each of the four scenario and configuration pairs. Following Table 5 is an explanation of how each component sizing range listed is determined.

Table 5: Combinations of model parameters for the ST array, SAT, TES, and WF used in combinations simulated in TRNSYS

Scenario & Configuration	ST array size (m^2)	% Area of Maximum ST Array Size	SAT Volume (m^3)	TES Volume (m^3)	# of Turbines in WF
S1C1	0	0	N/A	500	0-6
	3318	25	N/A	125	0-6
	6635	50	N/A	250	0-6
	9953	75	N/A	375	0-6
	13270 (max)	100	N/A	500	0-6
S1C2	0	0	0.5	300	0-6
	244	25	0.5	75	0-6
	487	50	0.5	150	0-6
	731	75	0.5	225	0-6
	974 (max)	100	0.5	300	0-6
S2C1	0	0	N/A	500	0-6
	3318	25	N/A	125	0-6
	6635	50	N/A	250	0-6
	9953	75	N/A	375	0-6
	13270 (max)	100	N/A	500	0-6
S2C2	0	0	0.5	300	0-6
	244	25	0.5	75	0-6
	487	50	0.5	150	0-6
	731	75	0.5	225	0-6
	974 (max)	100	0.5	300	0-6

The maximum ST array size is different for each of the two system configurations. The maximum ST array size for the S1C1 and S2C1 energy system combinations (employing a direct ST system) is selected based on the area of roof space available for collector installation on the 140 homes. This value is approximated as 13, 000 m^2, assuming an average roof area of 93 m^2 per

house. Though this study assumes the ST array will be installed as a single centralized plant, the surface area of the 140 homes is employed as a logical stopping point for the increase in the ST array's size. Logically, it serves that the larger a ST array, the larger the solar fraction provided by the array. However, it is infeasible to continue building larger ST arrays after a point due to the rising cost. The flat plate collector (FPC) type implemented in the combinations is modeled after the Vitosol 200-FM SH2F model FPCs, built by Veissmann. These FPCs have an absorber area of 2.32 m^2 [41], which means the full-sized ST array S1C1 and S2C1 combinations have 5720 FPCs installed. The ST array is reduced by increments of 25% from the maximum ST array size down to 0.

For the S1C2 and S2C2 combinations (employing a HPA-ST system), the HPA-ST system is found to require a much smaller collector area in order to provide solar fractions comparable to the S1C1 and S2C1 combinations. The maximum number of FPCs installed in the S1C2 and S2C2 combinations is therefore set to 420, roughly 14 times fewer than the number used in the S1C1 and S2C1 combinations.

Maximum TES and SAT volumes are selected using the following method. First, the initial values for tank sizing used are based on industry standards. These values vary between 41 to 61 L/m^2 of ST array installed, with the caveat that colder climates require smaller ratios [52], [70], [71]. By running combinations with variations of these industry standards and recording how the installation cost of the tank varies against the fraction of yearly energy load served by the DH grid, an optimal ratio of 20 L/m^2 of ST array installed is selected.

To determine the maximum capacity for the TES, combinations of the configuration 1 and configuration 2 models are run with all parameters listed in Table 5 fixed except the TES volume. To gauge the effectiveness of each component in the proposed energy system, the thermal energy

contributed by each system component is listed as a fraction of the total yearly thermal energy load. These energy fractions are generated for the direct ST, the HP, the EH, and the FFH. The effect that varying tank size has on the proposed energy system component energy fractions is recorded and examined for a trend that suggests an optimized TES volume. These energy storage results are then compared to the cost of building the TES using costing estimations from Xu et al. [77]. The maximum TES size (determined to be 300 m^3 for configuration 1 combinations, and 500 m^3 for configuration 2 combinations) is reached by determining the TES volume at which the marginal increase in the EH, direct ST, and HP energy fractions obtained by increasing the TES volume becomes too small to justify the corresponding increase in cost.

For all combinations in which there is no ST array, the TES size is reverted to its maximum value. This permits the EH to provide the largest possible fraction of yearly energy demand.

The TES volume in the model is linked with the ST array size and is decreased in linear proportion with each decrease in the ST array size, shown in Table 5. The S1C2 and S2C2 designs have small, unchanging SAT volumes of 0.5 m^3. The addition of the SAT is necessary for the HP to operate properly; however, the size of the SAT has little impact on the system performance. It is therefore set to an arbitrarily small volume in the S1C2 and S2C2 combinations.

The wind energy conversion system (WECS) type in the TRNSYS combinations emulates a Xant M-24 wind turbine. These turbines are selected since they are designed for operation in colder climates, have relatively low cut-in wind speeds, and are designed such that they can be transported in standard 12 m containers and assembled using a simple gin-pole and winch or crane. This makes them especially easy to transport and assemble in remote areas without the need for large pieces of machinery. The turbines are rated for 95 kW output and have a hub height of 24 m. The turbines begin generating power when wind speeds reach or exceed 2.5 m/s, which occurs frequently in the

area as seen in Figure 7 [53], [54]. The maximum WF size of 6 is determined due to the high cost of a larger farm, the large spacing requirements for such a farm, and the concern that a larger farm would feed back too much electricity to the OEG. The number of wind turbines in the WF is reduced from 6 to 0 for each ST array sizing increment, shown in Table 5.

The HP in the S1C2 and S2C2 TRNSYS models is implemented using an auxiliary heater and cooler (respectively types 659 and 1246 in TRNSYS, see Table 3), which emulate the movement of energy through a HP. Heat is exchanged between the SAT and the water flowing through the HP with the use of the auxiliary heater and cooler. When operating at full load (*i.e.* the HP is functioning at its maximum capacity), the coefficient of performance (COP) of the system is determined using Equation (1). The difference between the heat rejected from the condenser into the TES flow stream, $Q_{condenser}$, and the heat absorbed into the condenser from the SAT flow stream, $Q_{evaporator}$, is termed the useful energy generated by the HP, Q_{useful}. The COP of the HP at any given time step is given by dividing Q_{useful} by the energy required to run the compressor, $E_{compressor}$.

$$\boldsymbol{COP = \frac{Q_{useful}}{E_{compressor}} = \frac{Q_{condenser} - Q_{evaporator}}{E_{compressor}}} \quad (1)$$

The HP also runs at less than full load. To determine the COP of the HP when it is operating at what is referred to as part load, the part-load factor (PLF) method described by Bettanini et al. [78] is employed. This method uses Equation (2) to calculate the COP of the HP when it is being run at part load, COP_{PL}. The HP can't operate at full load if the compressor requires more energy to run than there is excess power available from the WF, $E_{excess\ power}$ (see **Figure 14** and **Figure 15** in Section 3.2.4 for a detailed account of how $E_{excess\ power}$ is determined), or if there is insufficient capacity in the TES to store the HP energy generated at full load. The ratio of $E_{excess\ power}$ over $E_{compressor}$ is defined as the part load factor by Bettanini et al [78]. The COP_{PL}

can be found by multiplying the COP by the part load factor.

$$\boldsymbol{COP_{PL} = COP * \frac{E_{excess\ power}}{E_{compressor}}} \quad (2)$$

The HP in the model mimics the functionality of a Trane water-to-water HP, chosen due to its high operating temperature range. The Trane HP evaporator can operate between -4°C to 50°C, and the condenser can operate between 4°C to 50°C. The Trane HP supplies water at 78°C [79]. These values are in line with the temperatures yielded by the proposed energy system combination results.

3.2.4 Scenario dispatch strategies

The dispatch strategies utilized in the model combinations of this study are classified into the following component groups: electrical, ST array/SAT, TES, DH system, and CT. A description of each of these strategies follows. The dispatch strategies can be understood more easily with reference to Figure 11 and Figure 12.

Electrical dispatch strategy for S1C1 and S1C2

The first step in each hourly time step of the TRNSYS simulation is to serve the electrical load via the GCU. Figure 14 shows this dispatch strategy as employed in TRNSYS for the grid connected models S1C1 and S1C2. The strategy determines the amount of excess electricity generated by the WF (excess power), and the amount of electricity that must be drawn from the OEG (grid power). If the WF generates any power during a time step wherein an electrical load is present, it is sent first to serve this load. Any leftover electricity is then utilized in a method determined by the TES dispatch strategies (see Figure 17 and Figure 18), to ascertain whether the leftover electricity is converted to thermal power and used or sold back to the OEG. If the wind generation is insufficient to serve the electrical load, the grid supplies the remainder. The values for excess power and grid power are used in the TES dispatch strategies for S1C1 and S1C2.

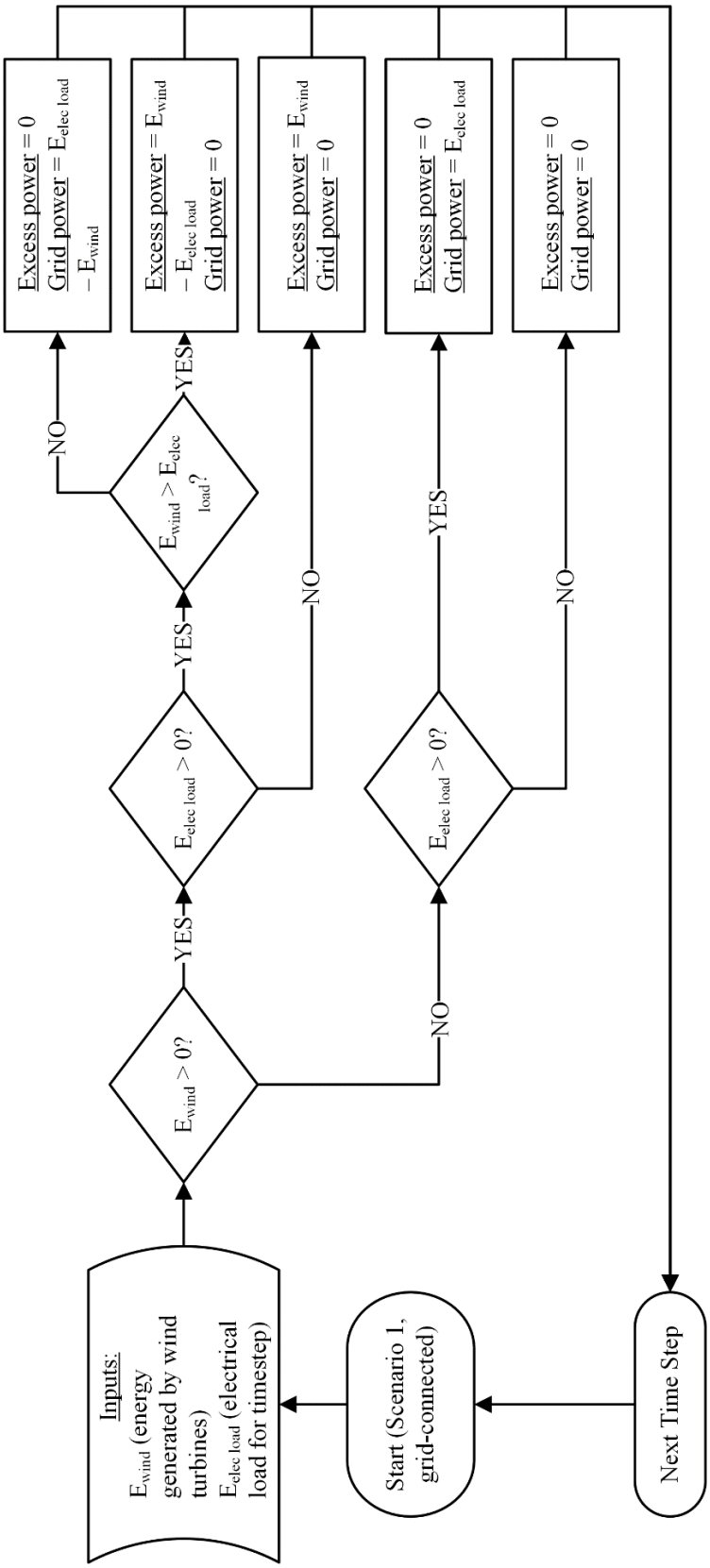

Figure 14: S1C1 & S1C2 electrical dispatch strategy

Electrical dispatch strategy for S2C1 and S2C2

The GCU for the grid-connected (S1) and the off-grid (S2) systems operate close to identically. Figure 15 shows the off-grid electrical dispatch strategy, which determines the amount of excess electricity generated by the WF (excess power) and the amount of electricity required from the diesel generator plant (diesel power). Since the regional electricity grid is not available to provide extra power in an off-grid scenario, a diesel generator plant is added to supply supplemental electricity as needed. The only difference between the grid-connected and off-grid electrical dispatch strategies is the electrical grid penetration limit imposed on the WF output. Wind power penetrations do not exceed 30% in these off-grid models [48], [49]. The values for excess power and diesel power are used in the TES dispatch strategies for S2C1 and S2C2.

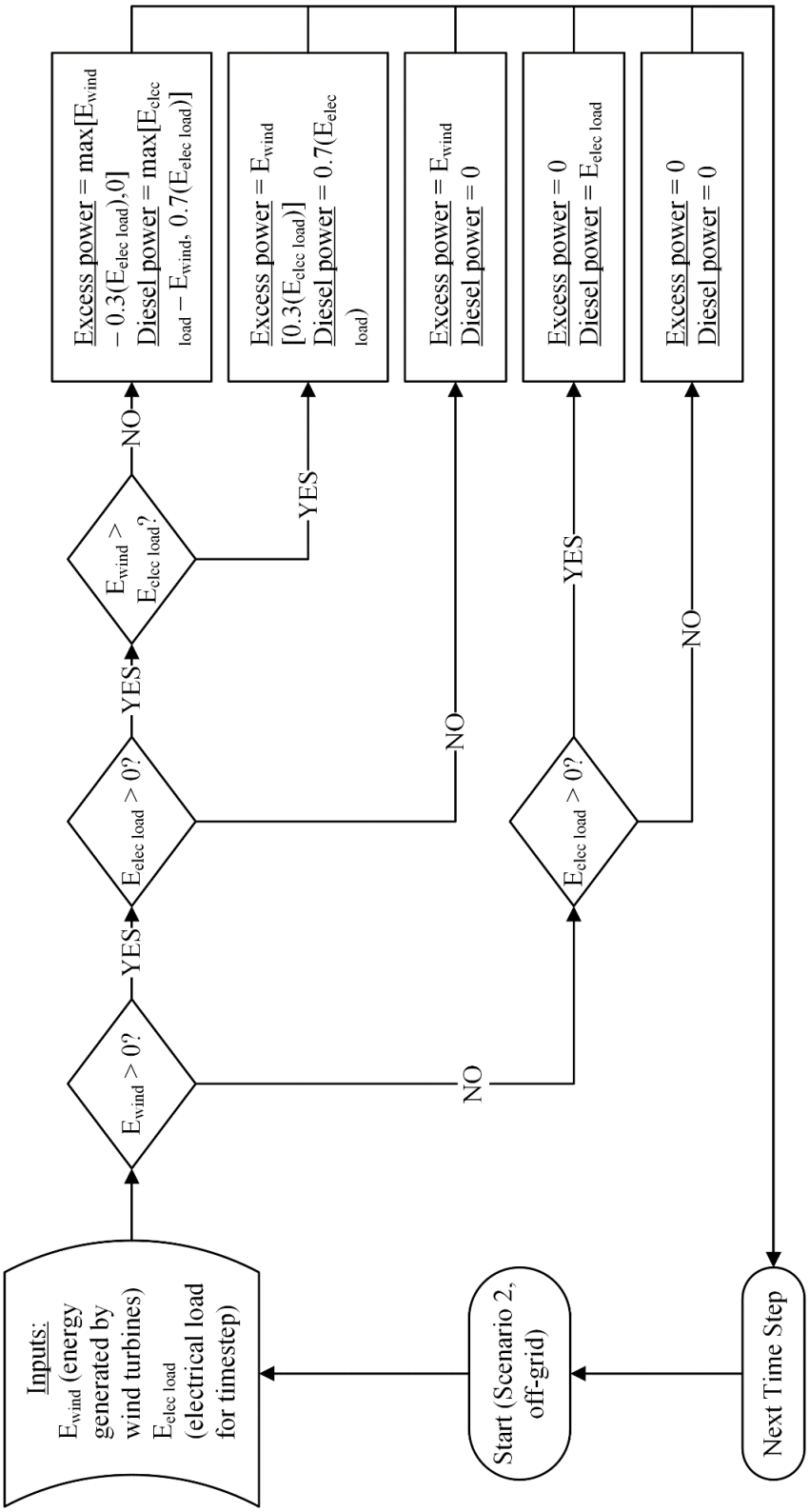

Figure 15: S2C1 & S2C2 electrical dispatch strategy

Dispatch strategy for the ST array and the SAT

The charging strategy for the SAT from the ST array is shown in Figure 16. If the heat transfer fluid at the exit of the ST array is at a temperature that is greater than the SAT, then the ST array control circulates the working fluid through the SAT to heat it. If not, the ST array control diverts the working fluid through the solar thermal array diverter loop (STADL) until it reaches a temperature that is greater than that of the SAT. This dispatch strategy applies to both configurations 1 and 2, as direct ST charging has precedence over HPA-ST charging. The resultant SAT temperature is used in the TES dispatch strategy (for all scenarios and configurations).

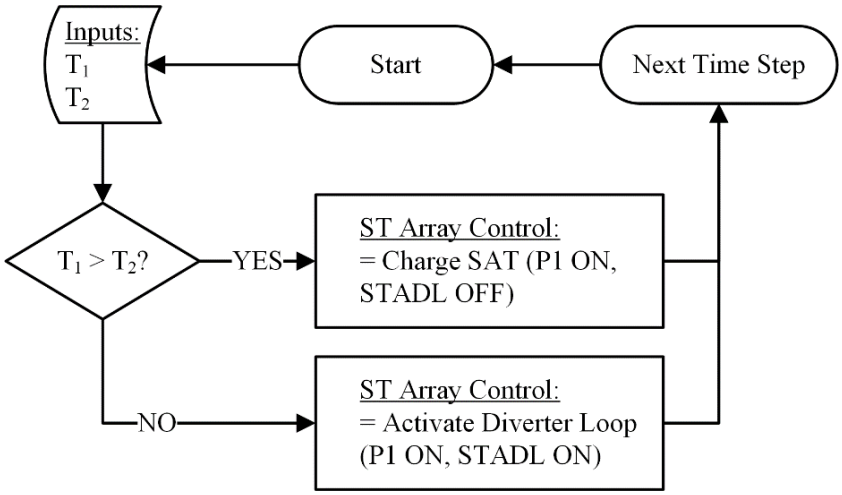

Figure 16: Dispatch strategy for the ST array and SAT

TES dispatch strategy for S1C1

Once the electrical load is served, the S1C1 system must then determine the control logic for the direct ST (ST power), the EH (EH power), as well as determining if there is excess electricity to send back to the OEG (grid sellback). The EH and ST power serve to charge the TES. Figure 17 shows the dispatch strategy for a grid-connected direct ST system.

If the temperature of the heat transfer fluid in the ST array is greater than the temperature of the TES and there is room in the TES to store this thermal energy, the system sends all the useful

energy from the ST array to the TES. The system then checks to see if there is any excess electricity available to be converted to thermal energy. If there is excess electricity available, the system checks whether there is a need for it (*i.e.* whether the TES is at a temperature that is below 95°C). If the answer to both these queries is 'yes', the system uses PtH through the EH to heat the TES to a maximum of 95°C. If afterwards there is still excess electricity, the system feeds it back to the electrical grid.

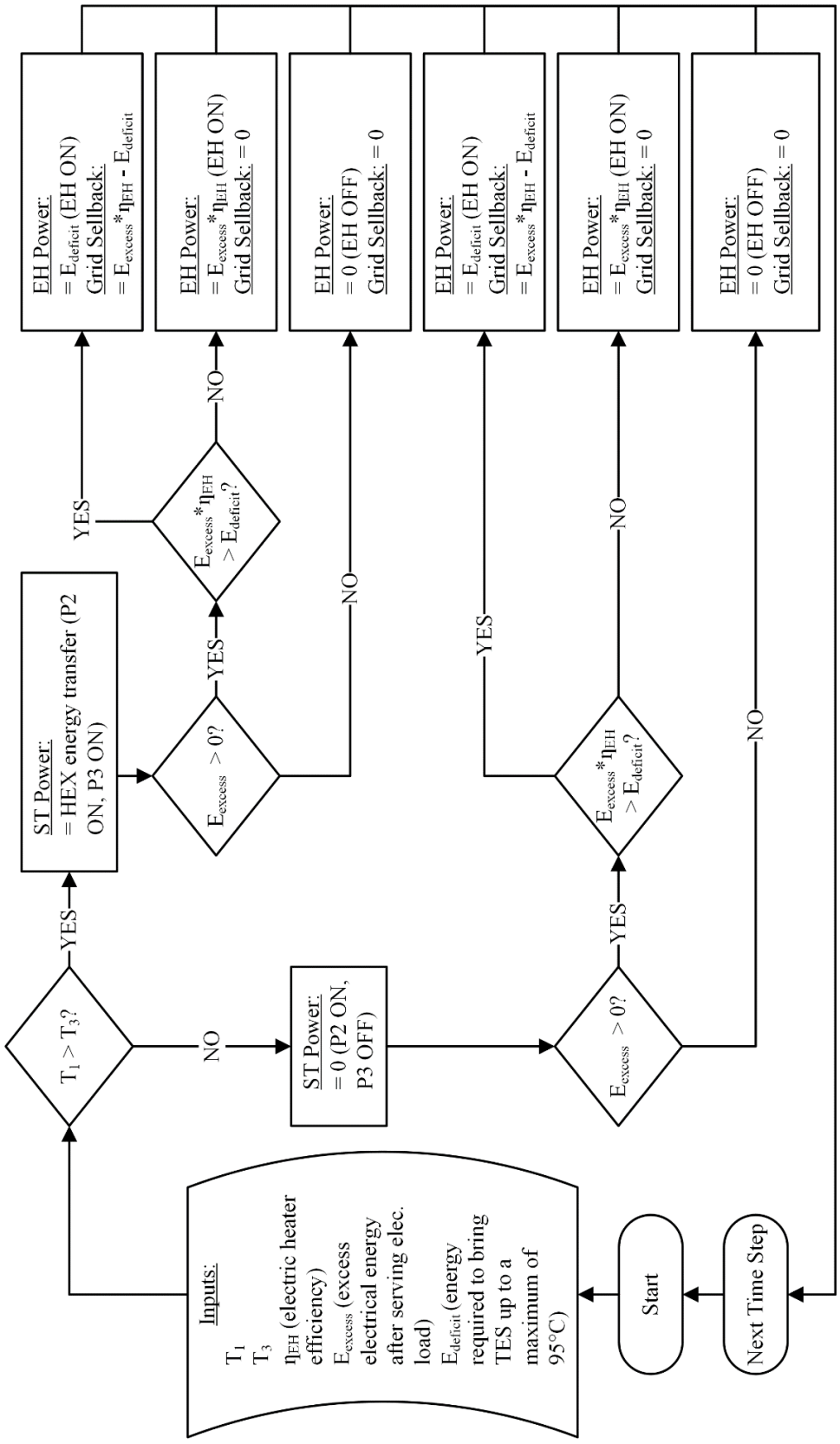

Figure 17: S1C1 TES dispatch strategy

TES dispatch strategy for S1C2

The TES operates differently in S1C2 to accommodate the HPA-ST system. Figure 18 displays a similar dispatch strategy to Figure 17 with identical outputs (*i.e.* "EH power" and "grid sellback"). The only difference is the existence of the HP, and that ST power now includes the energy from the direct ST system and the HPA-ST system.

The HP only operates at night. This gives the SAT as much time as possible to charge and provide direct ST energy through the HEX during the day. The electrically-powered HPA-ST system is activated only if the following criteria are met: the SAT is at a temperature that is below that which is required to directly charge the TES, the sun has set, there is enough excess wind generation to run the HP compressor, and activating the HP will not drop the SAT temperature down below 20°C (an arbitrarily set minimum). If these conditions are met, $E_{compressor}$ is sent to the HP ($E_{compressor}$ is taken from excess power determined in Figure 14).

If there is still excess power available after running the HP, the excess power is considered for PtH conversion. This excess electricity is converted to thermal energy and stored in the TES until the TES reaches its maximum setpoint of 95°C. At that point, if there is still excess electricity available, it is sold back to the electrical grid.

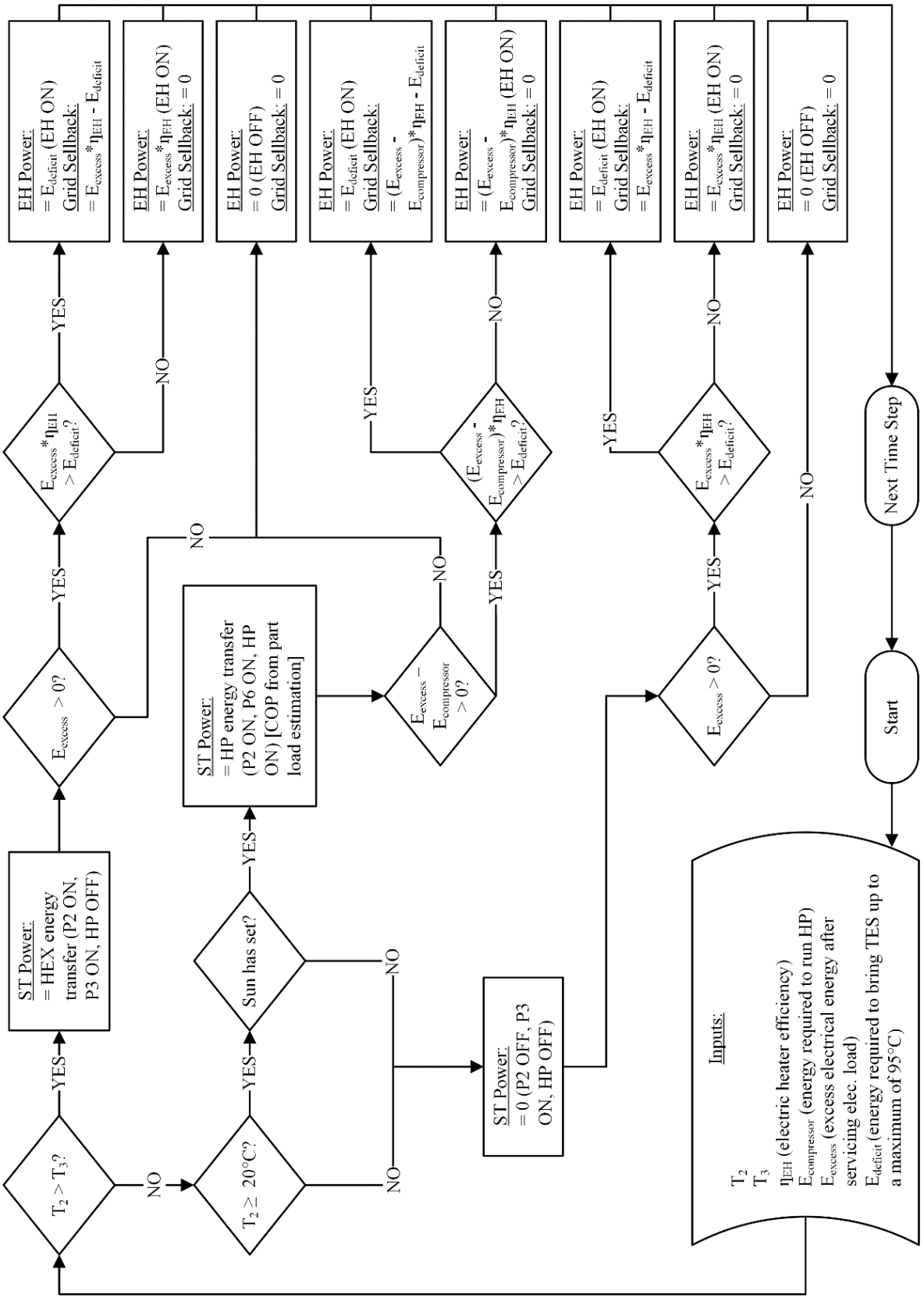

Figure 18: S1C2 TES dispatch strategy

As the dispatch diagrams for S2C1 and S2C2 are nearly identical to Figure 17 and Figure 18, they have not been shown here. The only difference between the S2C1 and S2C2 dispatch strategies is where the excess electricity is directed. These strategies have been included in Appendix A: Off-Grid TES Dispatch Strategy Diagrams.

Dispatch strategy for DH

The DH dispatch strategy is shown in Figure 19 and applies to all scenarios and configurations. The dispatch strategy is used to determine the district heating diverter loop (DHDL) setting. If there is a DH load and the fluid supply temperature from the TES is above the DH setpoint temperature of 70°C, then the system activates the DHDL to temper the fluid down to the setpoint temperature. The DHDL diverts cooled fluid returning from the DH grid back into the hot DH supply fluid to bring down the temperature. If there is a DH load and the supply temperature from the TES is below 70°C, then the FFH is activated to bring the supply fluid up to the setpoint temperature. The DH grid provides enough energy to serve the heating load as well as the heating and pumping losses incurred by the DH grid. District heating losses and pumping flow rate are discussed in Section 3.2.6 and 3.2.7, respectively.

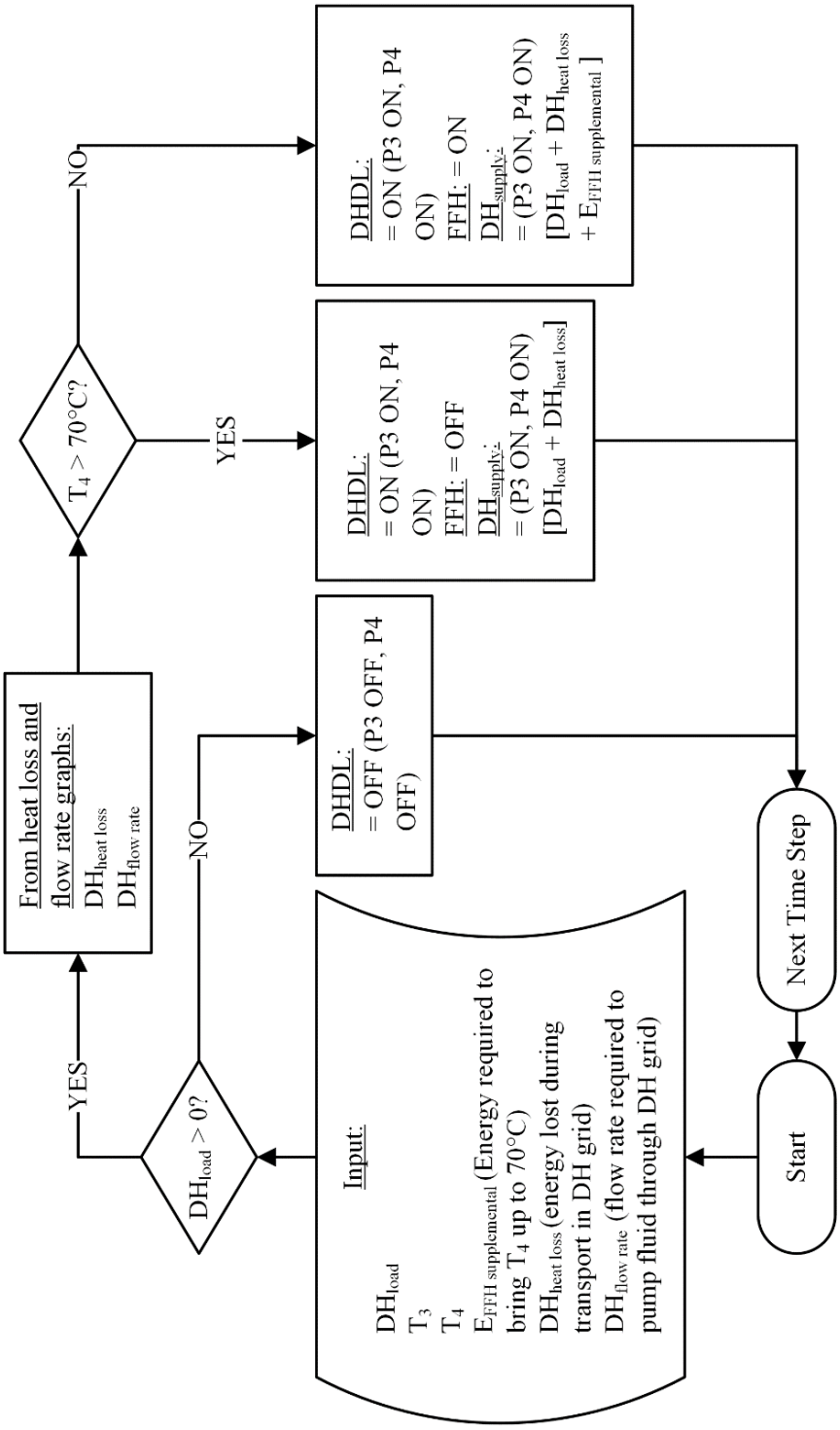

Figure 19: DH dispatch strategy

Dispatch strategy for the CT

The dispatch strategy for the CT determines whether the CT needs be activated at all and, if so, how much cooling is required to bring the TES temperature down to 95°C (CT power). The CT is activated only when the TES is in danger of overheating (*i.e.* when the TES is at a temperature greater than 95°C). The CT is implemented in TRNSYS with an auxiliary cooler for simplicity. The algorithm in Figure 20 calculates and subsequently removes the required amount of heat directly from the fluid flow to bring the TES temperature back down to 95°C. The CT otherwise remains idle.

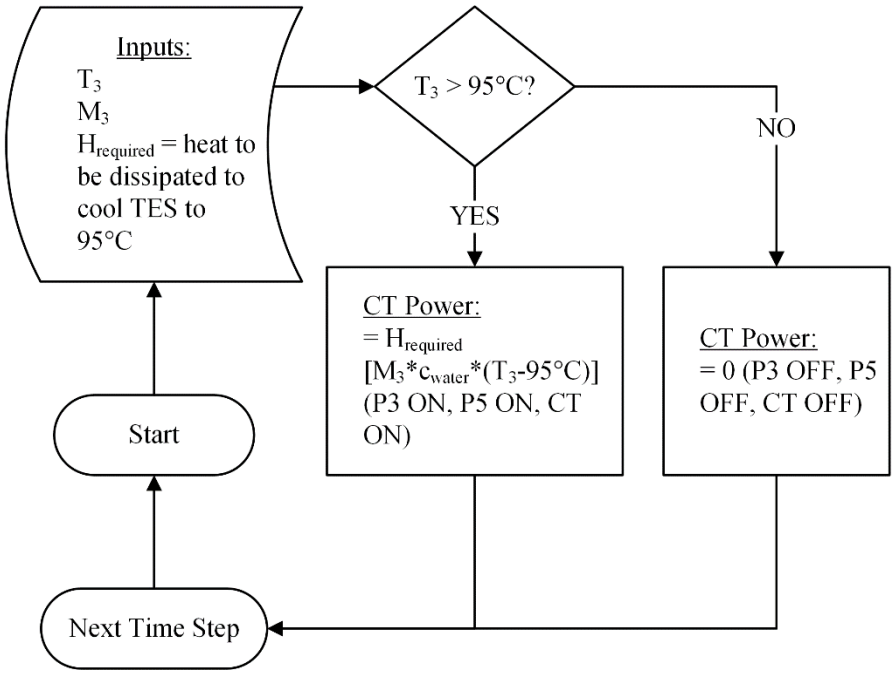

Figure 20: CT dispatch strategy

3.2.5 Estimation of hourly electrical and heating load distributions

The MoCreebec hourly electrical and heating load distributions are estimated from measured electricity load data gathered from the community from 2016, 2017, and 2018. Since the community primarily uses electric baseboard heaters, electric furnaces, and electric water heaters, these bills represent both thermal and electrical loads given in terms of energy consumed per hour.

The acquired data is disaggregated from a single lumped sum of energy into three vectors; DHW, space heating, and plug-in loads.

The DHW load profile is generated using a tool developed by NREL and Hendron et al. [73]. Hendron's tool generates random DHW usage event profiles based on realistic probability distributions for the event durations, flow rates, and time between the events. The effect of vacation periods, weekend versus weekday use, seasonality, and geographic location are also accounted for. These realistic probability distributions are derived from the measured data of over 1200 residences.

This tool is employed to generate a year's worth of hot water events for the community. For each event, the tool outputs the flow rate, $\dot{V}_{event}$, flow duration, t_{event}, and temperature, $T_{DHW\ supply}$. Using this information in conjunction with the average water mains temperature, T_{mains}, and the specific heat of water, c_{water}, the DHW energy demand for each event, Q_{DHW}, is determined, as shown in Equation (3) [80].

$$\boldsymbol{Q_{DHW} = \dot{V}_{event} t_{event} c_{water} (T_{DHW\ supply} - T_{mains})} \quad (3)$$

An average mains temperature of 10°C is assumed in this study. This value is assumed to be reasonable based on the climate data obtained from the One Building online repository of climate data for use in building performance simulation [53].

Since the NREL tool uses probability distributions to generate realistic DHW draw profiles, there is an element of randomness to the generated profiles. In order to accurately represent the DHW profile of 140 houses, the NREL tool is run 140 times based on the housing stock distribution (*i.e.* by number of bedrooms per house). These 140 profiles are summed to represent a net distribution for 140 homes. Fairbanks, AK is chosen as it is the location most closely matched to Moose Factory's climate available with the NREL tool [73].

One issue encountered with the tool is the assumption of a 14-day vacation taken every year by the simulated home's occupants [53]. This results in a 14-day period in which there is no DHW usage. This does not align with the lifestyle of the MoCreebec residents, whom do not take vacations with such frequency or regularity. To adjust for this, loads from similar times of the year (*e.g.* weekends, weekdays) are copied into the blank spaces left by the vacations so that an entire year's worth of DHW loads is obtained.

The second issue is that the tool was developed to emulate a typical home located in an urban centre [53]. To account for the more conservative use of water typified in Moose Factory, the DHW energy demands are reduced by a factor of 25% [81].

Once the annual DHW load profile is estimated for the community, it is subtracted from the lumped sum energy load for the community. The remainder of the lump sum load comprises the combined space heating and plug-in loads. In order to separate these two remaining loads, a heating degree hour (HDH) method for calculating heating load, adapted from Duquette et al. [82], is utilized for estimating the community space heating load. The steps taken to determine the space heating load are depicted in Figure 21.

Step 1: If the outdoor ambient temperature, $T_{ambient}$, is at a temperature that is less than or equal to the setpoint temperature T_H (assumed to be 17°C, assumed to be one degree higher than more typical averages based on correspondence with community residents that indicated more liberal use of space heating [82], [83]), the temperature difference for this hourly time step, ΔT_i, is calculated as the difference between $T_{ambient}$ and T_H. Otherwise, ΔT_i for this time step is set as zero. The result is a vector of 8760 temperature differences, ΔT; one entry for each hour of the year.

Step 2: Each entry of ΔT is then altered as follows- the difference between ΔT_i and the

smallest entry of ΔT is divided by the difference between the largest and smallest entries of ΔT. This generates another vector with 8760 entries, $\Delta T_{interim}$. $\Delta T_{interim}$ is normalized by dividing each hourly entry by the sum of the entire vector, which generates $\Delta T_{normalized}$. The entries of $\Delta T_{normalized}$ equal one when summed.

Step 3: To find the yearly space heating load profile, $E_{space\ heating}$, each hourly entry from $\Delta T_{normalized}$ is multiplied by the total profile, $E_{space\ heating\ total\ for\ 140\ homes}$. This gives an hourly space heating profile that varies according to the ambient temperature.

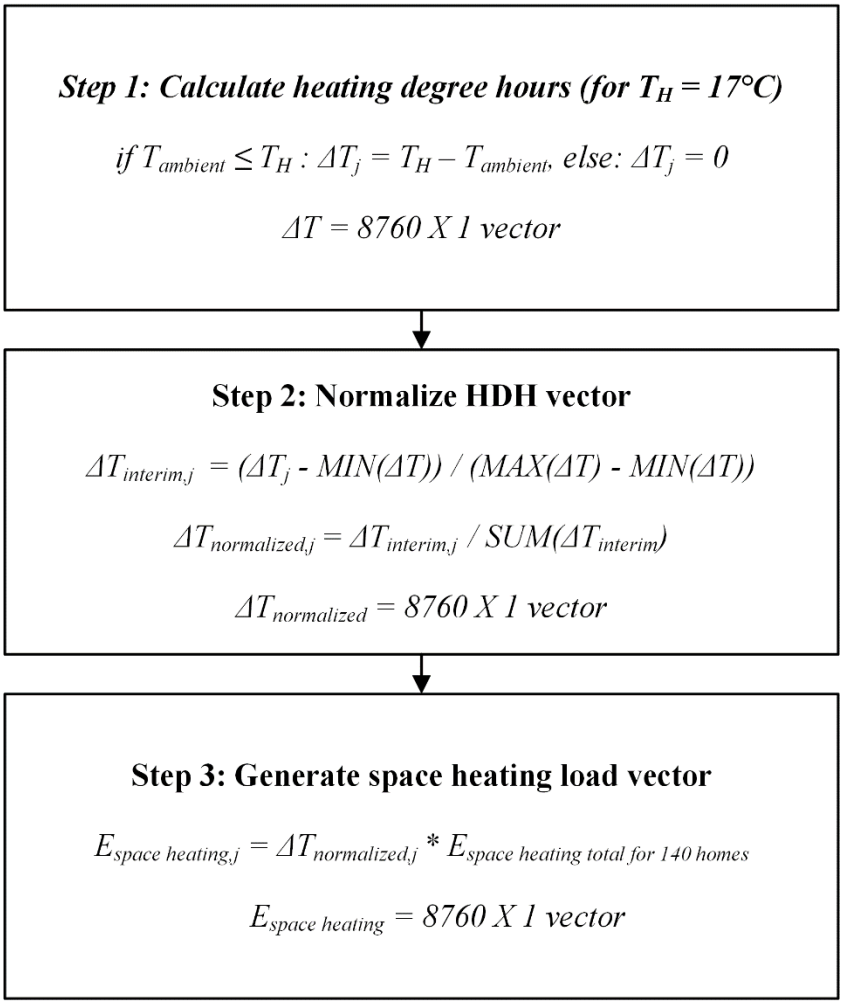

Figure 21: Algorithm to disaggregate heating load from community energy usage

By process of elimination, the plug-in loads are what is left after the space heating and DHW

loads have been removed from the lump sum value given by the load data gathered from MoCreebec. Space cooling is not considered for this study, due to the cold climate of the region.

3.2.6 Estimation of hourly thermal grid heating loss distributions

Heating losses in the DH system are calculated and added to the thermal energy load. This is done to ensure that the required thermal load for the community occupants is met, despite energy losses occuring during transit of the fluid through the DH piping network [84]. Figure 22 shows the heat loss values calculated for this DH system in terms of the total heat load (DHW and space heating) being served in hourly time steps for one year. These heat loss values are obtained from a study conducted by Coady [68]. A DH grid model for MoCreebec, consisting of interconnected buried steel pipes, was built in this study. The model was built in Simulink and executed for a period of one year in hourly time steps. The DH system working fluid was assumed to be water, which operated in steady state with incompressible, one dimensional flow. Heat was assumed to be distributed equally throughout the DH grid. Frictional losses from pipes, fittings, valves, and heat exchangers, as well as convective losses from the piping itself, were calculated and totalled to determine the heat loss in the DH grid.

The large dispersion seen in Figure 22 as the heat load increases is assumed to be due to variations in the ambient air temperature. The heat load used in this study was the hourly heat load (DHW and space heating combined) calculated in Section 3.2.5. The same magnitude of heat load occurs more than once throughout the year of heat load data. However, at each of these time steps with multiples of the same heat load, the ambient temperature differs. This results in multiple values for heat loss in the DH system occurring for the same total heat load value.

The values in Figure 22 are used directly in the TRNSYS model combinations (refer to Figure 19). Due to the dispersion present, some error is introduced to the model.

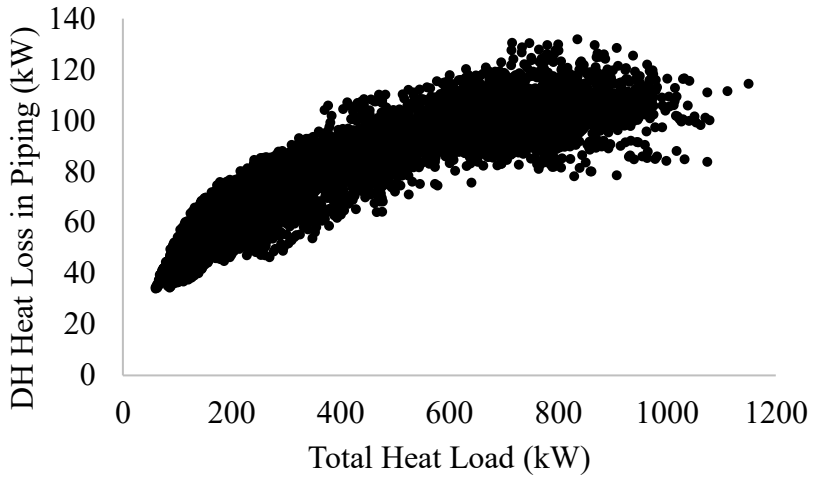

Figure 22: Heat loss in DH piping network compared against time step DH heat load input [68]

3.2.7 Estimation of hourly flow rates in the DH grid

A variable speed pump is employed in the TRNSYS model to serve as the DH pump (shown as P4 in Figure 11 and Figure 12). The flow rates through the DH VSP required to serve the thermal load are also supplied by Coady's work [68]. They were generated by calculating the energy balance across the DH variable speed pump and expressing the work of the variable speed pump as a function of total system head. These resultant flow rates are given in Figure 23, and are used directly in the TRNSYS model DH dispatch strategy. Normalized values for the pump flow rates are inputted to the DH variable speed pump component in the TRNSYS model (refer to Figure 19).

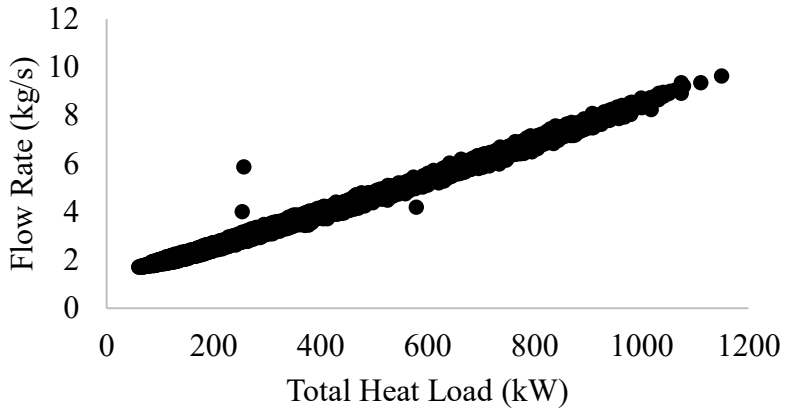

Figure 23: Flow rate inputted to DH VSP corresponding to time step DH heat load input [68]

3.2.8 Estimation of hourly wind distribution

Hourly climatic data from the OneBuilding online climate data repository from 2016 is used by TRNSYS as an input to the WECS type to determine WF energy output in the model [53].

Both wind velocity and wind direction are provided to the WECS type in the TRNSYS model by the data file found in the OneBuilding climate data online repository [53]. The WECS type in TRNSYS reads in the height at which the wind data has been collected and the hub height of the turbine, then uses Equation (4) to model the vertical wind shear. Vertical wind shear is the change in wind speed per change in unit of height [59].

$$\boldsymbol{U_2 = U_1 \left(\frac{z_2}{z_1}\right)^{\alpha}} \quad (4)$$

In Equation (4), U_1 represents the known wind speed at height z_1. U_2 represents the calculated wind speed at height z_2. The U_2 value in Equation (4) is the hub height of the turbines. For this study, it is assumed to be 24 m [54]. z_1 is the data collection height, and is assumed to be 4 m for this study according to a rough estimate for the anemometer height as reported by the community. α represents the power law exponent. This value changes based on the topology of the area. A smooth surface (*i.e.* the ocean or flat ground) has a power law exponent of 0.1, whereas an

urban centre has a power law of approximately 0.4. An α of 0.2 was selected for this study. This α value is used for topologies consisting of occasional trees and small buildings, an appropriate representation of the surface in and around the Moose Factory area [85].

$$\boldsymbol{U_2 = U_1 \left(\frac{z_2}{z_1}\right)^{\alpha}} \quad (4)$$

TRNSYS then uses the newly calculated wind speed along with its other WECS parameter inputs to calculate the electricity generated by the turbines [59].

3.2.9 Estimation of hourly solar thermal radiation distribution

Hourly solar radiation information for Moosonee for the year 2016 is acquired from the OneBuilding climate data online repository [53]. This radiation information, along with additional climatic inputs, is inputted to the FPCs in TRNSYS to determine the outlet temperature for the ST array [61]. Following standard practice, the FPCs modeled in TRNSYS are assumed to be tilted at an angle that is equivalent to the latitude of Moose Factory [86].

3.2.10 Model validation

All TRNSYS components used in this model have been thoroughly validated in a number of studies. A catalogue of studies that validate these TRNSYS components can be found on the University of Wisconsin-Madison website [60].

To ensure that the various TRNSYS components are operating correctly within the system proposed in this thesis, energy balances are performed across a range of input values. For example, the temperature gain between the inlet and outlet streams of the ST array is compared to the insolation of the array during the same time step to ensure the energy output by the SAT matches the energy gain from the ST array. This is done by ensuring that the first law of thermodynamics is never broken across any energy flow in the system (*i.e.* the total energy of a system remains constant, regardless of its conversion from one form to another) [87]. Similarly, flow streams

across the TES, the SAT, and the DH network are checked to ensure the energy is being transmitted through the model as intended. No discrepancies are found.

3.2.11 Energy system economic assessment assumptions

An economic analysis is conducted for each of the 140 combinations of the proposed energy system. In this section, various data are shown regarding components used in the model and their economic parameters.

For the purposes of this study, the overall system lifetime is set to 60 years [88]. The DH system is installed at year 0 of the project and remains in use for the duration of the 60-year project lifetime. All other system components are replaced in their entirety every 20 years (a rough estimation of their aggregated lifetimes [89]) at a cost determined by the values given in Table 6. For all calculations, a discount rate of 6% is assumed. This discount rate is chosen as it is a middle-range rate according to Zhuang et al [90]. It is assumed that the community pays out-of-pocket for the entire cost of the system (capital costs, recurring costs, and fuel costs).

Table 6: Component costing data for economic analysis

Component	Cost	Unit	Costing assumptions
Ethylene glycol (75% by volume)	5,283	$\$/m^3$	Cost acquired from Dynalene Inc. [91], [57]
ST Array	141	$\$/ft^2$	Cost from 2016 NREL renewable energy estimation of costs [92]
TES/SAT	933	$\$/m^3$	Estimation based on de Wit's free-standing insulated heat storage tanks costs [93]
DH trenching	4,493,400	$	Cost calculated by Coady [68] using values taken from RetScreen
DH connection	7,500	$/connection to grid	Cost calculated by Coady [68] using values taken from RetScreen
WF	1,960	$/kW	IEA average wind capacity installation cost [49]
CT	397	$/kW	Average wet CT installation cost

			according to a 2011 Tenaska Trailblazer Partners LLC report to the Global Carbon Capture and Storage Institute [94]
Condensing propane heater (FFH)	122	$/kW	US Department of Energy 2008 gas-condensing water heater costing estimate [95]
EH	167	$/kW	US Department of Energy 2008 electric water heater costing estimate [95]
Diesel	37.9	$/GJ	Natural Resources Canada retail fuel pricing from Yellowknife, NWT (closest geographical approximation with costing data available) [96] combined with a 2011 appendix of heating values for gas, liquid, and solid fuels, released by Argonne National Laboratories [97] (lower heating value used).
Propane	35.9	$/GJ	Natural Resources Canada retail fuel pricing from Yellowknife, NWT [98] (closest geographical approximation with costing data available) combined with a 2011 appendix of heating values for gas, liquid, and solid fuels, released by Argonne National Laboratories [97] (higher heating value used)
Operations and maintenance (O&M)	0.5	% of capital cost	Average O&M cost from 2016 NREL renewable energy estimation of costs [92]

Electricity costs are modeled after Ontario's time-of-use (TOU) pricing scheme and a tiered pricing scheme. TOU pricing changes the cost of electricity based on the time of day, the day of the week, and the season. During periods of historically high electricity use, electricity rates are increased. Conversely, during periods of historically low use, electricity rates are lowered. This method of pricing attempts to lessen peaking electricity use. Pricing periods and electricity prices in the current Ontario TOU policy are displayed in Figure 24.

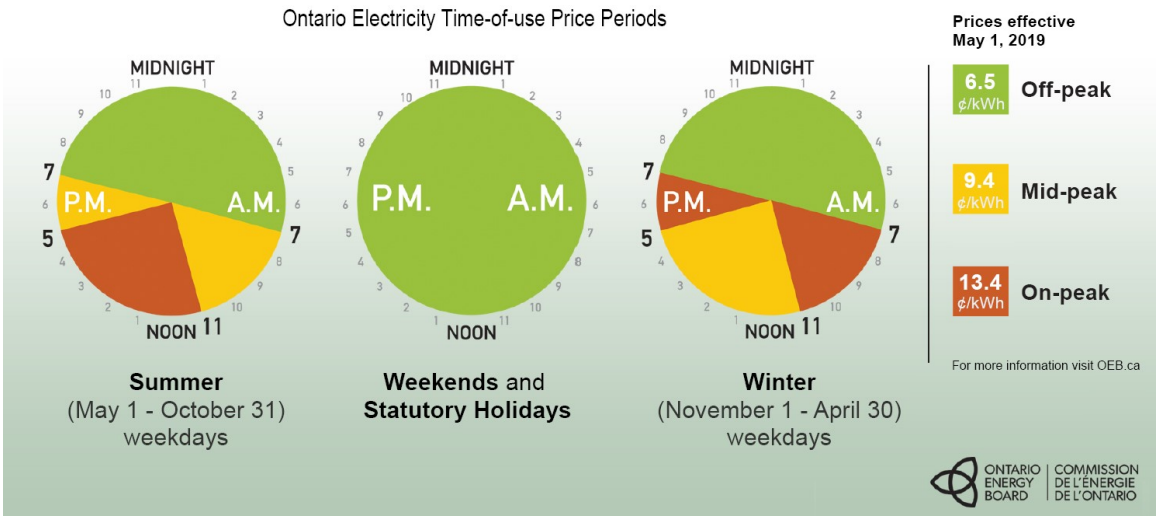

Figure 24: Ontario TOU pricing [99]

Electricity use in some areas of Ontario is also priced according to tiered rates. The price of tiered rates depends on the season, as well as the current sum of energy already consumed during the pricing period. After a certain amount of energy use, the electricity rates increase. Table 7 shows these tiered electricity pricing rates.

Table 7: Ontario tiered electricity pricing [100]

When	Power used (kWh)	Rate (¢/kWh)
Summer (May 1 - Oct 31)	< 600	7.7
	≥ 600	8.9
Winter (Nov 1 - Apr 30)	< 1000	7.7
	≥ 1000	8.9

This study examines the effect of two different electricity pricing policies on the system economics in the grid-connected scenarios. The first pricing policy is the current Ontarian net metering policy, which adheres to the rules as laid out by Ontario Regulation 541/05 [101]. The net metering policy is described in Figure 25. *A* represents the electricity bill incurred by the generator (the client), employing TOU pricing (see Figure 24). *B* represents the regulatory and

delivery fees charged to the generator. *C* represents the cost of electricity used by the generator during the billing period. *D* represents the total value of the electricity sent to the generator, before losses are incurred during transmission. *E* represents any electricity credits leftover from previous billing periods that can be applied to the current billing period. A credit is defined as a unit of electricity generated by the generator and fed back into the OEG. This credit can be used to 'pay' for an equivalent unit of electricity consumed by the generator. If *D* and *E* combined are worth less than *C*, then *A* is assigned to be the difference between *B* plus *C* and *D* plus *E*. Otherwise, *A* is equal to *B*.

The billing period is monthly in Ontario net metering. For simplicity, the billing period is expanded to be one year for the economic analysis in this study [101].

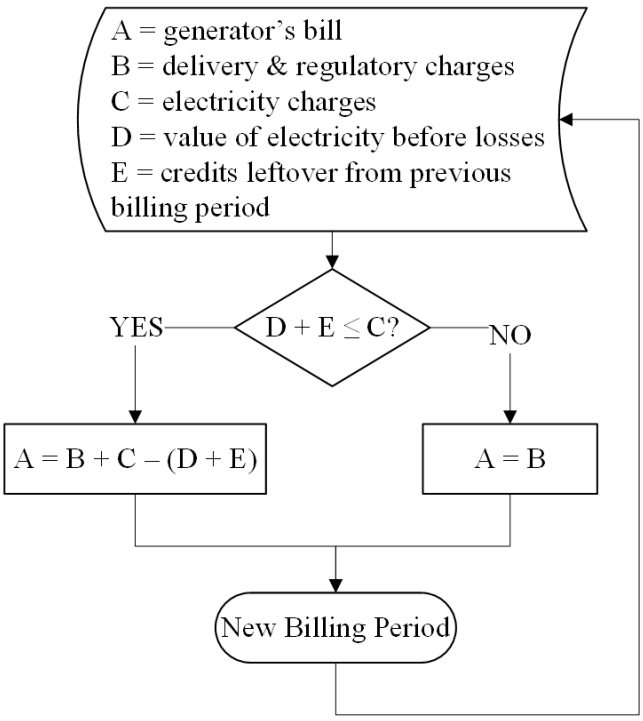

Figure 25: Net metering pricing guide [101]

The second pricing policy considered is a system similar to the now-defunct feed-in-tariff (FIT) program, which was in operation in Ontario from 2009 to 2018 [102].This proposed policy

(referred to hereafter as the two-way tiered pricing [TTP] policy) allows electricity to be bought and sold to the OEG according to tiered pricing regulations (see Table 7). The TTP policy does not deal in credits as the net metering policy does. Instead, the profit from the selling of excess electricity to the OEG is considered an income stream. This income stream does not have an upper limit, unlike the credit system in the net metering policy.

All grid-connected scenarios examined in this research follow the expense flow diagram in Figure 26. Individual consumers (the residents of the 140 homes considered) pay their electricity bills to the OEG based on tiered or TOU pricing, depending on the pricing policy being considered. The OEG sends either the accrued net metering credits or direct TTP income to the MoCreebec municipality. Individual consumers pay the MoCreebec municipality for their heating costs. These heating costs are incurred through the usage of the proposed DH grid, and are set such that the system's net present value (NPV) is maximized at the project lifetime's end. The municipality of MoCreebec generates a profit through the management of these expenses.

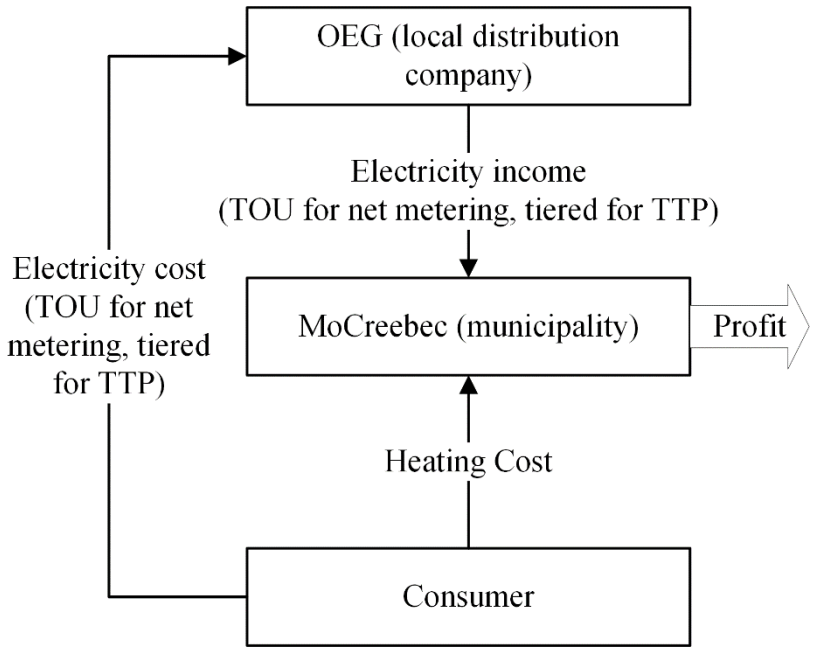

Figure 26: Flow of electricity and heating costs between the consumer, the local distribution company, and the municipality

The results obtained from the TRNSYS simulation work in this study are economically evaluated based on what is termed 'yearly household energy cost'. The yearly household energy cost is the average annual dollar amount that must be charged to each of the 140 households for both electrical (electricity cost in Figure 26) and thermal energy (heating cost in Figure 26) in order for the MoCreebec municipality to at least break even by the end of the 60-year project lifetime.

Yearly household energy cost is calculated using the NPV equation shown in Equation (5) [103]. The NPV is the difference between the present value of all incoming cash flows and the present value of all outgoing cash flows over the project lifetime, m. Equation (5) sums these cash flows from initial year, or n, 0, to the end of m. For each of these m years, the net cash flow of year n, NCF_n, is determined. NCF_n is the sum of all cash inflows (assumed to be positive) and cash outflows (assumed to be negative). NCF_n is then multiplied by a factor determined by the discount rate, d, and n.

$$\boldsymbol{NPV} = \sum_{\boldsymbol{n=0}}^{\boldsymbol{m}} \boldsymbol{NCF_n} \left(\frac{\mathbf{1}}{\boldsymbol{(1+d)^n}}\right) \quad (5)$$

The annual heating cost from Figure 26 is set for each proposed energy system combination such that the NPV for each combination is at least zero (*i.e.* the combination has broken even). The yearly household energy cost is then equivalent to the sum of the yearly heating cost and the yearly electricity cost.

3.2.12 Greenhouse gas accounting

For the purposes of the greenhouse gas (GHG) analysis in this study, only emissions arising from operational energy usage are considered. As such, the three GHG emission sources are the OEG power grid, the FFH (which uses propane as fuel), and the diesel generator plants in the off-grid scenarios.

The OEG power grid is assumed to have an average carbon intensity of 30 gCO_2 eq./kWh

[90], propane a carbon intensity of 214.5 gCO_2 eq./kWh [106], and diesel a carbon intensity of 247.7 gCO_2 eq./kWh [107].

Chapter 4: Results

Simulation results of the system combinations considered in this study are analyzed under three different scopes; energy analysis, economic analysis, and greenhouse gas (GHG) emissions analysis.

4.1 Energy analysis

Energy performance is measured in terms of the yearly residential energy fractions (see Section 3.2.3) served by each major component of the model. A system combination is considered to be 'high-performing' if the renewable energy system components contribute a higher net energy fraction than the fossil fuel-powered components. The goal is to minimize the fossil fuel energy fraction in each combination. The thermal energy and electrical energy analyses are separated for the sake of clarity.

In accordance with Table 5, the solar thermal (ST) array size of each combination is referred to as 0 ST (no ST array), 25 ST (25% full size ST array), 50 ST (50% full size ST array), 75 ST (75% full size ST array), and 100 ST (full size ST array).

Figure 27 shows the S1C1 combination with 100 ST energy results, in terms of percentage of yearly thermal load served from each source. The S1C1 100 ST results are presented by the size of the wind farm (WF) considered in each combination. The direct ST system provides a maximum of just under 30% of the yearly thermal energy load with a WF of 0, with the propane heater (a.k.a. the fossil fuel heater [FFH]) supplying the remainder. However, with a WF of 1, the electric heater EH contributes 40% of the yearly thermal energy load supplied by excess wind generation.

Increasing the size of the WF increases the fraction of thermal energy provided by the EH, as well as decreasing the thermal energy production fractions of both the FFH and the direct ST. The marginal benefit that adding a turbine to the WF has on the FFH consumption is found to be

inversely proportional to the size of the WF. The community electrical load does not always temporally coincide with periods of wind generation, and therefore cannot be served solely with the WF, no matter its size.

Figure 27 also displays a notable lack of cooling tower (CT) usage. Due to the optimized sizing of the thermal energy storage tank (TES), the system provides power to the DH grid, as well as stores a significant amount for later use with little risk of overheating the tank. The TES has a large storage capacity owing to the difference between the maximum TES storage temperature of 95°C and the district heating (DH) supply temperature of 70°C.

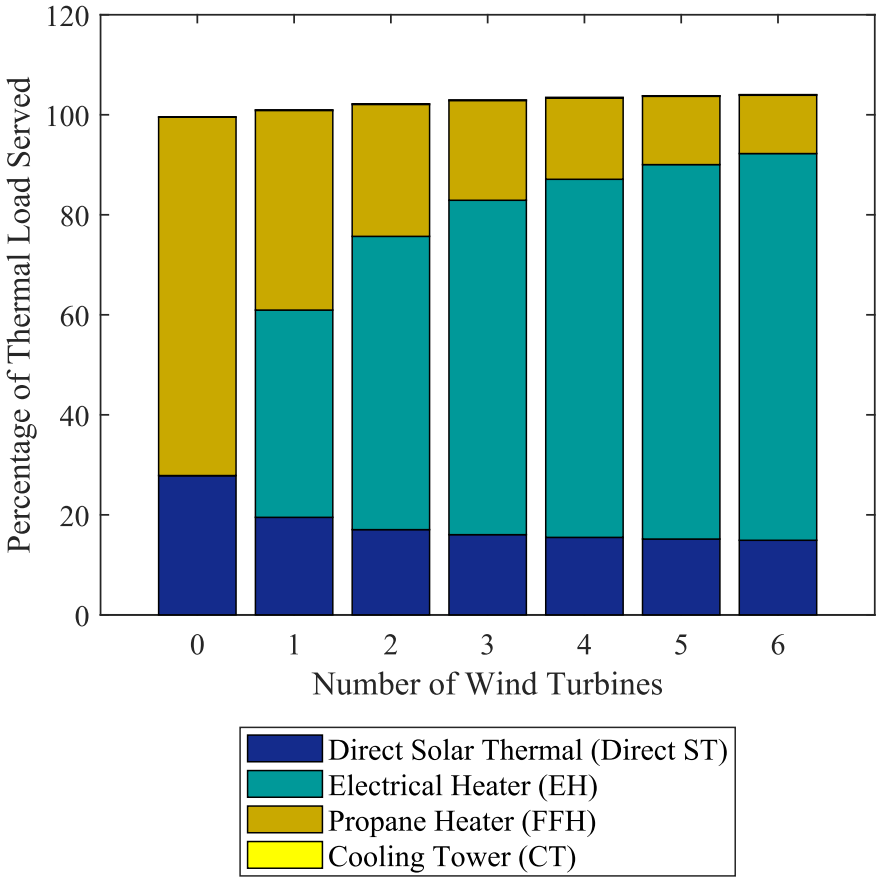

Figure 27: S1C1 100 ST thermal energy production results

The addition of a heat pump-assissted solar thermal (HPA-ST) system largely reduces the

direct ST's yearly energy load fraction, as demonstrated in Figure 28. This is because the heat pump (HP) draws out energy from the solar accumulator tank (SAT) to charge the TES overnight. The ST array is typically unable to recharge the SAT to a temperature exceeding that of the TES over the course of the next day before the HP activates again the following night and cools the SAT again.

The S1C2 models have a maximum ST array size that is approximately 14 times smaller than the maximum ST array size of the S1C1 models. In the absence of a WF to power the HP and the EH, this smaller ST array size results in a much smaller direct ST energy fraction than in the S1C1 model combination energy results. Consequently, the FFH supplies nearly the entire year's thermal energy load. A WF of 1 allows the EH and the HPA-ST system to operate, drastically reducing the FFH's energy fraction. With a larger WF, the EH usage increases and the FFH usage decreases. As in Figure 27, the subsequent WF size increase has an inversely proportional marginal impact on these energy fractions.

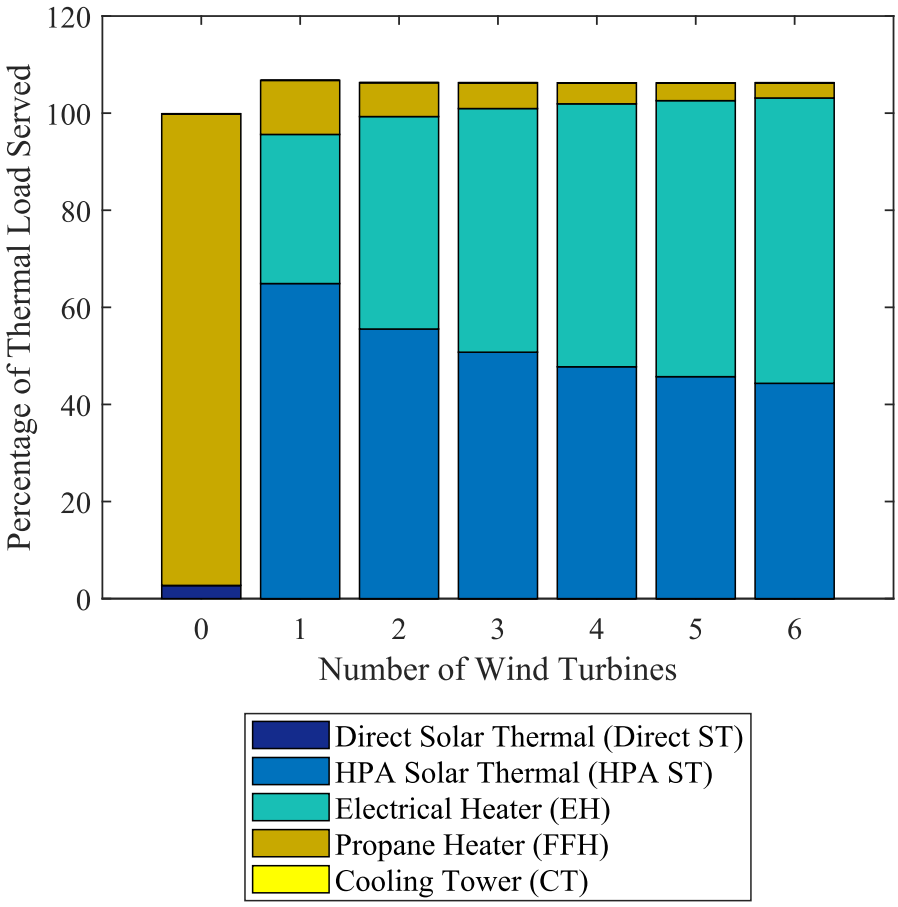

Figure 28: S1C2 100 ST thermal energy production results

The results of the electrical energy generation analysis vary between S1C1 and S1C2. However, this difference is so slight that Figure 29 suffices to represent the results of both combinations. Figure 29 shows the S1C1 and S1C2 electrical production results presented in terms of fraction of yearly electrical load provided by either the WF or the Ontario energy grid (OEG). In Figure 29, the positive y-axis represents electricity used to serve the community electrical load. The negative y-axis represents excess electricity generated in the combination. With no WF, the entirety of the load is served by the OEG. A WF of 1 generates enough electricity to reduce the OEG's contribution from 100% down to approximately 30%, with roughly 1.5 times the yearly plug-in load being generated in excess. This excess electricity is used to power the EH, the HPA-

ST, or is fed back into the OEG.

Each additional turbine in the WF results in a narrow reduction in the fraction of yearly electrical load served by the OEG. The WF can only provide power when the wind is blowing and there is an electrical load. Figure 29 shows that roughly 20% of the community electrical load does not temporally coincide with periods of wind generation.

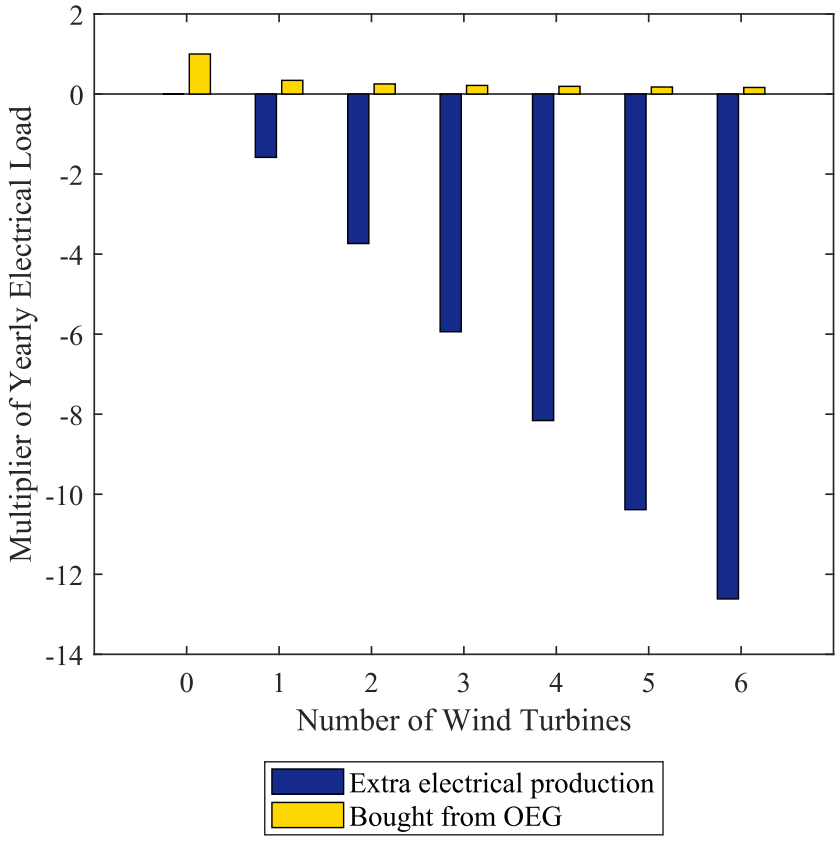

Figure 29: S1C1 & S1C2 electrical energy production results

Figure 30 shows the 100 ST thermal energy results for the S2C1 model. The results are similar to the S1C1 model. The only difference between the functionality of the scenario 1 & 2 models is the percentage of wind power permitted to penetrate the community electrical grid. There is a 30% limit imposed on the WF penetration in off-grid systems (see Section 3.2.4), whereas the grid-connected systems have no such limitation. This increases the amount of electrical energy

available for the EH and the HPA-ST system in the S2C1 and S2C2 models, compared to the S1C1 and S1C2 models with WFs of identical size. It follows that the EH energy fraction in Figure 30 is larger than that in Figure 27, having supplanted more FFH production due to the higher amount of electricity available for use in the EH.

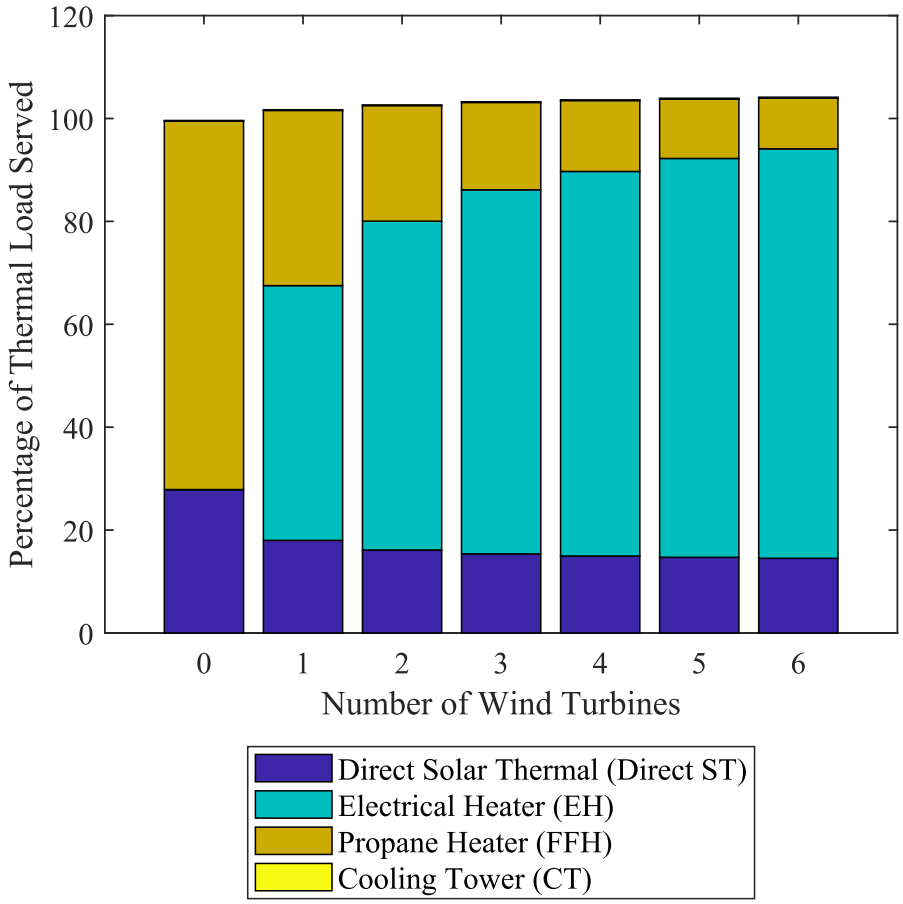

Figure 30: S2C1 100 ST thermal energy production results

The energy results for the S2C2 model combinations shown in Figure 31 also bear resemblances to the S1C2 results shown in Figure 28. For the same reasons as outlined above, the EH energy fraction has increased, further reducing the fraction of the yearly energy load provided by the FFH.

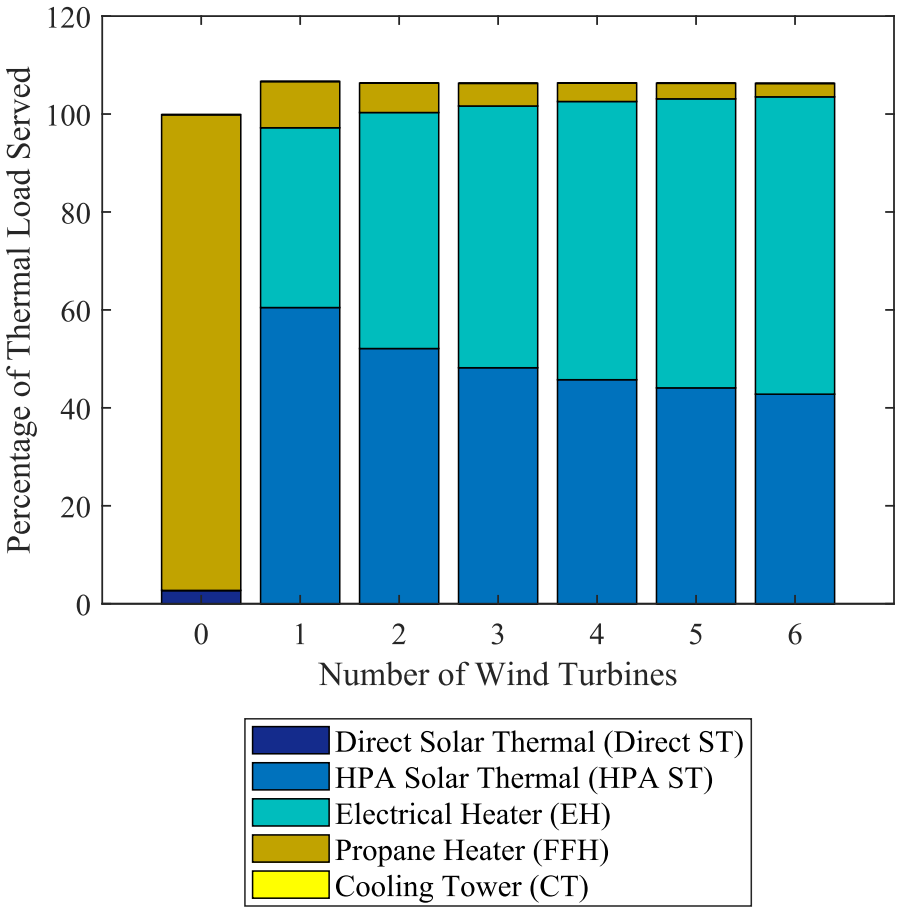

Figure 31: S2C2 100 ST array thermal energy production results

The S2C1 and S2C2 models are off-grid, and therefore have no way to sell or purchase additional electricity from the OEG. Figure 32 shows the S2C1 and S2C2 model electrical energy outputs in terms of fraction of yearly electrical load provided by either the WF or the diesel generator plants. Excess electrical energy is sent to the HPA-ST, the EH, or failing both those options, is converted to thermal energy and sent to the CT to be vented. The wind power penetration is never high in the off-grid scenarios, due to its imposed 30% cap.

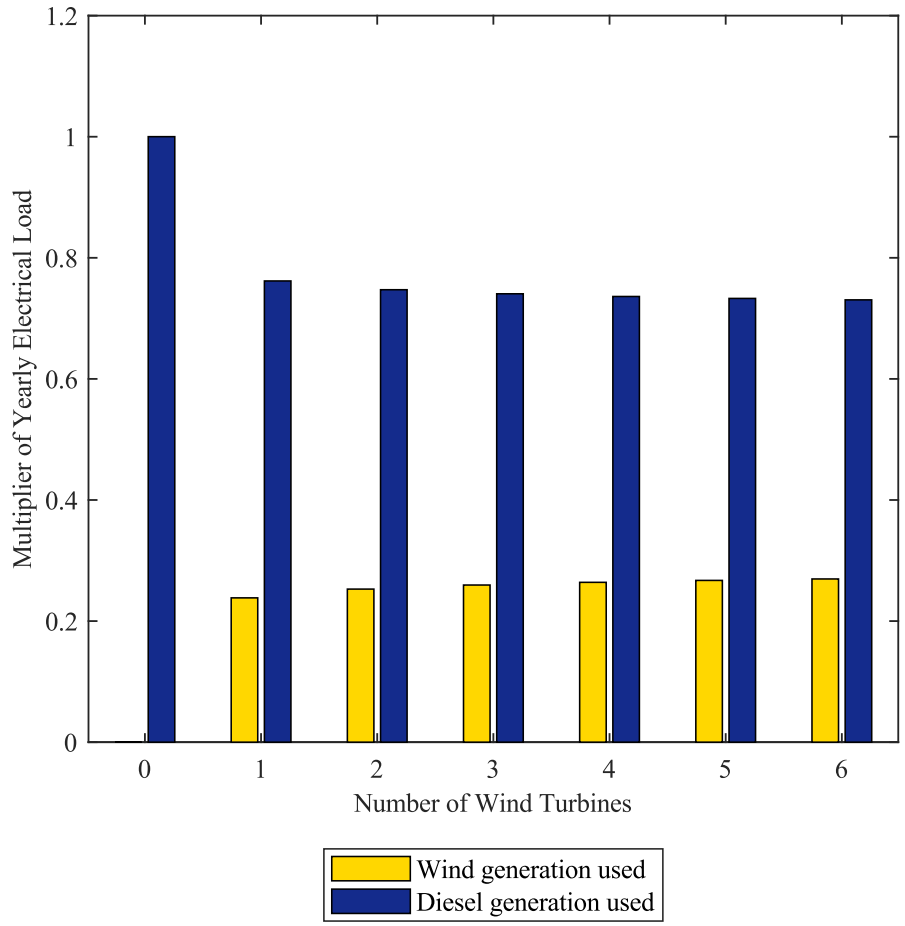

Figure 32: S2C1 & S2C2 electrical energy production results

No matter the scenario or configuration, the CT usage is minimal to nonexistent. Owing to the HPA-ST and EH components available to make use of extra wind generation, as well as the generously sized TES tanks to permit large amounts of thermal energy storage, the combinations rarely have to activate the CT to cool the TES.

Simulations were run for all other combinations shown in Table 5. The energy fractions served by each system component do not change much when decreasing the ST array size. Therefore, the graphs detailing the results for 0, 25, 50, and 75 ST for all four system scenario and configuration pairs have been included in Appendix B: S1C1 0, 25, 50, 75 ST array energy generation results through to Appendix E: S2C2 0, 25, 50, 75 ST array energy generation results.

4.2 Economic analysis

The base-case scenario economic result is defined as the current yearly cost of energy for a single residence. The base-case scenario is hereafter referred to as the Business-as-Usual (BaU) scenario. For all grid-connected scenarios considered in this study, the BaU cost is $1.4k CAD per MoCreebec household.

Figure 33 shows the economic combination results for S1C1 compared to the BaU scenario when a net metering pricing policy is considered for the sale of excess electricity generated by the WF. Every combination's price drops with each increase in the WF's size until the third turbine is installed. After a WF of size 3, the combinations become increasingly expensive with each added turbine. None of the combinations produce a less expensive alternative to the BaU scenario.

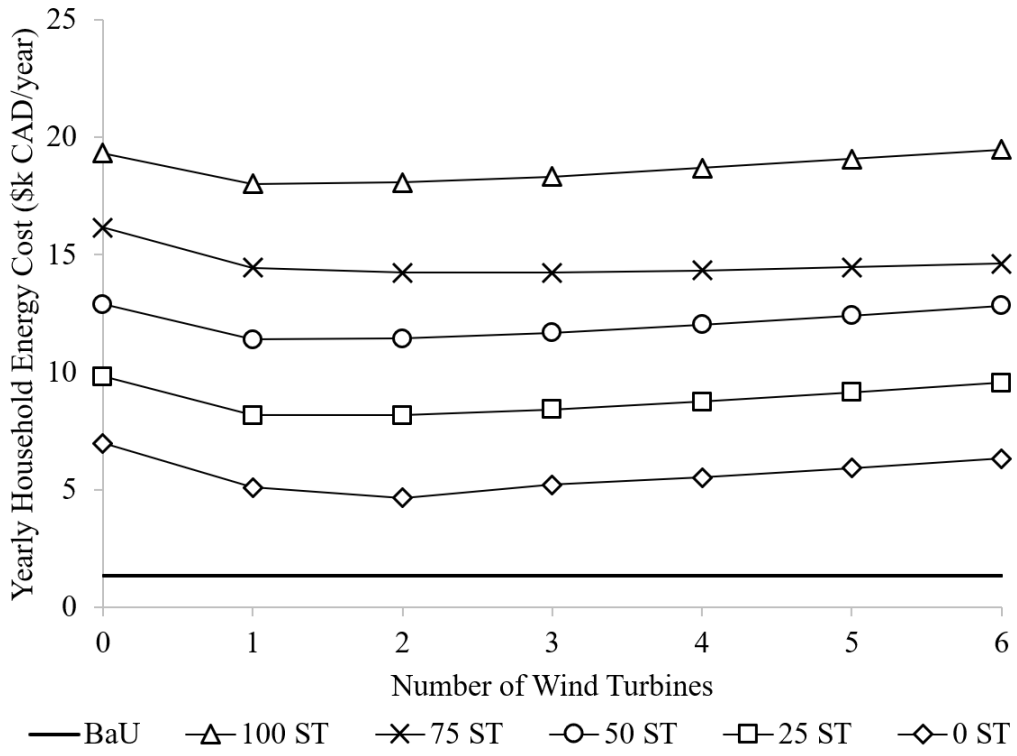

Figure 33: S1C1 yearly household energy cost analysis with net metering electricity pricing policy

The yearly household energy cost results for the S1C2 model combinations are shown in

Figure 34. For all combinations with an ST array, a similar trend to that seen in the S1C1 results repeats itself. Yearly household energy costs drop with a WF of 1, and then increase steadily with each increase in the number of turbines in the WF.

The 0 ST combination with no WF is much less expensive than the other combinations with no WF. The 0 ST combination's capital costs are considerably lower than the other combinations without WFs, since no ST array or associated components are installed. A WF of 1 in conjunction with the 0 ST combination greatly increases the price due to the increase in capital cost necessary to install the wind turbine. A second wind turbine installation decreases costs, as the marginal increase in capital expenditure is small compared to the marginal increase in EH use. Any additional turbine installations increase the yearly household energy costs in the same way they do for the combinations with ST arrays. The results show that the household energy cost is still relatively high for all combinations relative to the BaU scenario.

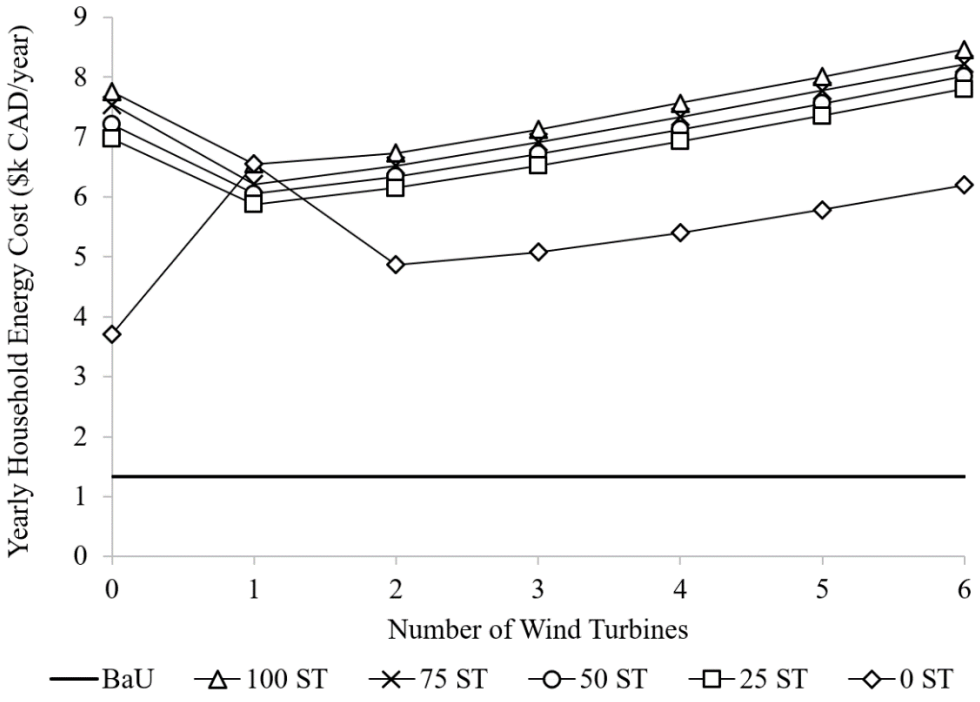

Figure 34: S1C2 annual household energy cost analysis with net metering electricity pricing policy

The implementation of a hypothetical two-way tiered (TTP) pricing scheme increases income from excess electricity significantly. The TTP income increases as the WF is increased in size, as a larger WF produces more excess electricity. The large income stream to the municipality allows for it to charge a much lower heating cost (see Figure 26), making the combinations more economically attractive compared to the BaU scenario. Therefore, as the WF increases in size, yearly household energy cost decreases with a TTP pricing scheme. Figure 35 shows the S1C1 combination results with a TTP pricing scheme. The TTP program decreases the yearly household energy cost an average of $1 - 2k CAD for every additional increase in the WF size.

Some of the S1C1 combinations yield yearly household energy costs low enough to undercut the BaU scenario. In the 0 ST combinations with a WF of size 3 or larger, it becomes possible to give away thermal energy to community residents for free and conclude the 60-year project term with a profit, rather than only breaking even (see Table 8 for more combination results yielding a profit at the end of the project lifetime). Note that while thermal energy may be given away for free, consumers must still pay for their electricity use (see Figure 26). Implemented in reality, the combinations yielding free thermal energy would continue to charge a rate for thermal energy to generate a larger profit. The thermal energy is listed as free for the purposes of comparison only.

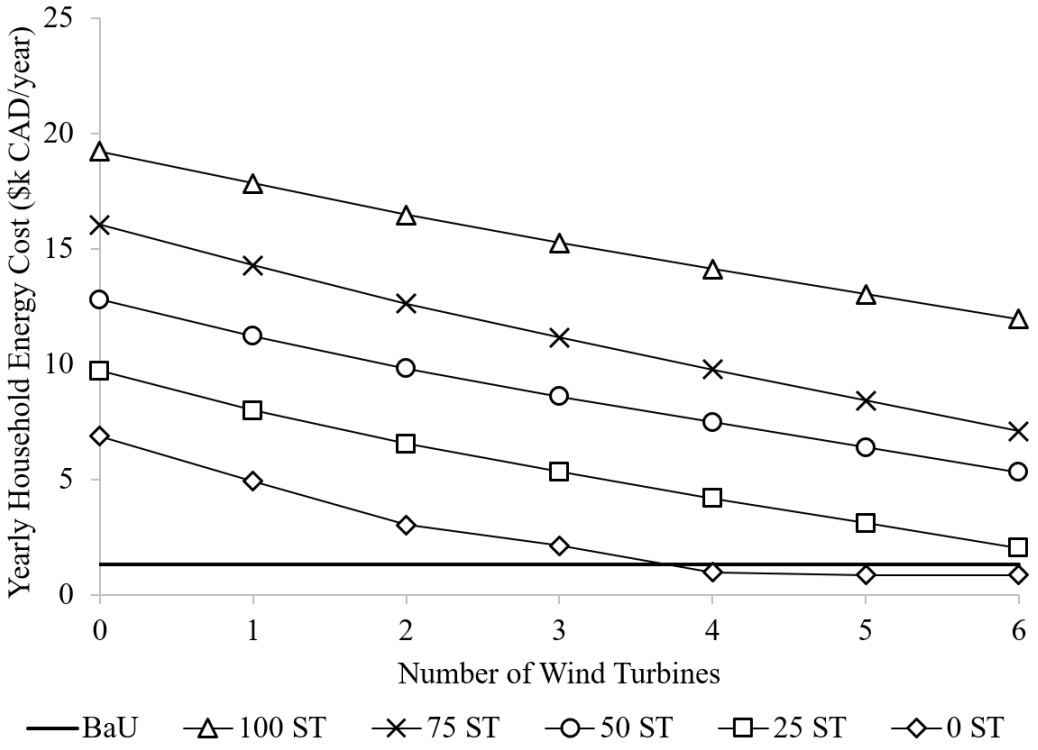

Figure 35: S1C1 annual household energy cost analysis with TTP electricity pricing policy

Using the TTP pricing policy for excess electricity in the S1C2 model combinations produces even more yearly household energy costs that are lower than the BaU case, as shown in Figure 36. With a WF of 6, every iteration of the ST array size results in a lower household energy cost than the BaU scenario. Any combination with a WF of 6 yields a yearly thermal energy cost lower than the BaU scenario. The 25 ST- 5 WF combination has a household energy cost equal to the BaU scenario. The 0 ST- 0 WF combination and the 0 ST- 5 WF combination both produce yearly household energy costs lower than the BaU scenario. The price for 0 ST combinations increases until the WF is size 2, and thereafter decreases for the same reason the 0 ST combinations decreases as described in Figure 34 and Figure 35.

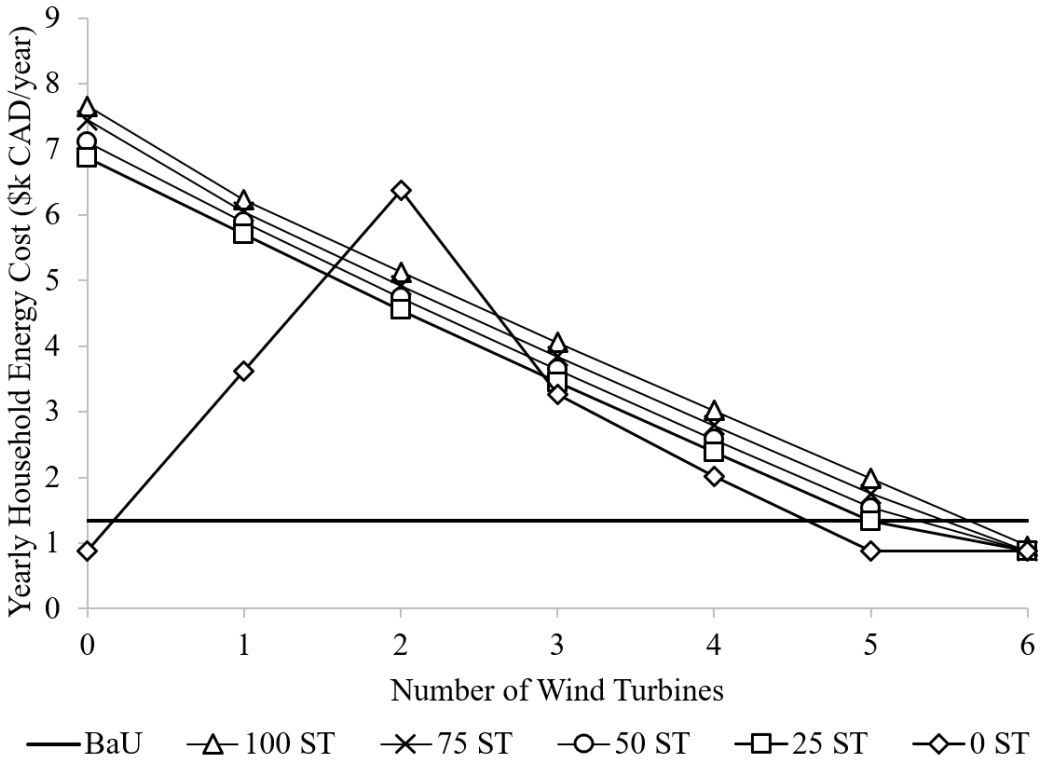

Figure 36: S1C2 annual household energy cost analysis with TTP electricity pricing policy

Table 8 enumerates all grid-connected model combinations that result in free household heating costs as well as a profit at the end of the project lifetime under a TTP electricity pricing policy. Consumers still pay for their electricity bills, which amount to just under $1k CAD per year per household.

Table 8: Combinations with zero household energy cost resulting in a profit at the end of project lifetime under a TTP policy for a grid-connected system

Combination & Configuration	Model Parameters	End-of-project-lifetime Profit ($M CAD, NPV)
S2C1	0 ST, 5 WF	2.2
S2C1	0 ST, 6 WF	4.6
S2C2	75 ST, 6 WF	0.35
S2C2	50 ST, 6 WF	0.81
S2C2	25 ST, 6 WF	1.3
S2C2	0 ST, 4 WF	0.0055
S2C2	0 ST, 5 WF	2.5
S2C2	0 ST, 6 WF	4.9

The proposed energy system model economics are also compared to an off-grid BaU scenario. In the off-grid BaU scenario, all energy needs are served by propane heaters and diesel generator plants. The off-grid BaU scenario has a yearly household energy cost of $9k CAD and is assumed to have the same energy profile as the MoCreebec case study. The lack of electrical grid connection forces the BaU scenarios to rely on more costly and carbon intensive fossil fuels to provide both electrical and thermal energy.

Figure 37 shows the annual household energy costs for the S2C1 combinations compared to an off-grid BaU scenario. All combinations with a WF of 1 or more, except for the 0 ST combinations, produce annual household energy costs greater than the BaU scenario. After the initial drastic decrease in price that precipitates from the installation of the first turbine, the yearly household energy cost decrease per turbine added to the WF is less than $100 CAD.

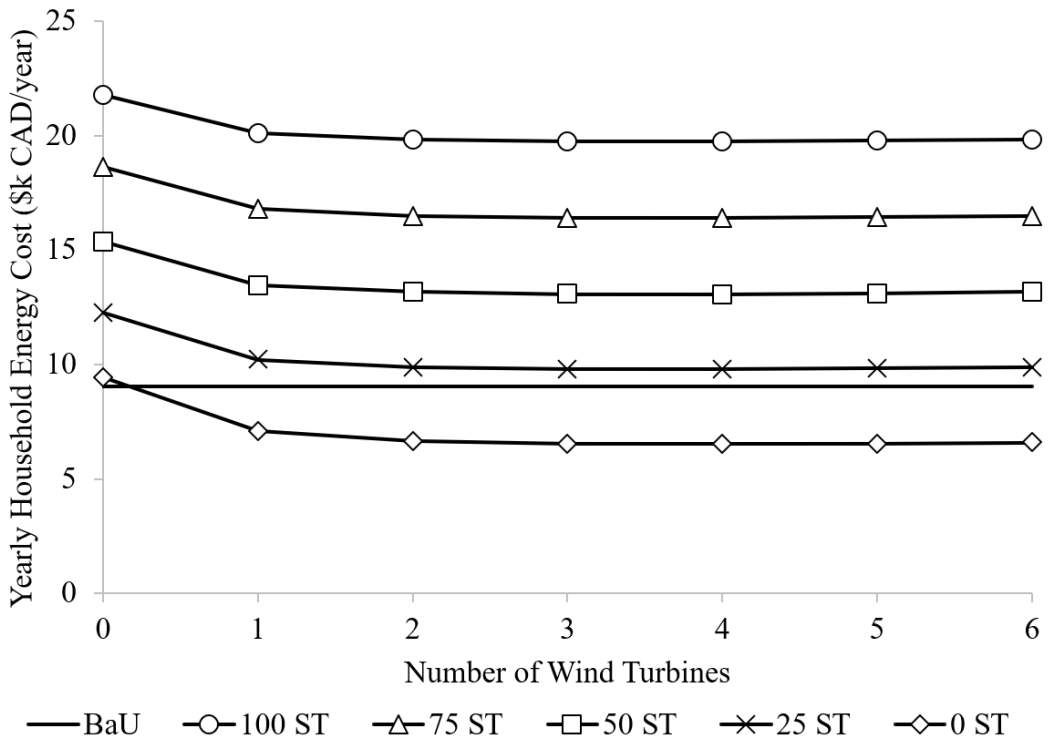

Figure 37: S2C1 annual household energy cost analysis

The addition of a HPA-ST system drops the annual household energy costs even further. The S2C2 results in Figure 38 show that every combination with a WF of at least 1 results in a cheaper yearly household energy cost than the BaU case. As in the S1C2 results, the yearly household energy cost lowers significantly with a WF of 1. With a WF of 2 or more, the yearly household energy cost begins to increase again for all combinations with ST arrays.

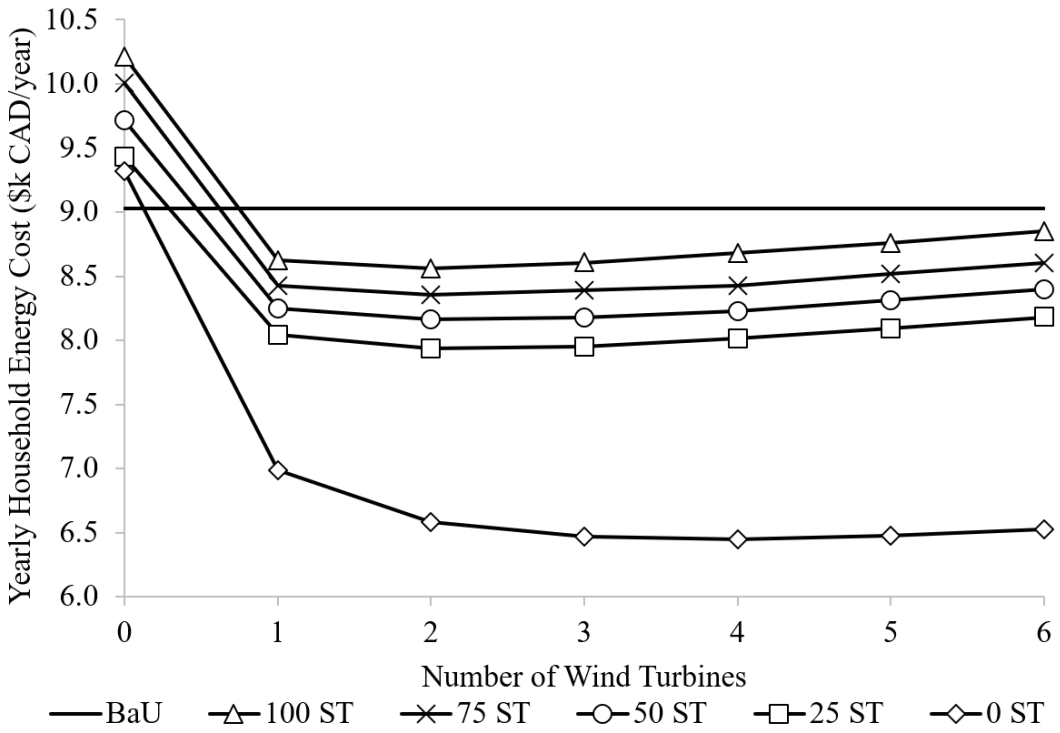

Figure 38: S2C2 annual household energy cost analysis

4.3 GHG emissions analysis

The grid-connected BaU scenario GHG emissions result is defined as the current yearly GHG emissions for 140 typical MoCreebec residences. This is set to 114 tonnes of CO_2 eq. per year.

The GHG results of the S1C1 combinations, shown in Figure 39, yield annual GHG emissions larger than that of the BaU case with six exceptions; the 100 ST combinations with a WF of 5 and 6, the 75 ST combinations a WF of 5 and 6, and the 50 ST combination with a WF of 6.

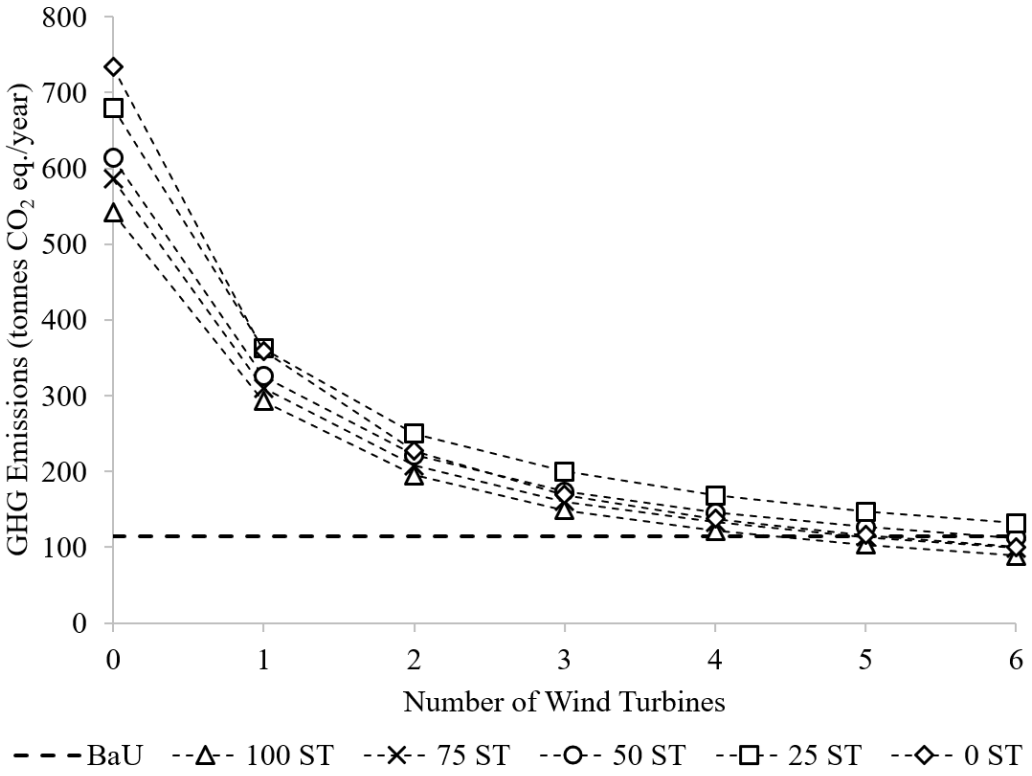

Figure 39: S1C1 GHG emissions analysis

The S1C2 model combinations, shown in Figure 40, overall yield more results with fewer GHG emissions than the BaU scenario than results with greater GHG emissions. Of the 0 ST models, only the combination with a WF of 6 yields fewer GHG emissions than the BaU scenario. All ST array sizes without a WF produce more GHG emissions than the BaU scenario, as well as the 25 ST and 75 ST combinations with a WF of 1. All other combinations result in fewer GHG emissions than the BaU scenario.

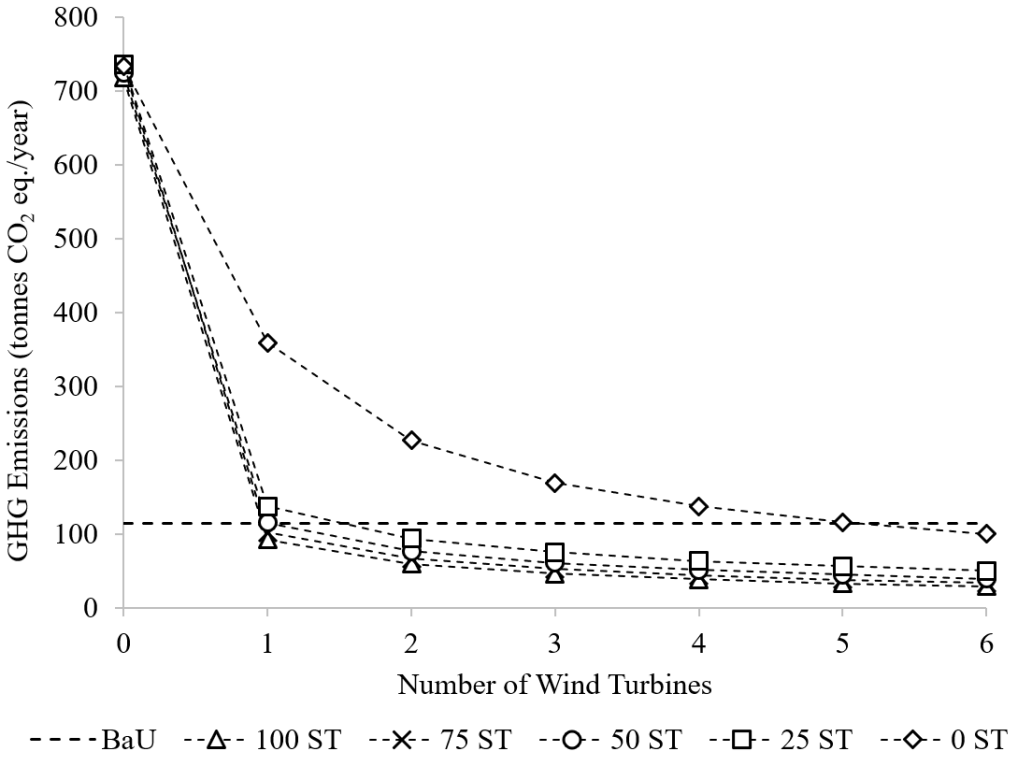

Figure 40: S1C2 GHG emissions analysis

The off-grid BaU scenario GHG emissions result is defined as the current yearly GHG emissions for 140 typical remote residences. This is set to 2053 tonnes CO_2 eq. per year.

Both configurations of the proposed energy system produce fewer GHG emissions than the off-grid BaU scenario for every model combination. Figure 41 shows that, excepting the combinations with a WF of 0, every S2C1 combination results in half the GHG emissions or less than the off-grid BaU case. The same is true of the S2C2 combinations shown in Figure 42.

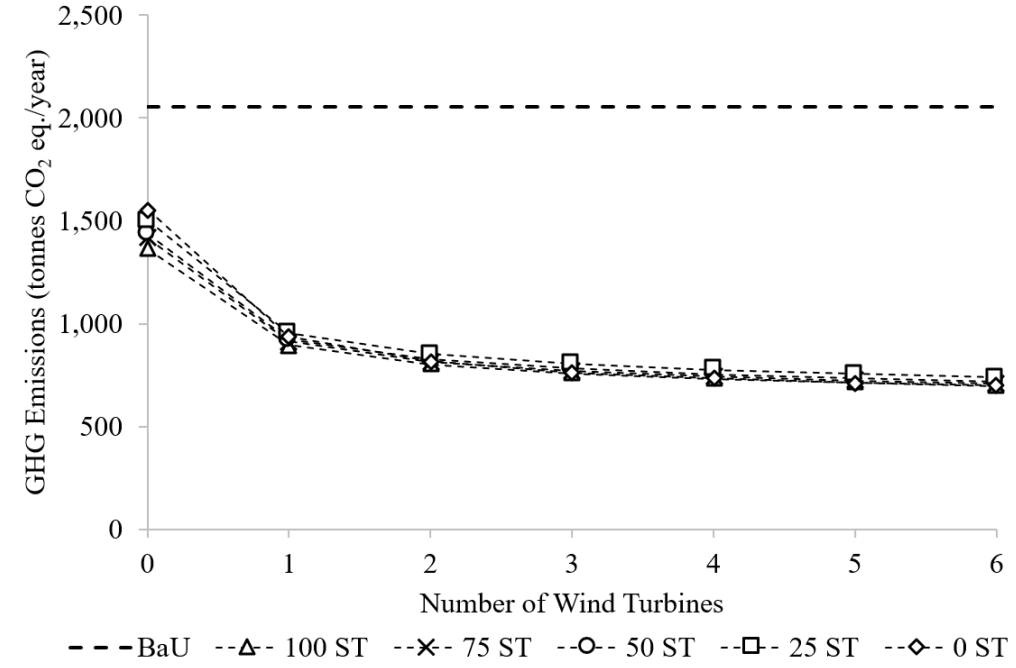

Figure 41: S2C1 GHG emissions analysis

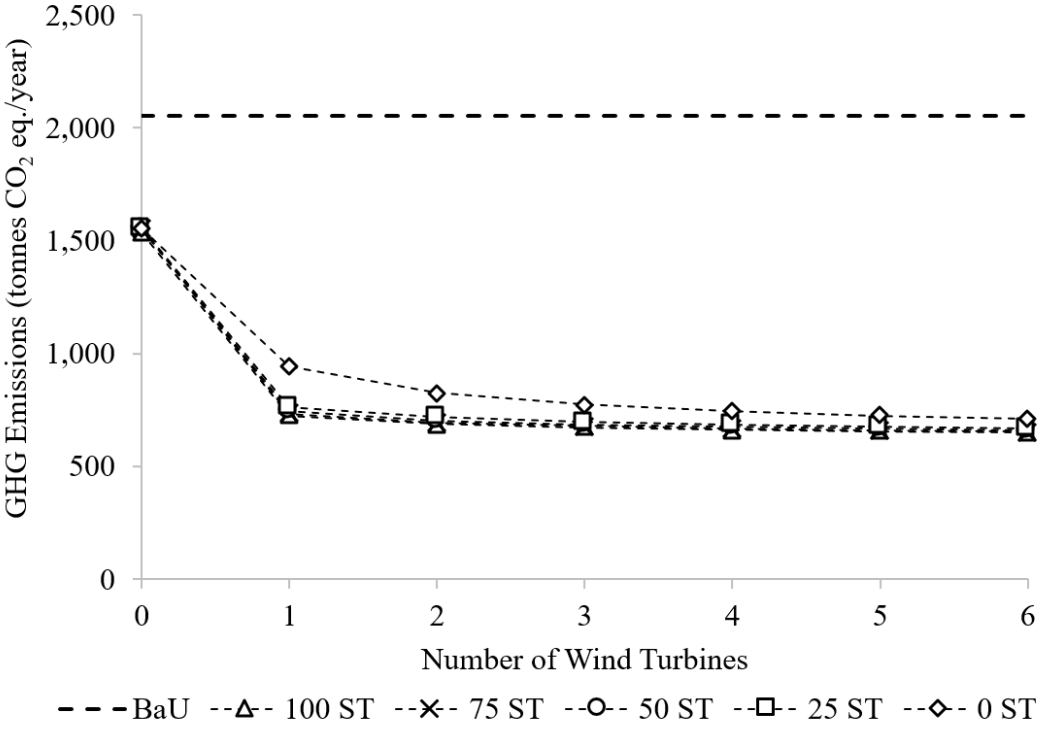

Figure 42: S2C2 GHG emissions analysis

4.4 Sensitivity analysis

The effects of altering the O&M cost, the discount rate, the cost of propane, and the capital cost of the grid-connected combinations are examined to determine which of these variables has the greatest effect on the economic performance of the model. Changes in the yearly household energy cost charged by the municipality produced by alterations of the initial values of the variables listed are used to determine system sensitivity to these variables. The economic results using the TTP pricing policy are investigated for both grid-connected model combinations. Only the 100 ST, 6 WF combinations of each configuration are examined. These combinations are chosen since they are the most economically lucrative configurations when considered under a net metering policy.

Figure 43 shows the sensitivity analysis results for the S1C1 combination. Increasing the O&M cost decreases the yearly household energy cost, and does so with a slightly larger impact than increasing the cost of propane. Adjusting the capital cost has the single largest impact on system economics. Increasing or decreasing the capital cost by 20% correspondingly increases or decreases the yearly household energy cost by just under $4k. The system is also found to be highly sensitive to changes in the discount rate. Increasing the discount rate largely increases yearly household energy cost, and vice-versa. A discount rate reduction of 20% (from 6% to 4.8%) results in a $2100 decrease in yearly household energy cost. An additional reduction of 20% (down to 3.6%) results in a $2000 decrease in yearly household energy cost.

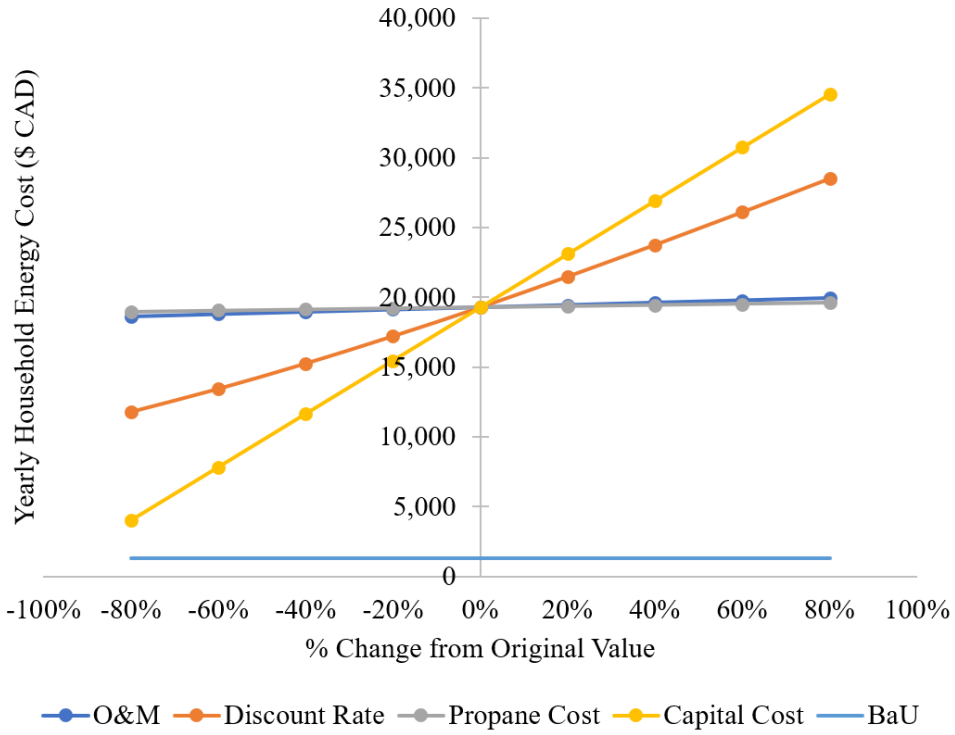

Figure 43: S1C1 sensitivity analysis for 100 ST and 6 WF with net metering, analyzing O&M, discount rate, propane cost, and capital cost

Figure 44 shows the sensitivity analysis results for S1C2 combination. The same trends that are true in Figure 43 are true in Figure 44. The key difference is that while the trends remain the same, the S1C2 combination is a little less than half as sensitive to all variables than the S1C1 combination. A 20% increase or decrease in capital cost results in a corresponding $1.7 k increase or decrease in yearly household energy cost, roughly half that of the S1C1 combination. The same is true for the S1C2 discount rate sensitivity analysis results; a discount rate reduction of 20% (from 6% to 4.8%) results in a $1000 decrease in yearly household energy cost. An additional reduction of 20% (down to 3.6%) results in another $1000 decrease in yearly household energy cost. The S1C2 combination is less sensitive to changes in propane costs because the combinations employing configuration 2 use less fossil fuels than those employing combination 1.

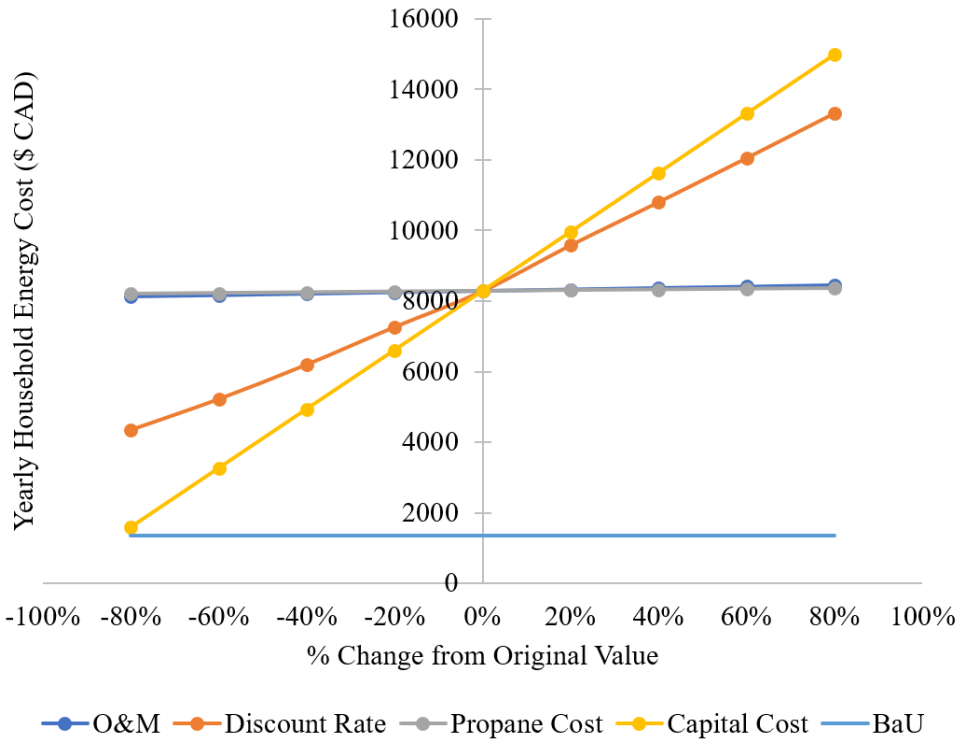

Figure 44: S1C2 sensitivity analysis for 100 ST and 6 WF with net metering, analyzing O&M, discount rate, propane cost, and capital cost

The effects of altering the O&M, the discount rate, the cost of propane, the cost of diesel, and the capital cost of the off-grid combinations are examined to determine which of these variables has the greatest effect on the economic performance of the model. Only the 100 ST, 6 WF combinations of each configuration are examined.

The S2C1 combination sensitivity analysis results in Figure 45 are very similar to the S1C1 combination results in Figure 43. The S2C1 combination is less sensitive to adjustments in propane costs than the S1C1 combination, as the combination uses much less of it than the S1C1 combination. However, the S2C1 combination is very sensitive to the cost of diesel. A 20% reduction in diesel cost results in a $500 decrease in yearly household energy cost. As in both Figure 43 and Figure 44, the system is most sensitive to changes in capital cost. A 20% reduction in capital cost results in a ~$3.5 k decrease in yearly household energy costs. A 20% reduction in

discount rate results in a $1900 decrease in yearly household energy costs. A further reduction by 20% drops costs by another $1600. The S2C1 combination is only slightly less sensitive to all variables analyzed than the S1C1 combination.

Only the reduction of the capital cost of at least 60% results in a better yearly household energy costs than the BaU scenario.

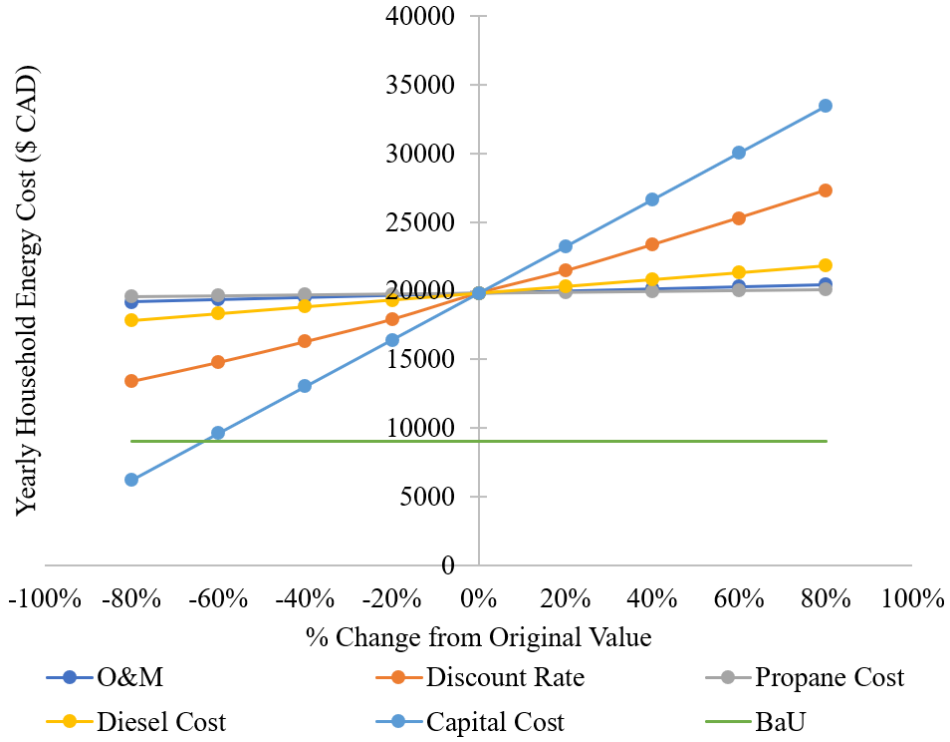

Figure 45: S2C1 sensitivity analysis for 100 ST and 6 WF, analyzing O&M, discount rate, propane cost, diesel cost, and capital cost

Figure 46 shows the S2C2 combination sensitivity analysis results. As with the grid-connected results, the S2C2 configuration is less sensitive overall to the fuel costs as it consumes less fossil fuel than the S2C1 combination. The combinations are most sensitive to changes in capital cost, diesel cost, and discount rate. A 20% reduction in capital cost decreases yearly household energy cost by $1300. A 20% reduction in diesel cost decreases yearly household energy costs by $500. A 20% reduction in discount rate reduces costs by $850, and a further reduction by

20% drops costs by another $700. As seen in the comparison between the S1C1 and S1C2 combinations, the S2C2 combination is consistently half as sensitive to all variables as the S1C1 combination.

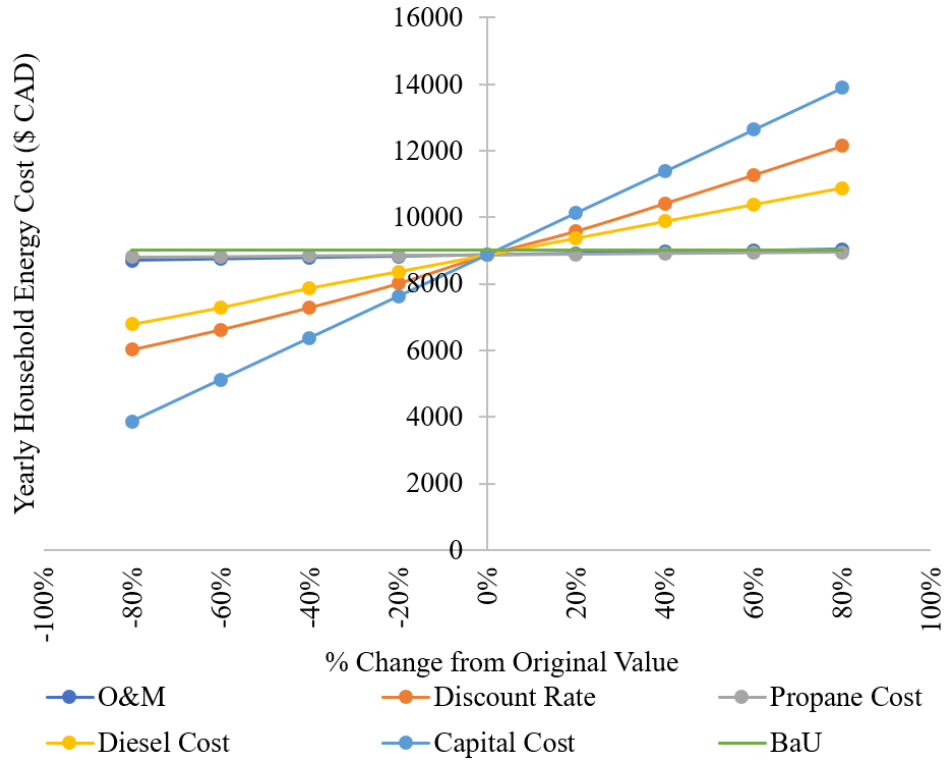

Figure 46: S2C2 sensitivity analysis for 100 ST and 6 WF, analyzing O&M, discount rate, propane cost, diesel cost, and capital cost

The results of the sensitivity analysis indicate that all variables affect the yearly household energy cost linearly except for discount rate, which increases costs at a higher rate corresponding to higher discount rates. Changes in fuel costs and O&M costs have little effect on the yearly household energy costs when compared to changes in capital costs and the discount rate, with the exception of S2C2, which is also highly sensitive to diesel costs. To maximize system profitability,

the lowest possible system capital cost should be obtained through acquiring optimized finance rates or gaining access to preferential loads (for example).

The S2C2 combimation analyzed already provides a better yearly household energy cost than the BaU scenario. The adjustment of several of these factors further reduce the costs, however, making the system that much more economically appealing.

Of note is the higher incidence of vandalism sometimes seen in Northern communities [108]. As such, O&M costs may in fact be higher than the 0.5% assumed in this study. In all cases examined, O&M was found to be the second least sensitive variable, which means economics will be minimally affected even with the assumption of a higher O&M cost to account for vandalism.

Chapter 5: Discussion

5.1 Key findings and contributions

Finding 1: The proposed energy system does not currently offer an economically preferable option to the BaU scenario for MoCreebec, the case study for this thesis; however, the combinations offer social benefits that should be considered

All the S1C1 and S1C2 combinations with net metering pricing schemes result in higher yearly household energy costs than that of the grid-connected business-as-usual (BaU) scenario (see Figure 33 and Figure 34). This study assumes that the community pays out-of-pocket for the entire cost of the system- capital costs, recurring costs, and fuel costs- at a discount rate of 6%. With no financial aid for these costs, the system proves to be much more expensive than the BaU case, the costs for which consist only of the price of electricity usage.

Although the grid-connected economic results using the net metering electricity pricing scheme do not compare favourably to the BaU case in the MoCreebec community, the proposed energy system also generates energy completely on-site. There is no need to import fuels or transmit energy across long distances, which increases system reliability and community autonomy. The results may still hold value owing to this, despite their comparatively poor financial performance, as MoCreebec has expressed interest in increasing self-reliance for energy generation and distribution.

The Ontario long term energy plan forecasts that residential energy prices will increase by 53% between 2019 and 2029 [109]. Conversely, the costs calculated by the model will remain largely static. In fact, the capital costs of the model are likely to fall as the years pass, since renewable energy installations are expected to become cheaper in the coming decades [110]. As time passes, the model economics for both scenarios 1 & 2 will continue to look more attractive

when compared to the BaU scenario.

Finding 2: Several combinations of the proposed grid-connected energy system provide lower household energy costs relative to the BaU scenario when a two-way tiered (TTP) pricing policy is in place

Using a TTP pricing policy allows for an income stream from the excess electricity generated by the wind farm (WF). This means that a larger WF results in progressively lower household energy costs, dropping costs below the grid-connected BaU scenario in several combinations. In S1C1, the combinations with no solar thermal (ST) array and WF of 4 or more provides yearly household energy costs lower than the BaU scenario (see Figure 35). In S1C2, all combinations with a WF of 6 provide yearly household energy costs lower than the BaU scenario (see Figure 36). A few combinations yield not only free thermal energy to the community residents, but also generate a profit by the end of the system lifetime. The combination results that generate a profit are listed in Table 8.

Currently, the only pricing scheme available to Ontarians is the net metering approach, as the TTP program no longer exists in the province. Permitting remote communities to sell back extra electricity reduces the burden of generation on the provincial grid. The implementation of a TTP program improves the financials of this study's system to the point where several combinations of both grid-connected configurations offer lower yearly household energy costs than the BaU scenario, several of which generate profit by the end of the project lifetime. These results may be used as motivation for a community to negotiate with utility for a TTP pricing scheme.

Finding 3: The proposed grid-connected energy system lowers GHG emissions relative to the BaU scenario

All configuration 1 combinations are modeling the Ontario electricity grid (OEG) as the electricity grid. The OEG has very few greenhouse gas (GHG) emissions, as it derives less than 10% of its energy supply from GHG emitting sources [111]. All S1C1 combinations result in more GHG emissions than the grid-connected BaU scenario, excepting the following six combinations: the 100 ST combinations with a WF of both 5 and 6, the 75 ST combinations a WF of both 5 and 6, and the 50 ST combination with a WF of 6. In the S1C2 combinations, the results compare more favourably against the BaU GHG emissions. Of the 0 ST models, only the combination with a WF of 6 yields fewer GHG emissions than the BaU scenario. Combinations of every ST array size without a WF produce more GHG emissions than the BaU scenario, as well as the 25 ST and 75 ST combinations with a WF of 1. All other combinations result in fewer GHG emissions than the BaU scenario.

The proposed grid-connected energy system would fare much better in terms of GHG emissions analysis when compared to an electricity grid that is more reliant on fossil fuels (for instance, in the province of Ontario, the grid produces less than 10% of its energy through fossil fuels [111], whereas in the province of Alberta, the grid produces 89% of its energy through fossil fuels [112]).

Finding 4: The proposed off-grid energy system significantly reduces both yearly household energy costs and GHG emissions relative to the BaU scenario

In the S2C1 combinations, the proposed energy system with no ST array and a WF of at least 1 yields lower yearly household energy costs than the off-grid BaU scenario (see Figure 37). Every S2C2 combination with a WF of at least 1 results in a lower yearly household energy cost than that of the BaU scenario (see Figure 38).

The S2C1 and S2C2 model combinations are compared to a BaU scenario in which a remote

energy grid provides electricity from diesel generator plants and thermal energy from propane heaters. This increases the yearly GHG emissions from 114 tonnes of CO_2 eq. in the grid-connected BaU case to 2053 tonnes of CO_2 eq. in the off-grid BaU case. Compared to this off-grid BaU scenario, the S2C1 and S2C2 scenarios provide lower GHG emissions in every model combination.

The proposed energy system offers an attractive alternative energy supply for remote off-grid communities, both economically and environmentally.

Finding 5: The heat pump-assissted solar thermal (HPA-ST) system consistently provides a cheaper household energy costs and fewer GHG emissions than the direct ST system, regardless of scenario

The HPA-ST configurations provide cheaper household energy costs than the direct ST configurations of the same scenario (see Section 4.2). The HPA-ST configurations also generate fewer GHG emissions than the direct ST configurations of the same scenario (see Section 4.3). Additionally, the HPA-ST configurations are less sensitive to fossil fuel prices than the direct ST configurations.

Finding 6: The increase in the WF from size 0 to 1 in the proposed energy system has the largest marginal benefit in terms of fossil fuel displacement

Going from no WF to a WF of 1 in any of the proposed energy system designs has the largest marginal decrease on the fossil fuel heater (FFH) energy usage. This marginal benefit tapers off to nearly nothing with each subsequent increase in WF size. Increasing the size of the WF beyond a single wind turbine has more of an effect on system economics than it does on the system fossil fuel usage.

Finding 7: The implementation of a heat pump-assisted solar thermal system to the proposed energy system significantly reduces the share of energy provided by the FFH

In both the grid-connected and off-grid combinations with a WF of 1, the addition of a heat pump (HP) reduces the FFH energy share from approximately 35% to 12%. While the addition of the HPA-ST also reduces the yearly energy load fraction provided by the direct ST, this disbenefit is not outweighed by the reduction in fossil fuel usage.

Finding 8: The system is extremely sensitive to changes in the discount rate and the capital cost

For all scenarios and configurations, the system economics were highly affected by the alteration of the discount rate and the system capital cost. Should this model be pursued, the community implementing it should attempt to secure as low a finance rate as possible, as well as find funding sources to reduce the burden of the capital costs. This will greatly increase the overall system value (see Section 4.4).

Chapter 6: Conclusions, Recommendations, and Future Work

6.1 Conclusions and Recommendations

When compared to the current BaU scenario in Moose Factory, the proposed energy system model combinations with a net metering excess electricity pricing scheme, no preferential loan access, and a finance rate of 6%, result in more expensive household energy costs. However, the proposed energy system model combinations yield many scenarios that provide fewer greenhouse gas (GHG) emissions than the business-as-usual (BaU) scenario. The social benefits of the system are also significant. The system provides energy reliability and community autonomy. Fossil fuels need not be imported to the island, and Ontario energy grid (OEG) outages will no longer interrupt electrical energy supply to the community. With training, the system could be entirely managed by members of the MoCreebec community.

The S2C1 combinations with no solar thermal (ST) array and a wind farm (WF) of at least 1 can provide energy to off-grid communities at a lower cost than the off-grid BaU case, with a GHG emissions reduction of 50% or more in combinations with a WF of at least 1.

All S2C2 model combinations with a WF of at least 1 reduce yearly household energy costs. All S2C2 model combinations with a WF of at least 1 reduce GHG emissions by 60% or more. These models offer an attractive template with which to design reliable and autonomous remote energy systems.

The present net metering policy does not offer any system combinations that are cheaper than current energy costs for MoCreebec residences. However, the implementation of the hypothetical two-way tiered (TTP) pricing policy considered in this study results in several model combinations that provide for the energy needs of the 140-home residential energy load at a lower cost than the grid-connected BaU case. Negotiating or advocating for a TTP pricing policy or an

independent power purchasing agreement should be pursued if the project moves forward in MoCreebec.

The grid-connected model combination results considered under a net-metering policy do not yield economically attractive alternatives to the BaU scenario. However, they offer a significant increase in community energy independence. The community should discuss whether there is merit to paying higher energy costs, if that increase in price is accompanied by an increase in community energy autonomy.

It should be noted that for the purposes of this case study, the MoCreebec community is assumed to fund the full cost of the endeavour. Moving forward, it would benefit the community to investigate potential sources of financial aid in order to reduce the project capital costs. Grants and other income sources should be pursued.

6.2 Future work

One area that should be further explored is the effect of different electrical grid carbon intensities on the carbon analysis of the combination outputs. The carbon intensity of the OEG is very low compared to other electricity grids, as it is largely powered by nuclear power and renewable sources. It would be useful to see how the combinations fared against a fossil fuel heavy grid, such as the Albertan grid. In addition, a carbon tax could be added to the economic analysis of these more heavily polluting grids to see how drastically it alters the yearly household energy costs of the more carbon intensive combinations.

The combinations built in TRNSYS are highly idealized. Boilers function at 100% efficiencies, pumps have no losses and require no power to run, etc. (see Section 3.2.1 for all assumptions made in model). A more in-depth energy system model, including thermal losses, pumping energies (both the district heating (DH) variable speed pump and the smaller system

pumps), and system outages would give a more accurate representation of the system's functionality.

An analysis could be conducted to introduce electrical storage to the system, so that when the wind farm (WF) is generating power but the thermal energy storage (TES) has no room to store it, the energy does not go to waste. This would be particularly useful in the off-grid system, where there exists no grid to purchase and sell electricity as required. Waste heat from diesel generators could be harnessed in off-grid scenarios to further improve system efficiency.

Additional sources of renewable electricity and thermal energy generation could be investigated. Biomass generation is an example of a potential source.

The wind energy conversion system (WECS) system in TRNSYS assumes operation at the Betz limit, which is an impossible limit to reach. The implementation of a wind turbine component in the TRNSYS model that utilizes a power curve would yield more realistic combination results. Additionally, the simplified heat pump (HP) model used in this research could be replaced with one of the more sophisticated TRNSYS HP types.

Propane and diesel fuel prices from Yellowknife, NWT are used to estimate fuel costs in this study. This was the closest geographical approximation to Moose Factory for which reliable costing data was available. Costing data from Moose Factory or Moosonee could be obtained directly in the future to ensure a more accurate economic analysis.

The energy profile investigated in this study is purely residential. The addition of large, singular energy loads, such as a hospital, community centre, or any commercial centres, will undoubtedly alter the economic and emissions results. The study should be expanded in the future to more closely examine these altered results.

References

[1] Ontario Heritage Foundation, *Moose Factory: An Exploration of Frontier History*. Toronto, ON: Queen's Printer for Ontario, 2002.

[2] MacLeod Farley & Associates, "MoCreebec Eeyoud Community Energy Plan," Owen Sound, ON, 2015.

[3] Google, "Moose Factory, ON," *Google Maps*, 2019. .

[4] IESO, "Ontario's Electrical System," *Independent Electricity Systems Operator*, 2019. [Online]. Available: http://www.ieso.ca/localContent/ontarioenergymap/index.html. [Accessed: 23-Jun-2019].

[5] Hydro One Networks Inc (Transmission & Distribution), "Local Planning Report," 2016.

[6] Natural Resources Canada and Aboriginal Affairs and Northern Development Canada, "Remote Communities in Canada," Ottawa, ON, 2011.

[7] Statistics Canada, "Household energy consumption, Canada and provinces." Statistics Canada, Environment, Energy and Transportation Statistics Sector, 2019.

[8] Natural Resources Canada, "Water Heaters," 2019. [Online]. Available: https://www.nrcan.gc.ca/energy/products/categories/water-heaters/13735. [Accessed: 23-Jun-2019].

[9] Statistics Canada, "Households and the environment: Energy use," *11-526-S*, no. 11, pp. 1–41, 2007.

[10] IESO, "ECB Overview," 2019. [Online]. Available: http://www.ieso.ca/Get-Involved/Funding-Programs/Education-and-Capacity-Building-Program/Overview. [Accessed: 14-Sep-2019].

[11] Natural Resources Canada, "Reducing diesel energy in rural and remote communities," *Government of Canada*, 2019. [Online]. Available: https://www.nrcan.gc.ca/climate-change/green-infrastructure-programs/reducing-diesel-energy-rural-and-remote-communities/20542. [Accessed: 23-Jun-2019].

[12] B. Gilmour, E. Oldfield, H. Platis, and E. Wicks, "Toward a Positive Energy Future in and Remote Communities: Summary Report," 2018.

[13] S. Werner, "International review of district heating and cooling," *Energy*, vol. 137, pp. 617–631, 2017.

[14] S. Hsieh, A. Omu, and K. Orehounig, "Comparison of solar thermal systems with storage: From building to neighbourhood scale," *Energy Build.*, vol. 152, pp. 359–372, 2017.

[15] E. Ampatzi and I. Knight, "Modelling the effect of realistic domestic energy demand

profiles and internal gains on the predicted performance of solar thermal systems," *Energy Build.*, vol. 55, pp. 285–298, 2012.

[16] A. Hugo, R. Zmeureanu, and H. Rivard, "Solar combisystem with seasonal thermal storage," *J. Build. Perform. Simul.*, vol. 3, no. 4, pp. 255–268, 2010.

[17] L. M. Ayompe, A. Duffy, S. J. McCormack, and M. Conlon, "Validated TRNSYS model for forced circulation solar water heating systems with flat plate and heat pipe evacuated tube collectors," *Appl. Therm. Eng.*, vol. 31, no. 8–9, pp. 1536–1542, 2011.

[18] C. J. Banister, W. R. Wagar, and M. R. Collins, "Validation of a single tank, multi-mode solar-assisted heat pump TRNSYS model," *Energy Procedia*, vol. 48, pp. 499–504, 2014.

[19] X. Wang, M. Zheng, W. Zhang, S. Zhang, and T. Yang, "Experimental study of a solar-assisted ground-coupled heat pump system with solar seasonal thermal storage in severe cold areas," *Energy Build.*, vol. 42, no. 11, pp. 2104–2110, 2010.

[20] A. Rosato, G. Ciampi, A. Ciervo, and S. Sibilio, "Performance of Different Back-up Technologies for Micro-Scale Solar Hybrid District Heating Systems with Long-term Thermal Energy Storage," *Energy Procedia*, vol. 149, pp. 565–574, 2018.

[21] D. Wang, K. Orehounig, and J. Carmeliet, "A Study of District Heating Systems with Solar Thermal Based Prosumers," *Energy Procedia*, vol. 149, pp. 132–140, 2018.

[22] Z. Tian *et al.*, "Large-scale solar district heating plants in Danish smart thermal grid: Developments and recent trends," *Energy Convers. Manag.*, vol. 189, no. October 2018, pp. 67–80, 2019.

[23] L. Bird *et al.*, "Wind and solar energy curtailment: A review of international experience," *Renew. Sustain. Energy Rev.*, vol. 65, pp. 577–586, 2016.

[24] W. Dong, C. Dong, Y. Qi, and C. Huang, "Fixing Wind Curtailment with Electric Power System Reform in China Principal Investigator: Ye Qi a Field Work Lead: Wenjuan Dong a."

[25] H. Li, P. E. Campana, Y. Tan, and J. Yan, "Feasibility study about using a stand-alone wind power driven heat pump for space heating," *Appl. Energy*, vol. 228, no. January, pp. 1486–1498, 2018.

[26] D. Böttger, M. Götz, N. Lehr, H. Kondziella, and T. Bruckner, "Potential of the Power-to-Heat technology in district heating grids in Germany," *Energy Procedia*, vol. 46, pp. 246–253, 2014.

[27] K. Appunn and B. Wehrmann, "Germany 2021: when fixed feed-in tariffs end, how will renewable fare?," *Energy Post*, 2019. [Online]. Available: https://energypost.eu/germany-2021-when-fixed-feed-in-tariffs-end-how-will-renewables-fare/. [Accessed: 24-Nov-

2019].

[28] G. Schweiger, J. Rantzer, K. Ericsson, and P. Lauenburg, “The potential of power-to-heat in Swedish district heating systems,” *Energy*, vol. 137, pp. 661–669, 2017.

[29] H. Ü. Yilmaz, D. Keles, A. Chiodi, R. Hartel, and M. Mikulić, “Analysis of the power-to-heat potential in the European energy system,” *Energy Strateg. Rev.*, vol. 20, pp. 6–19, 2018.

[30] X. Chen *et al.*, “Increasing the Flexibility of Combined Heat and Power for Wind Power Integration in China: Modeling and Implications,” *IEEE Trans. Power Syst.*, vol. 30, no. 4, pp. 1848–1857, 2015.

[31] P. Meibom, J. Kiviluoma, R. Barth, H. Brand, C. Weber, and H. V. Larsen, “Value of electric heat boilers and heat pumps for wind power integration,” *Wind Energy*, vol. 10, no. 4, pp. 321–337, 2007.

[32] M. B. Blarke, “Towards an intermittency-friendly energy system: Comparing electric boilers and heat pumps in distributed cogeneration,” *Appl. Energy*, vol. 91, no. 1, pp. 349–365, 2012.

[33] P. Pinel, C. A. Cruickshank, I. Beausoleil-Morrison, and A. Wills, “A review of available methods for seasonal storage of solar thermal energy in residential applications,” *Renew. Sustain. Energy Rev.*, vol. 15, no. 7, pp. 3341–3359, 2011.

[34] S. Colclough and T. McGrath, “Net energy analysis of a solar combi system with Seasonal Thermal Energy Store,” *Appl. Energy*, vol. 147, no. 2015, pp. 611–616, 2015.

[35] O. Ozgener and A. Hepbasli, “A review on the energy and exergy analysis of solar assisted heat pump systems,” *Renew. Sustain. Energy Rev.*, vol. 11, no. 3, pp. 482–496, 2007.

[36] C. Winterscheid, “Integration of solar thermal systems in existing district heating systems,” *Euroheat Power (English Ed.*, vol. 14, no. 4, pp. 16–20, 2017.

[37] A. Bloess, W. Schill, and A. Zerrahn, “Power-to-heat for renewable energy integration : A review of technologies , modeling approaches , and fl exibility potentials,” *Appl. Energy*, vol. 212, no. August 2017, pp. 1611–1626, 2018.

[38] M. R. Patel, *Wind and solar power systems: Design, Analysis, and Operation*, 2nd ed. Boca Raton, FL: Taylor & Francis, 2006.

[39] S. A. Kalogirou, *Solar Energy Engineering: Processes and Systems*, 2nd ed. San Diego, CA: Elsevier Inc., 2014.

[40] BINE Information Service, “Energy research for application,” *BINE Information Service*, 2013. [Online]. Available: http://www.bine.info/en/publications/themeninfos/publikation/elektrisch-angetriebene-

waermepumpen/waermepumpen-plus-solar/. [Accessed: 05-Oct-2019].

[41] Viessmann, “Vitosol 200-FM Technical Data Manual.” Viessmann, p. 11, 2016.

[42] I. S. C. Sebarchievici, “Solar Water and Space-Heating Systems,” in *Solar Heating and Cooling Systems: Fundamentals, Experiments and Applications*, 1st ed., Academic Press, 2017, pp. 139–206.

[43] ASHRAE, “District heating and cooling,” in *2008 ASHRAE Handbook*, vol. 0, no. 0, ASHRAE, 2008, pp. 1–35.

[44] K. C. Kavvadias, A. P. Tosios, and Z. B. Maroulis, “Design of a combined heating, cooling and power system: Sizing, operation strategy selection and parametric analysis,” *Energy Convers. Manag.*, vol. 51, no. 4, pp. 833–845, 2010.

[45] A. Z. A. Saifullah, A. Karim, and R. Karim, “Wind Energy Potential in Bangladesh,” *Am. J. Eng. Res.*, no. 5, pp. 85–94, 2016.

[46] H. Bindner, *Power Control for Wind Turbines in Weak Grids : Concepts Development*, vol. 1118, no. March. 1999.

[47] D. Weisser and R. S. Garcia, “Instantaneous wind energy penetration in isolated electricity grids: Concepts and review,” *Renew. Energy*, vol. 30, no. 8, pp. 1299–1308, 2005.

[48] P. Lundsager and E. I. Baring-Gould, *Isolated Systems with Wind Power*. 2005.

[49] M. Arriaga, C. A. Canizares, and M. Kazerani, “Renewable energy alternatives for remote communities in Northern Ontario, Canada,” *IEEE Trans. Sustain. Energy*, vol. 4, no. 3, pp. 661–670, 2013.

[50] M. Vafaei, “Optimally-Sized Design of a Wind / Diesel / Fuel Cell Hybrid System for a Remote Community,” 2011.

[51] J. G. Kirkerud, T. F. Bolkesjø, and E. Trømborg, “Power-to-heat as a flexibility measure for integration of renewable energy,” *Energy*, vol. 128, pp. 776–784, 2017.

[52] J. Salpakari, J. Mikkola, and P. D. Lund, “Improved flexibility with large-scale variable renewable power in cities through optimal demand side management and power-to-heat conversion,” *Energy Convers. Manag.*, vol. 126, pp. 649–661, 2016.

[53] Climate.OneBuilding, “Repository of free climate data for building performance simulation: From the Creators of EPW,” 2019. [Online]. Available: http://climate.onebuilding.org/WMO_Region_4_North_and_Central_America/CAN_Canada/index.html#IDON_Ontario-. [Accessed: 17-Jan-2019].

[54] Xant, “XANT, Your Mid-Size Wind Partner.” Xant N.V., Brussels, Belgium, p. 2, 2018.

[55] A. Jolly, “RE: EB-2016-0004 OEB Natural Gas Heating Evidence Letter.” MoCreebec

Eeyoud, Moose Factory, ON, pp. 1–10, 2016.

[56] B. Lévesque, M. Lavoie, and J. Joly, “Residential water heater temperature: 49 or 60 degrees Celsius?,” vol. 15, no. 1, pp. 11–12, 2004.

[57] P. Applications and C. Protection, “Dynalene Ethylene Glycol Series,” *Eur. Chem. News*, vol. 9686, no. 610, 2008.

[58] Solar Energy Laboratory Univ. of Wisconsin-Madison, TRANSSOLAR Energietechnik GmbH, and Centre Scientifique et Technique du BatimentThermal Energy Systems Specialists, “TRNSYS 18, a TRaNsient SYstem Simulation program: Volume 1 Getting Started,” vol. 1. Thermal Energy System Specialists, LLC, pp. 1–9, 2018.

[59] Solar Energy Laboratory Univ. of Wisconsin-Madison, T. E. GmbH, and C. S. et T. du B. E. S. Specialists, “Trnsys 18, a TRaNsient SYstem Simulation program: Volume 4 Mathematical Reference,” vol. 4. Thermal Energy System Specialists, LLC, p. 705, 2018.

[60] Mechanical Engineering Department, “Papers and Validation,” *The University of Madison-Wisconsin*, 2006. [Online]. Available: https://sel.me.wisc.edu/trnsys/validation/index.html. [Accessed: 05-Jul-2019].

[61] J. W. Thornton *et al.*, “TESSLibs 17 - Component Libraries for the TRNSYS Simulation Environment Volume 10 Solar Library Mathematical Reference,” vol. 10. Thermal Energy System Specialists, LLC, pp. 1–166, 2012.

[62] J. A. Duffie and W. A. Beckman, *Solar Engineering of Thermal Processes*, 4th ed. Wiley, 2013.

[63] S. E. L. U. of Wisconsin-Madison, T. E. GmbH, and C. S. et T. du B. E. S. Specialists, “TRNSYS 18, a TRaNsient SYstem Simulation program: Volume 3 Component Library Overview,” vol. 3. Thermal Energy System Specialists, LLC, pp. 1–90.

[64] J. W. Thornton *et al.*, “TESSLibs 17 - Component Libraries for the TRNSYS Simulation Environment Volume 11 Storage Tank Library Mathematical Reference,” vol. 11. Thermal Energy System Specialists, LLC, pp. 1–93, 2014.

[65] J. W. Thornton *et al.*, “TESSLibs 17 - Component Libraries for the TRNSYS Simulation Environment Volume 6 HVAC Library Mathematical Reference,” *TESSLibs 17*, vol. 06. Thermal Energy System Specialists, LLC, pp. 1–262, 2012.

[66] Energy Star, “Energy Star Most Efficient 2019 - Boilers,” *US Department of Energy*, 2019. [Online]. Available: https://www.energystar.gov/products/most_efficient/boilers. [Accessed: 30-Oct-2019].

[67] S. E. L. U. of Wisconsin-Madison, T. E. GmbH, and C. S. et T. du B. E. S. Specialists, “TRNSYS 18, a TRaNsient SYstem Simulation program: Volume 3 Component Library

Overview," vol. 3. Thermal Energy System Specialists, LLC, pp. 1–90.

[68] J. Coady, "Quantifying the impacts of biomass driven combined heat and power based district heating grids in Canada's rural and remote communities," Ottawa, ON, 2019.

[69] A. D. Wills, "On the Modelling and Analysis of Converting Existing Canadian Residential Communities to Net-Zero Energy," p. 447, 2018.

[70] T. Adefarati and R. Bansal, *Pathways to a Smarter Power System*. Academic Press, 2019.

[71] E. Gunner, "Estimation of residences in MoCreebec Eeyoud that use wood burning heating in addition to electric baseboard heating." Moose Factory, ON, 2018.

[72] J. Russell, "Community Energy Preferences and Residential Occupant Behaviour of the MoCreebec Eeyoud," Carleton Univeristy, 2019.

[73] B. Hendron, J. Burch, and G. Barker, "Tool for Generating Realistic Residential Hot Water Event Schedules Preprint," in *NREL/CP-550-47685*, 2010, no. August, pp. 1–8.

[74] US Army Corps of Engineers, "Central Solar Hot Water Systems Design Guide," 2011.

[75] M. Schnauss, "Large-scale solar thermal systems for buildings," *Imprint*. FIZ Karlsruhe GmbH, Eggenstein-Leopoldshafen, Germany, 2008.

[76] Buderus, "Solar Technology for DHW and Space Heating," *Anti-Corrosion Methods and Materials*, vol. 49, no. 6. Bosch Thermotechnology Corp., Londonderry, NH, 2014.

[77] J. Xu, R. Z. Wang, and Y. Li, "A review of available technologies for seasonal thermal energy storage," *Sol. Energy*, vol. 103, pp. 610–638, 2014.

[78] E. Bettanini, A. Gastaldello, and L. Schibuola, "Simplified models to simulate part load performances of air conditioning equipments," *Eighth Int. IBPSA Conf. Eindhoven, Netherlands August 11-14, 2003*, pp. 107–114, 2003.

[79] Trane, "Product Catalog - Water Source Heat Pump Axiom Water-to-Water — EXW 5to20Tons–60Hz," no. August, 2017.

[80] M. J. Moran, H. N. Shapiro, D. D. Boettner, and M. B. Bailey, *Fundamentals of Engineering Thermodynamics*, 9th ed. Wiley, 2018.

[81] E. Gunner, "Estimation of MoCreebec resident DHW use." Moose Factory, ON, 2018.

[82] J. Duquette, P. Wild, and A. Rowe, "The potential benefits of widespread combined heat and power based district energy networks in the province of Ontario," *Energy*, vol. 67, pp. 41–51, 2014.

[83] E. Gunner, "Estimation of space heating use among MoCreebec residents." Moose

Factory, ON, 2018.

[84] K. Çomakli, B. Yüksel, and Ö. Çomakli, “Evaluation of energy and exergy losses in district heating network,” *Appl. Therm. Eng.*, vol. 24, no. 7, pp. 1009–1017, 2004.

[85] M. Ray, A. Rogers, and J. McGowan, “Analysis of wind shear models and trends in different terrains,” *Proc. AWEA Wind. Conf.*, pp. 1–14, 2006.

[86] C. Stanciu and D. Stanciu, “Optimum tilt angle for flat plate collectors all over the World - A declination dependence formula and comparisons of three solar radiation models,” *Energy Convers. Manag.*, vol. 81, pp. 133–143, 2014.

[87] B. Zohuri and P. McDaniel, *Thermodynamics in nuclear power plant systems*, no. May 2018. Springer, 2015.

[88] D. A. N. Kelley and R. Energy, “Low Grade Waste Heat Sources Impact on District Heating Systems – Design and Economics.”

[89] National Renewable Energy Laboratory, “Distributed Generation Renewable Energy Estimate of Costs,” *US Department of Energy*, 2016. [Online]. Available: https://www.nrel.gov/analysis/tech-lcoe-re-cost-est.html. [Accessed: 10-Jun-2019].

[90] J. Zhuang, Z. Liang, T. Lin, and F. De Guzman, “Theory and practice in the choice of social discount rate for cost-benefit analysis: A survey,” *ERD Work. Pap. Ser.*, no. 94, pp. 1–45, 2007.

[91] Dynalene Inc., “Ethylene Glycol Dynalene EG (5 Gal),” 2019. [Online]. Available: https://www.dynalene.com/product/ethylene-glycol-dynalene-eg-5-gal/. [Accessed: 07-Jun-2019].

[92] National Renewable Energy Laboratory, “Distributed Generation Renewable Energy Estimate of Costs,” *US Department of Energy*, 2016. .

[93] J. de Wit, “Heat Storages for CHP Optimisation,” *PowerGen Eur. 2007*, pp. 1–18, 2007.

[94] Tenaska TrailBlazer Partners LLC, “Cooling Alternatives Evaluation for a New Pulverized Coal Power Plant with Carbon Capture,” no. August, 2011.

[95] U.S. Department of Energy, “Residential Water Heaters: Final Criteria Analysis,” *Energy Star*, no. Abril, pp. 1–11, 2008.

[96] Natural Resources Canada, “Daily Average Retail Prices for Diesel in 2019,” *Government of Canada*, 2019. [Online]. Available: http://www2.nrcan.gc.ca/eneene/sources/pripri/prices_bycity_e.cfm?productID=5&locationID=7&frequency=D&priceYear=2019&Redisplay=. [Accessed: 30-Oct-2019].

[97] Argonne National Laboratory, “Appendix A: Lower and Higher Heating Values of Gas, Liquid and Solid Fuels.” US Department of Energy Office of Science, Argonne, IL, p.

2011, 2011.

[98] Natural Resources Canada, “Weekly Average Retail Prices for Auto Propane in 2019,” *Government of Canada*, 2019. [Online]. Available: http://www2.nrcan.gc.ca/eneene/sources/pripri/prices_bycity_e.cfm?productID=6&locationID=1&locationID=7&frequency=W&priceYear=2019&Redisplay=. [Accessed: 30-Oct-2019].

[99] Ontario Energy Board, “Electricity rates,” *OEB*, 2019. [Online]. Available: https://www.oeb.ca/rates-and-your-bill/electricity-rates. [Accessed: 10-Jun-2019].

[100] Ontario Energy Board, “Electricity rates,” *OEB*, 2019. .

[101] 1998 Ontario Energy Board Act, “ONTARIO REGULATION 541/05 NET METERING.” Ontario Energy Board, Ottawa, ON, p. 5, 2018.

[102] G. of Ontario, “Renewable energy development in Ontario: A guide for municipalities,” *Gov. Ontario*, pp. 1–63, 2018.

[103] J. Duquette, “Lecture 13 : Power Plant Economics.” pp. 1–10, 2018.

[104] J. Sotes, “A clearer view on Ontario’s emissions,” *Atmos. Fund*, no. June, 2019.

[105] British Columbia Ministry of Environment, “Best Practices Methodology for Quantifying Greenhouse Gas Emissions,” *Br. Columbia Minist. Environ.*, vol. 7, no. 1, pp. 1–44, 2014.

[106] Department for Business Energy & Industrial Strategy and Department for Environment Food & Rural Affairs, “UK Government GHG Conversion Factors for Company Reporting.” UK Government, 2018.

[107] Department for Business Energy & Industrial Strategy and Department for Environment Food & Rural Affairs, “UK Government GHG Conversion Factors for Company Reporting.” UK Government, 2018.

[108] Department of Justice, “Indigenous overrepresentation in the criminal justice system,” *Gov. Canada*, no. June, pp. 2014–2015, 2017.

[109] Government of Ontario, “Ontario’s Long Term Energy Plan 2017- Delivering Fairness and Choice,” Ottawa, ON, 2017.

[110] U.S. EIA, “Annual Energy Outlook 2019 with projections to 2050,” *Annu. Energy Outlook 2019 with Proj. to 2050*, vol. 44, no. 8, pp. 1–64, 2019.

[111] Canada Energy Regulator, “Canada’s Renewable Power Landscape 2017 - Energy Market Analysis,” *Government of Canada*, 2019. [Online]. Available: https://www.cer-rec.gc.ca/nrg/sttstc/lctrct/rprt/2017cndrnwblpwr/prvnc/on-eng.html. [Accessed: 20-Oct-

2019].

[112] Canada Energy Regulator, “Provincial and Territorial Energy Profiles - Alberta,” *Government of Canada*, 2019. [Online]. Available: https://www.cer-rec.gc.ca/nrg/ntgrtd/mrkt/nrgsstmprfls/ab-eng.html#:~:targetText=About 89%25 of electricity in,and 39%25 from natural gas. [Accessed: 26-Nov-2019].

Appendix A: Off-Grid TES Dispatch Strategy Diagrams

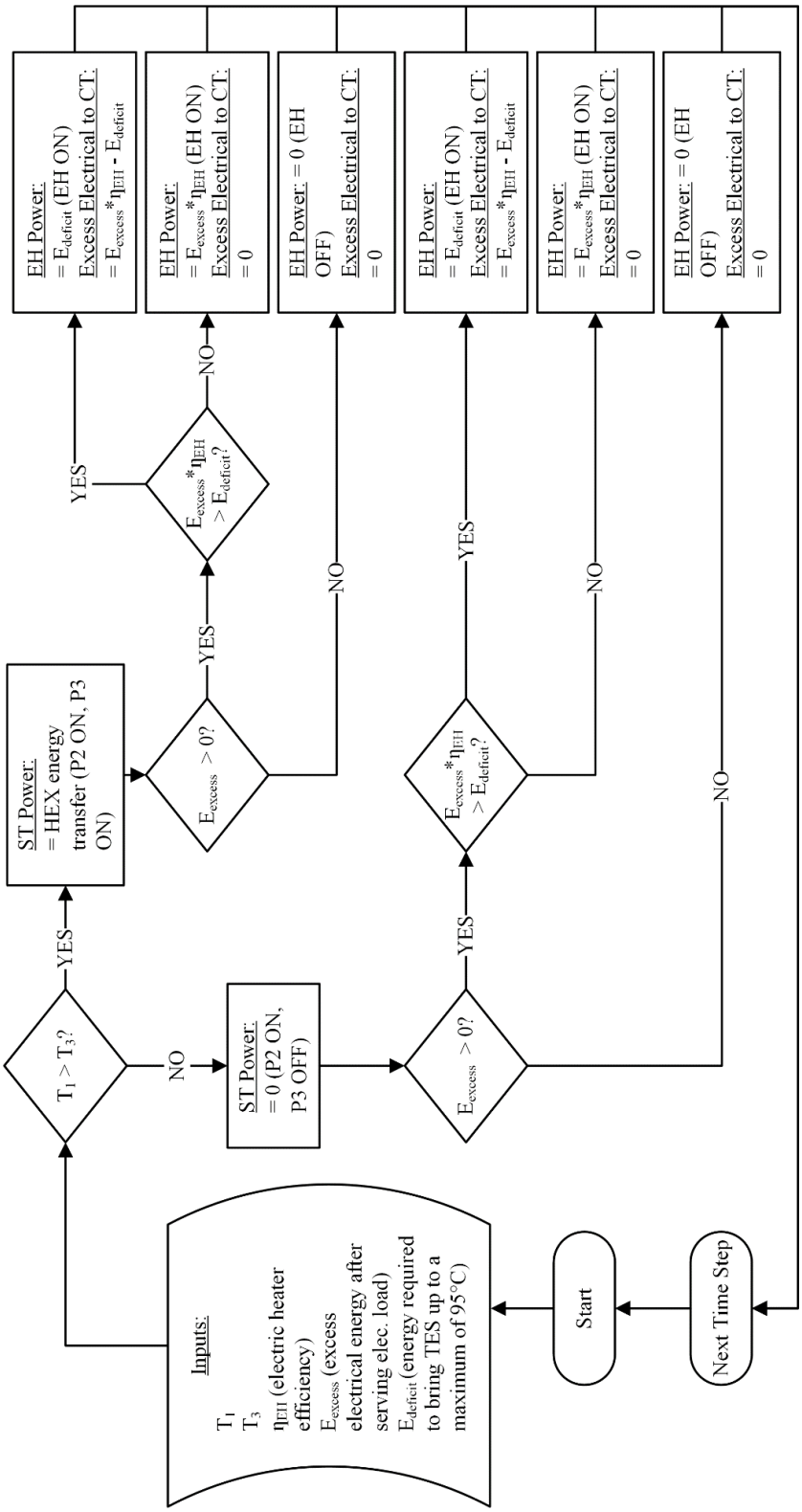

Figure 47: S2C1 TES dispatch strategy

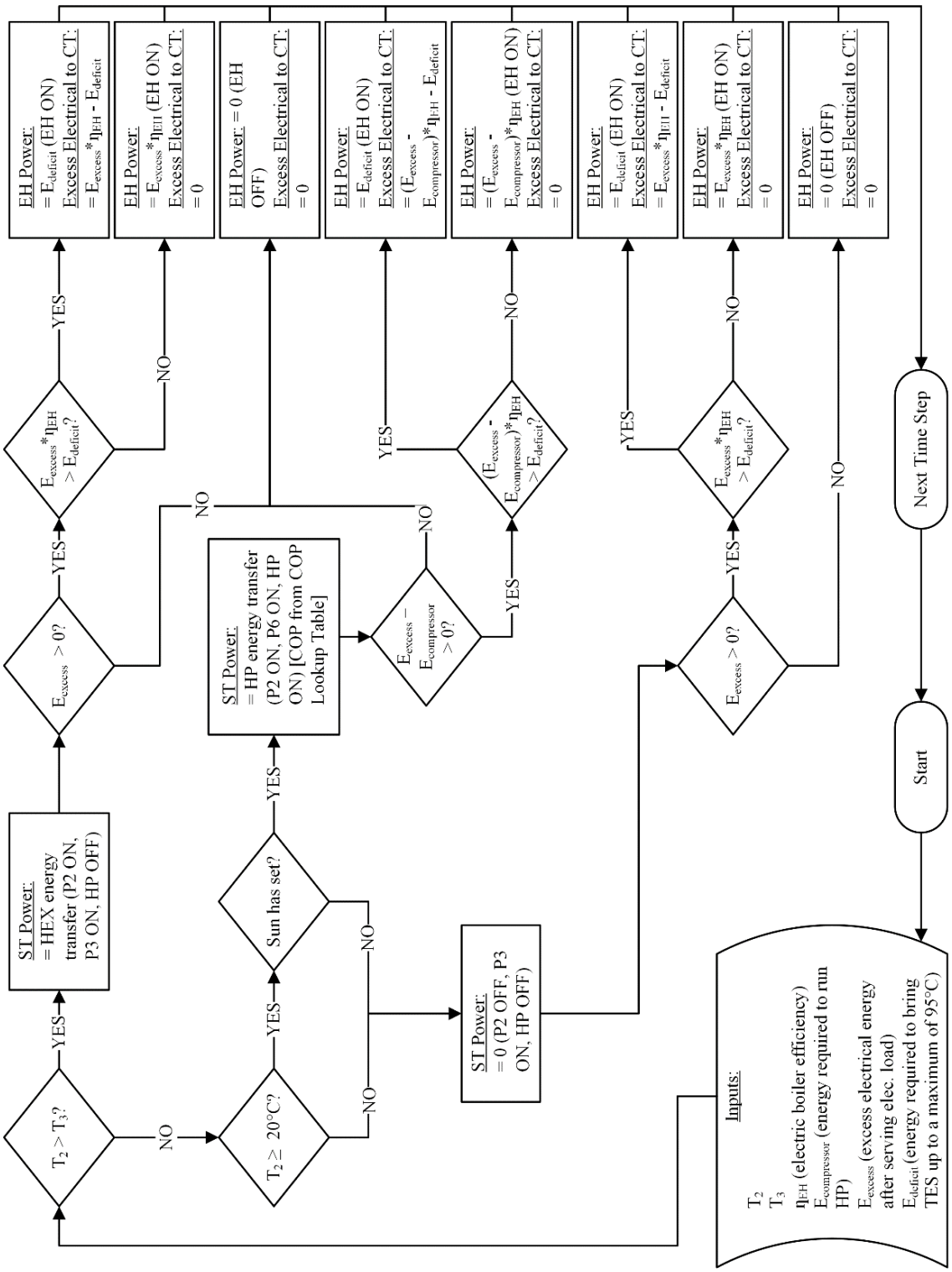

Figure 48: S2C2 TES dispatch strategy

Appendix B: S1C1 0, 25, 50, 75 ST array energy generation results

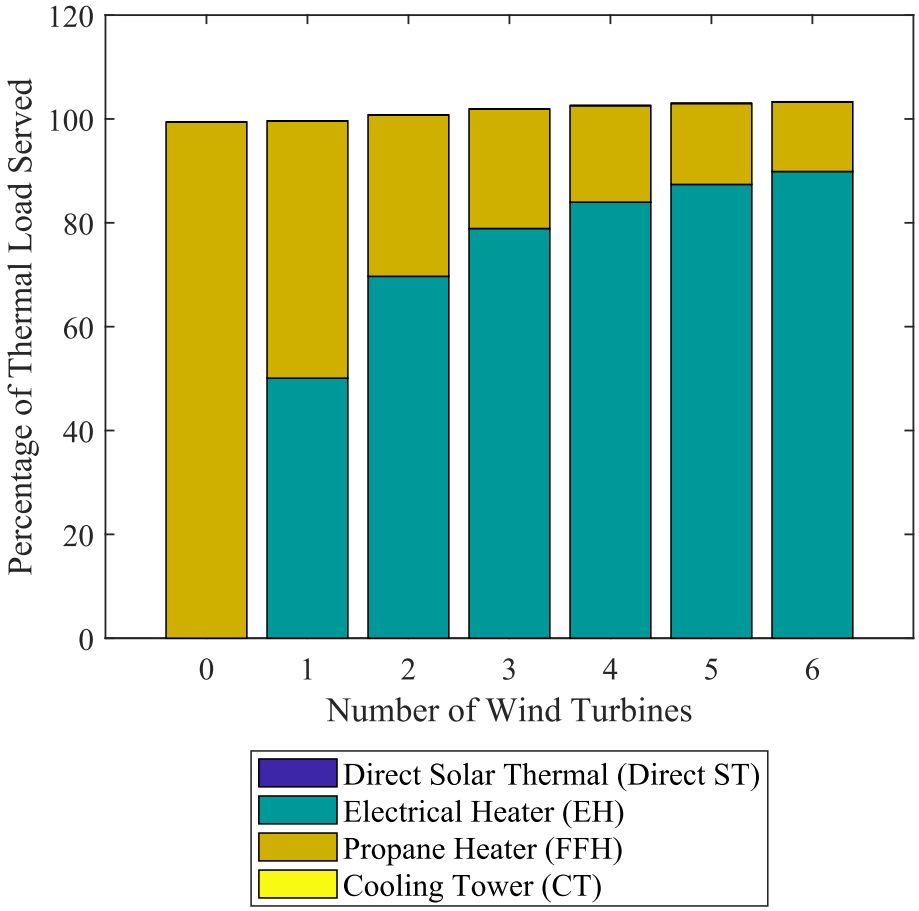

Figure 49: S1C1 0 ST thermal energy production results

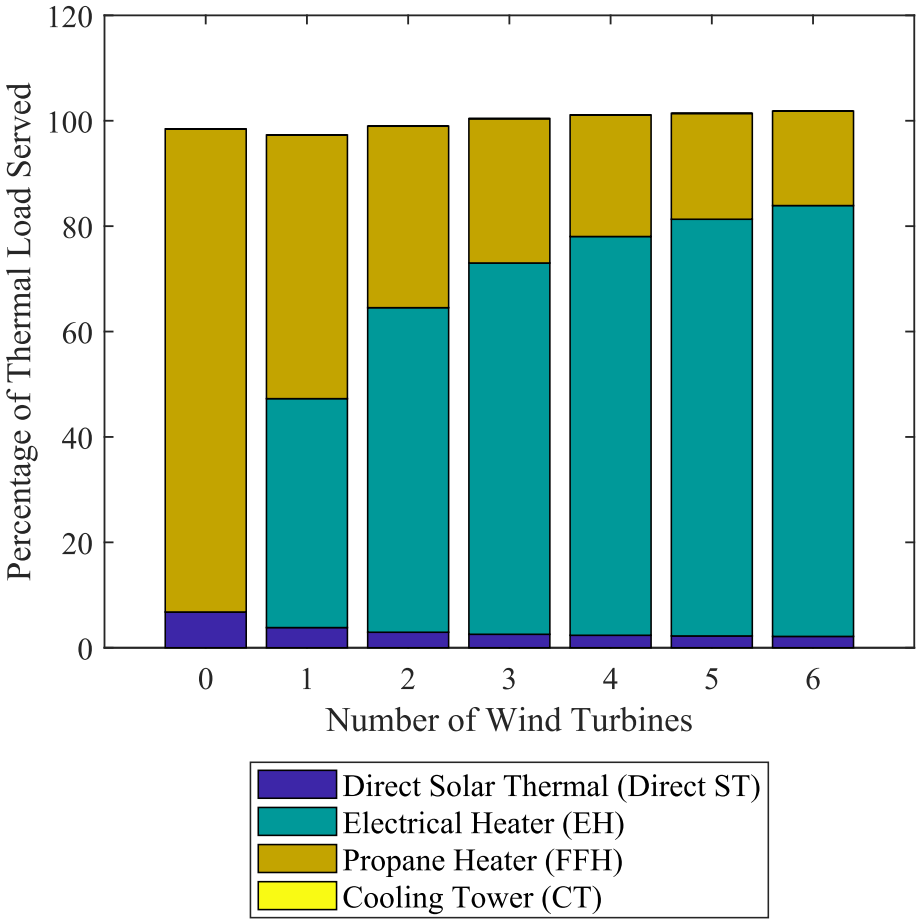

Figure 50: S1C1 25 ST thermal energy production results

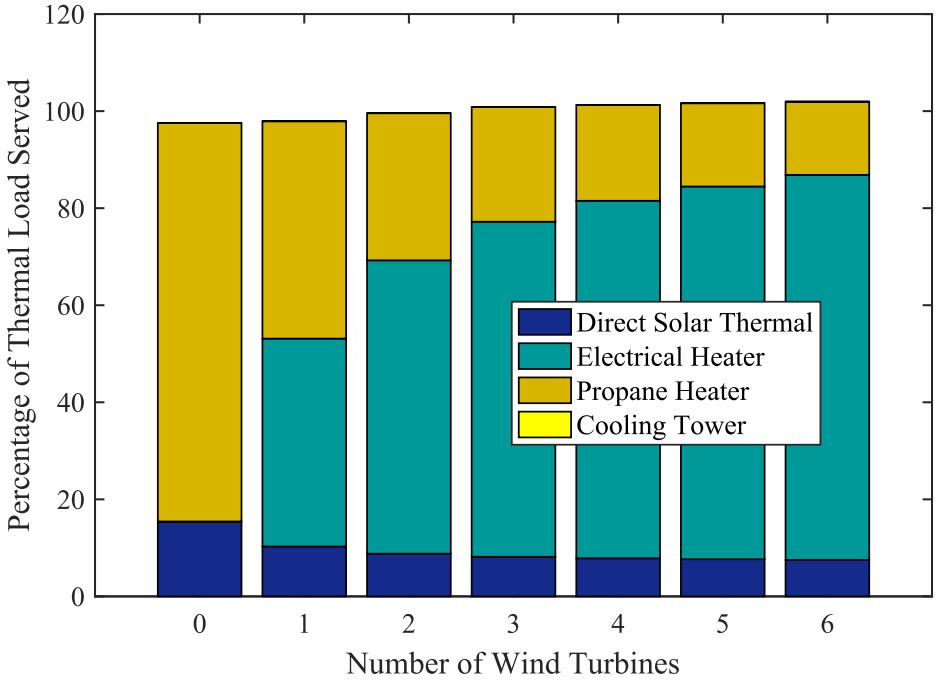

Figure 51: S1C1 50 ST thermal energy production results

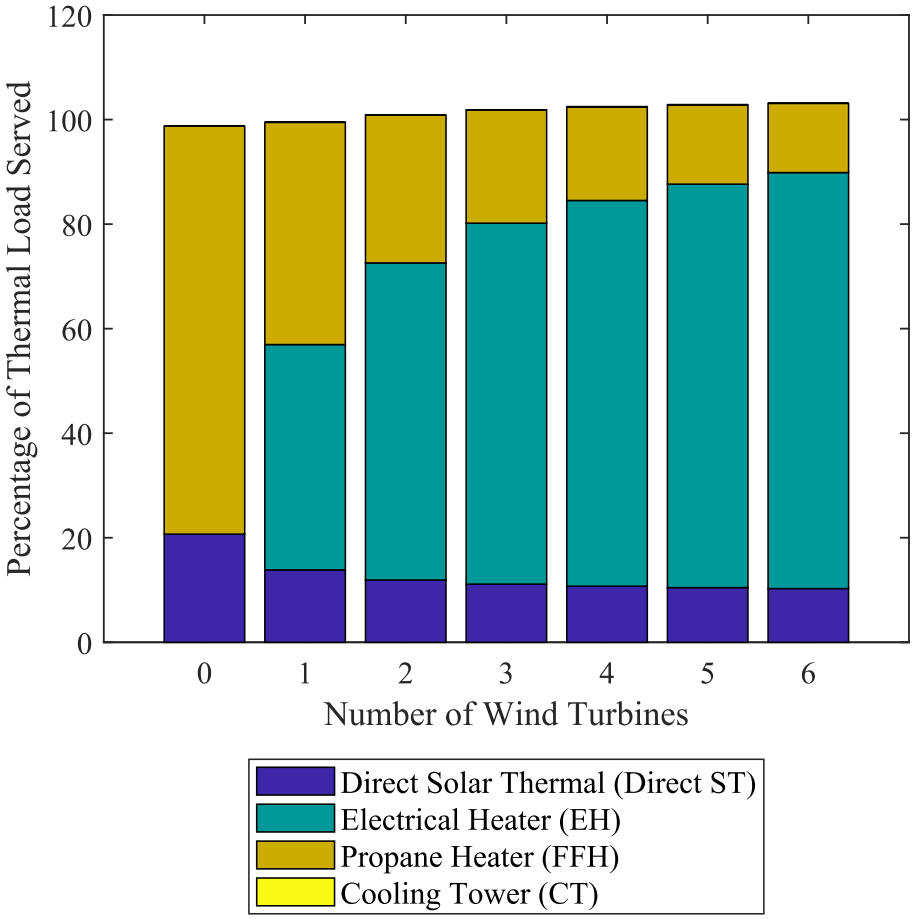

Figure 52: S1C1 75 ST thermal energy production results

Appendix C: S1C2 0, 25, 50, 75 ST array energy generation results

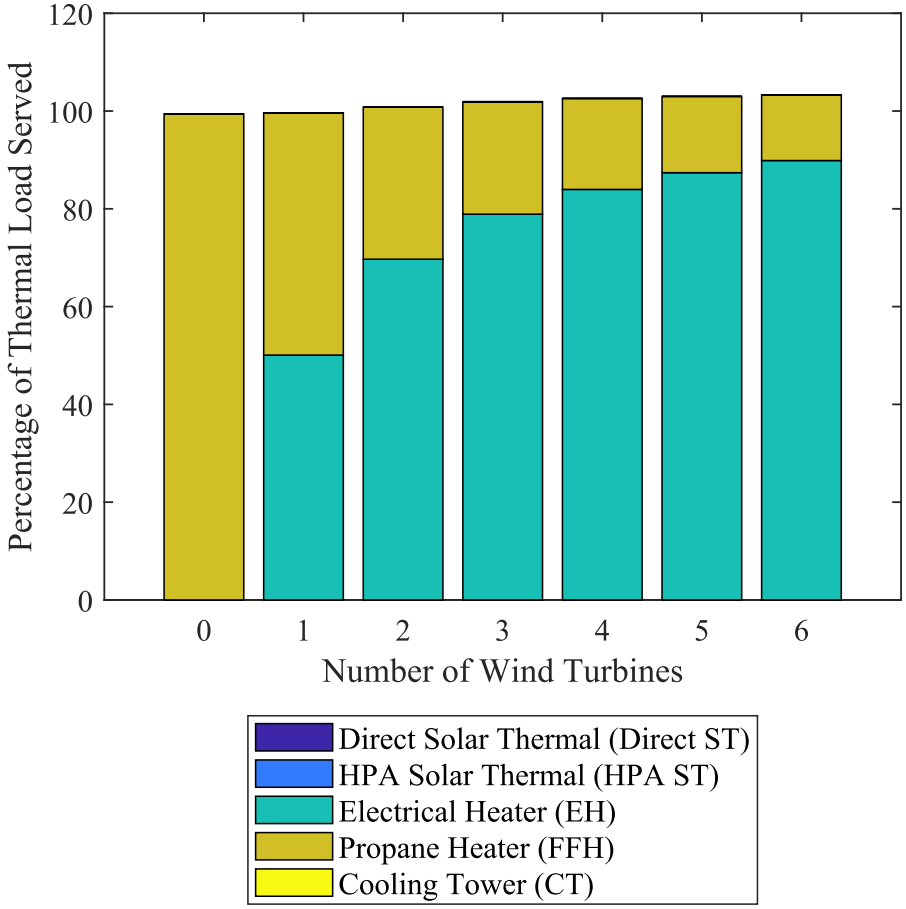

Figure 53: S1C2 0 ST thermal energy production results

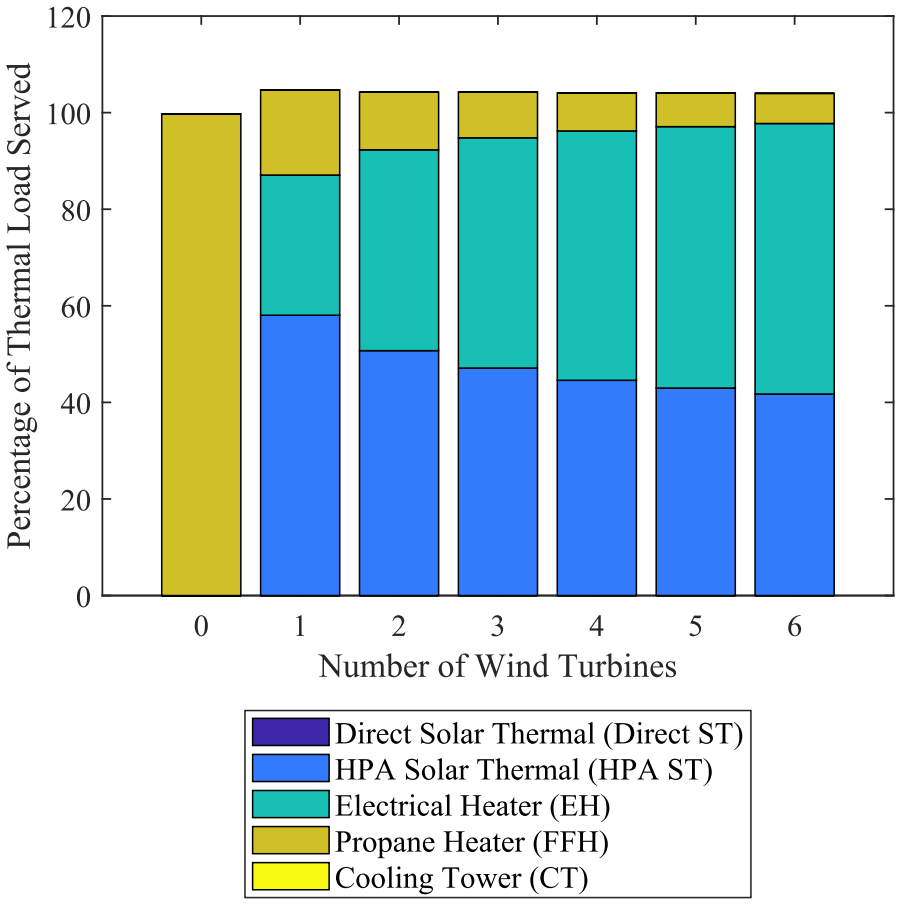

Figure 54: S1C2 25 ST thermal energy production results

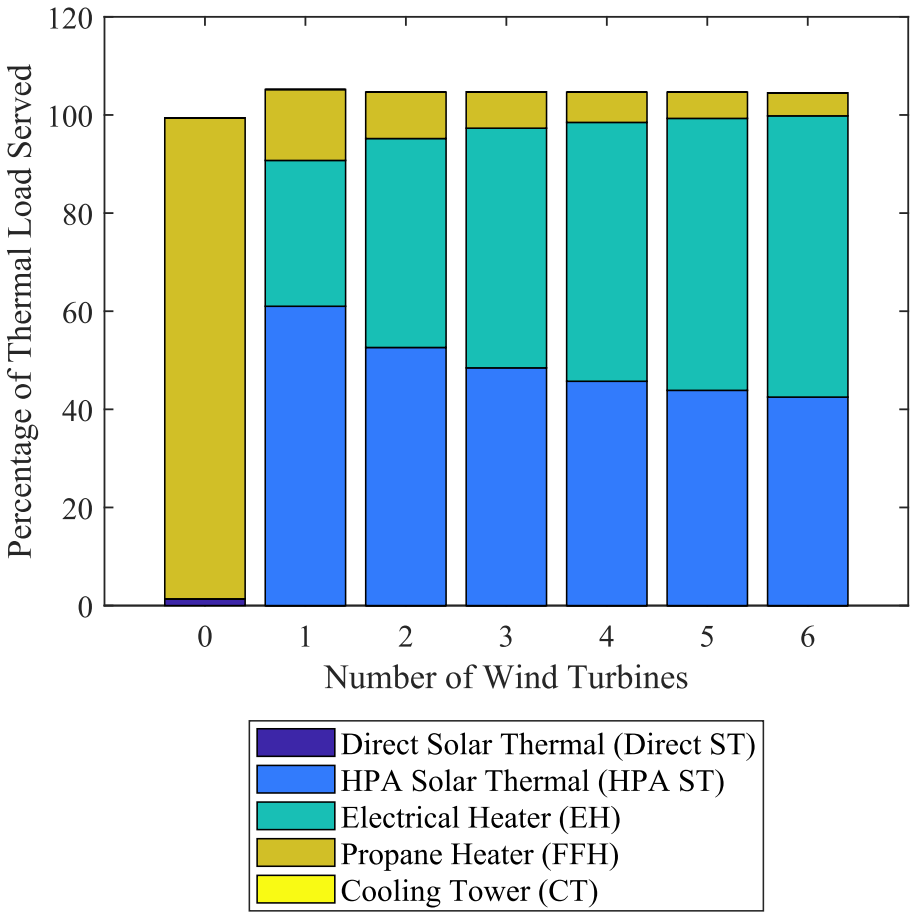

Figure 55: S1C2 50 ST thermal energy production results

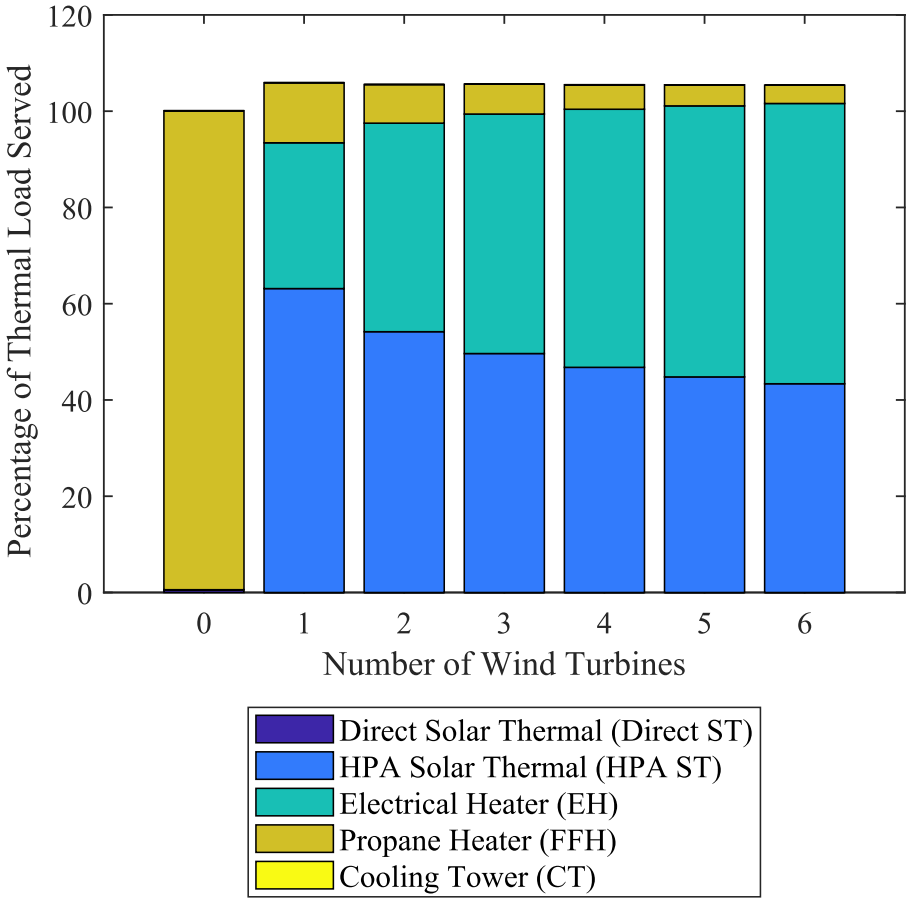

Figure 56: S1C2 75 ST thermal energy production results

Appendix D: S2C1 0, 25, 50, 75 ST array energy generation results

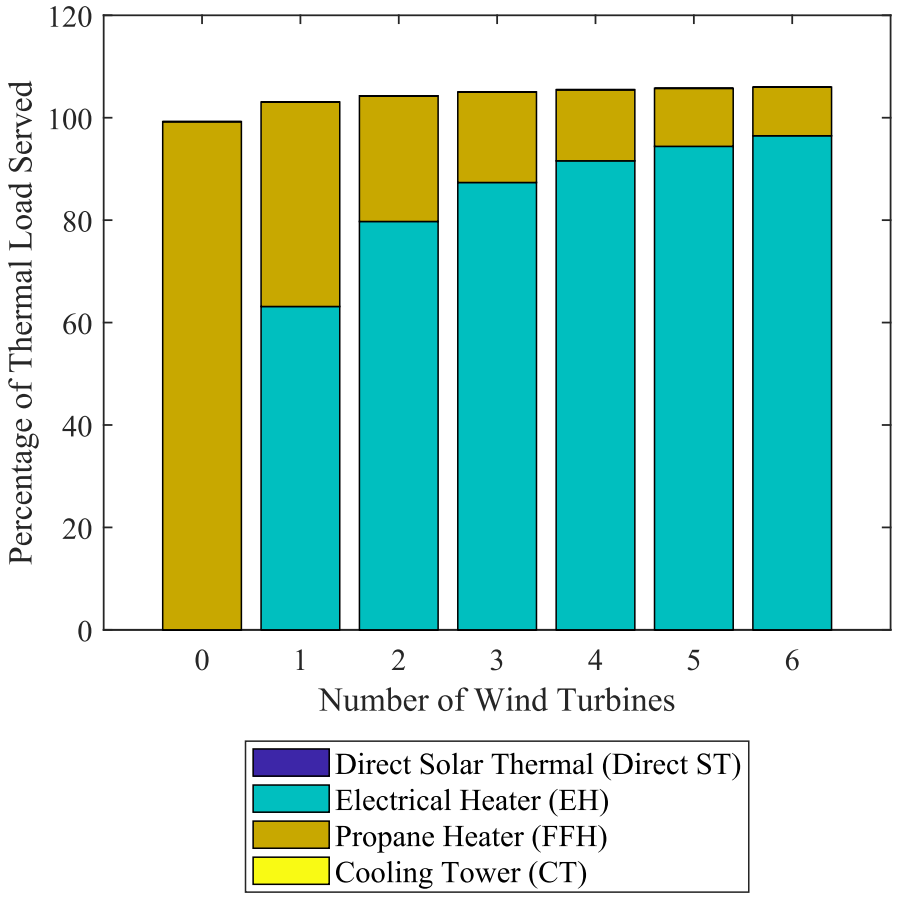

Figure 57: S2C1 0 ST thermal energy production results

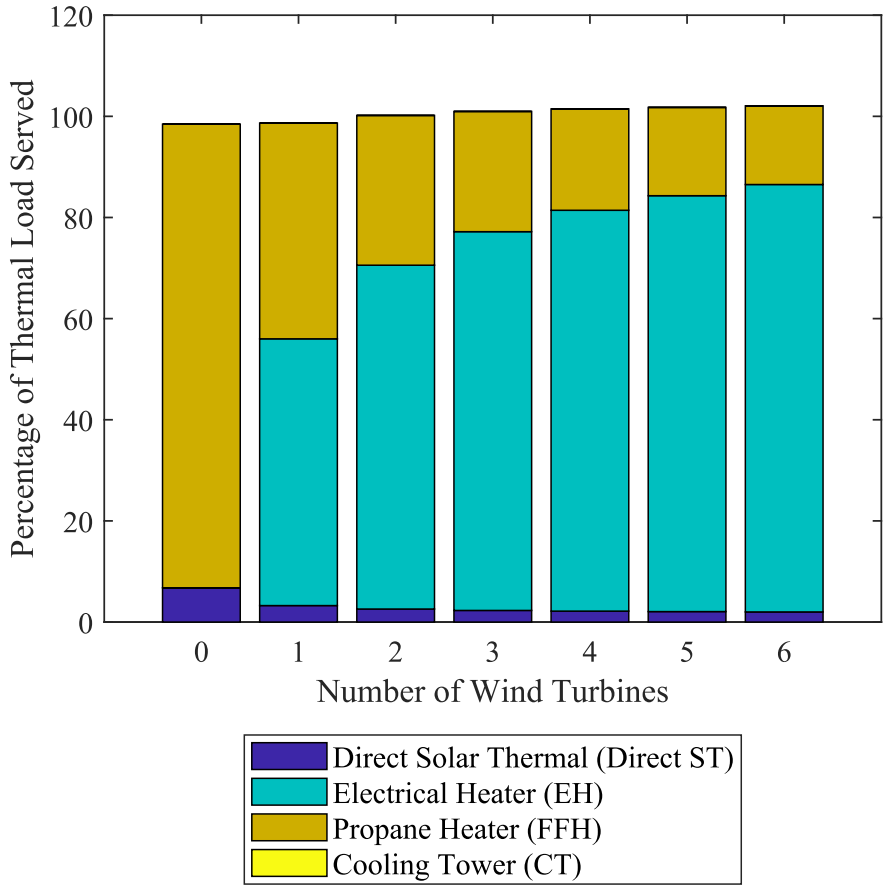

Figure 58: S2C1 25 ST thermal energy production results

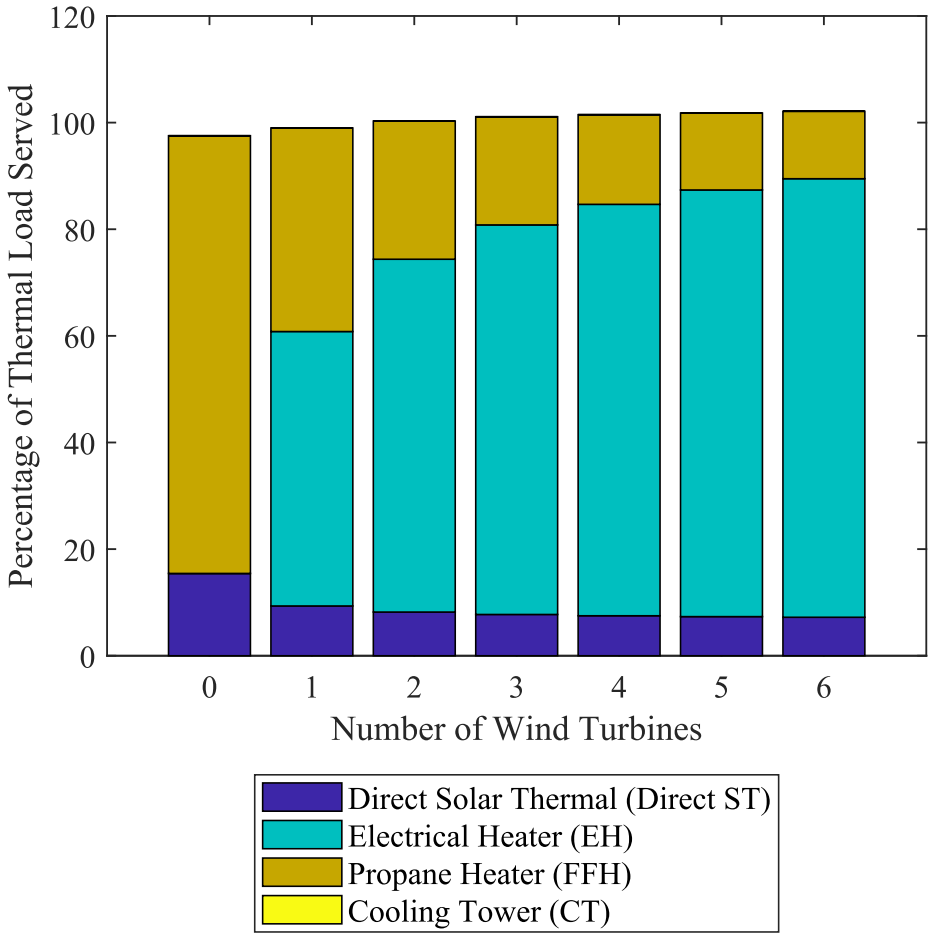

Figure 59: S2C1 50 ST thermal energy production results

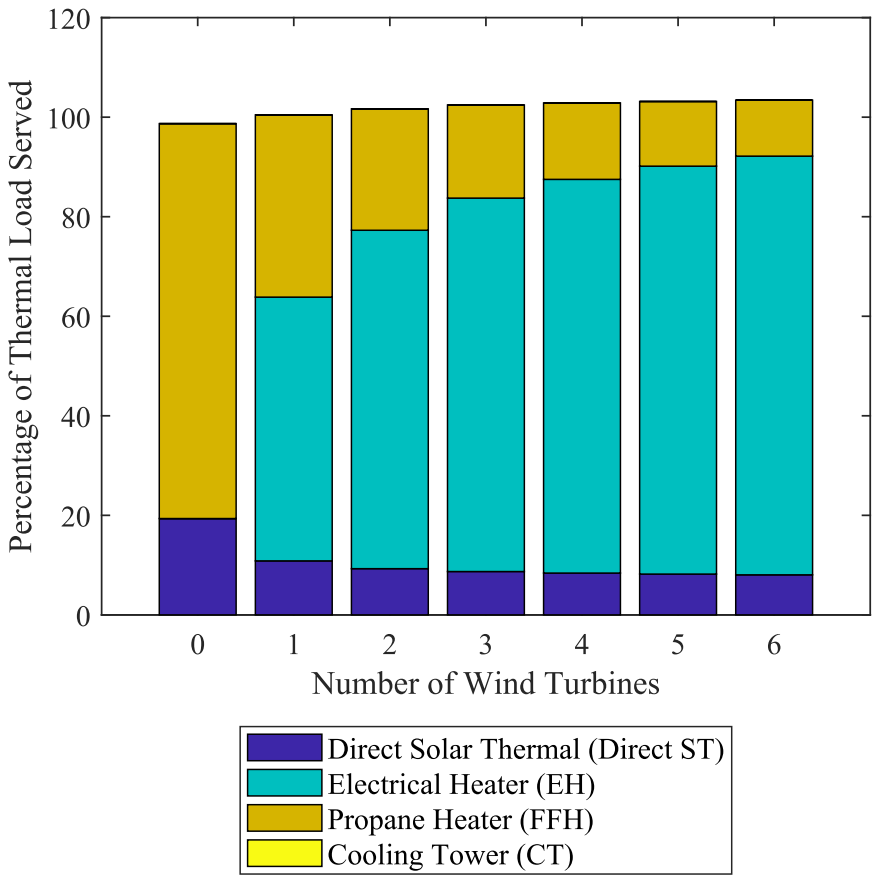

Figure 60: S2C1 75 ST thermal energy production results

Appendix E: S2C2 0, 25, 50, 75 ST array energy generation results

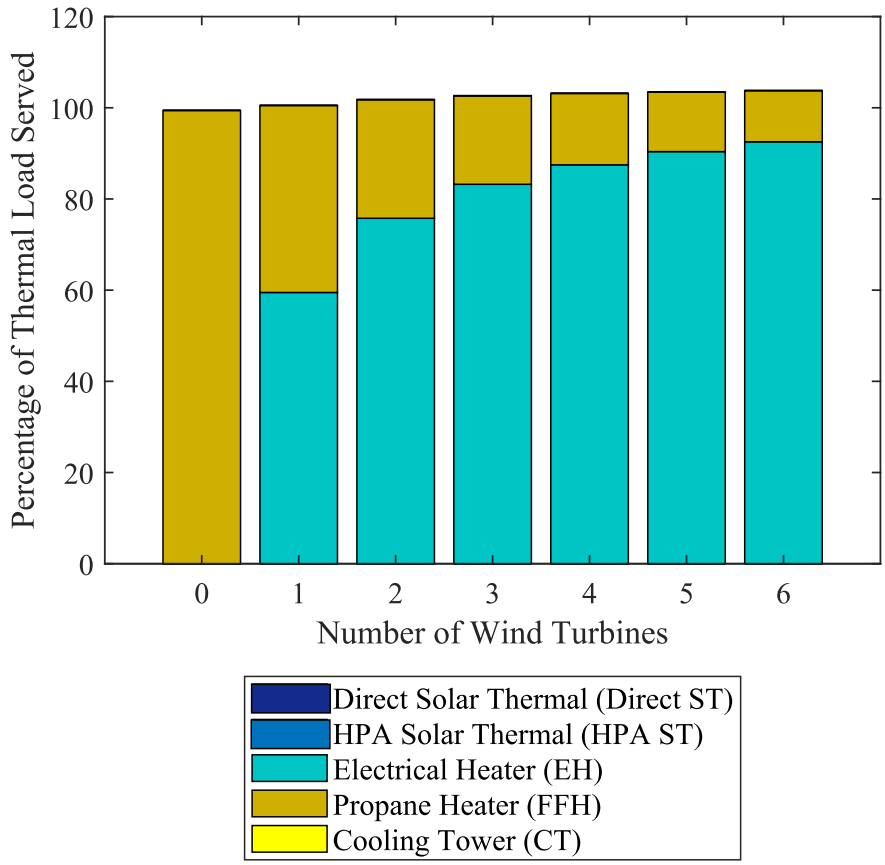

Figure 61: S2C2 0 ST thermal energy production results

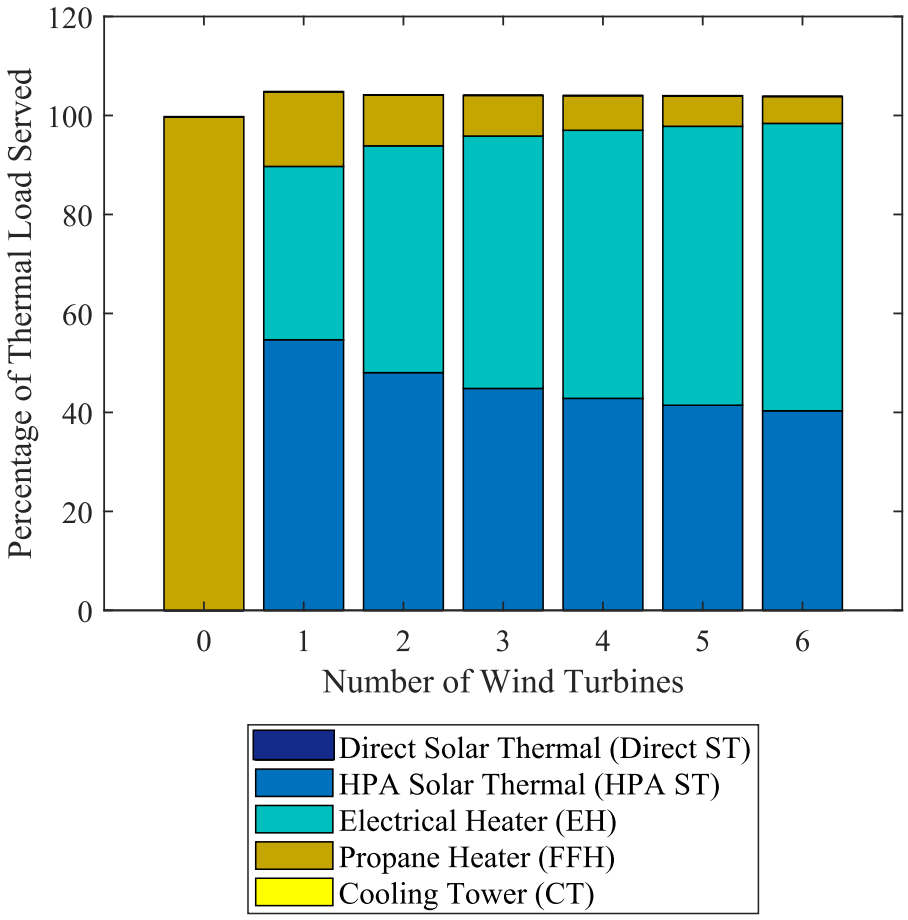

Figure 62: S2C2 25 ST thermal energy production results

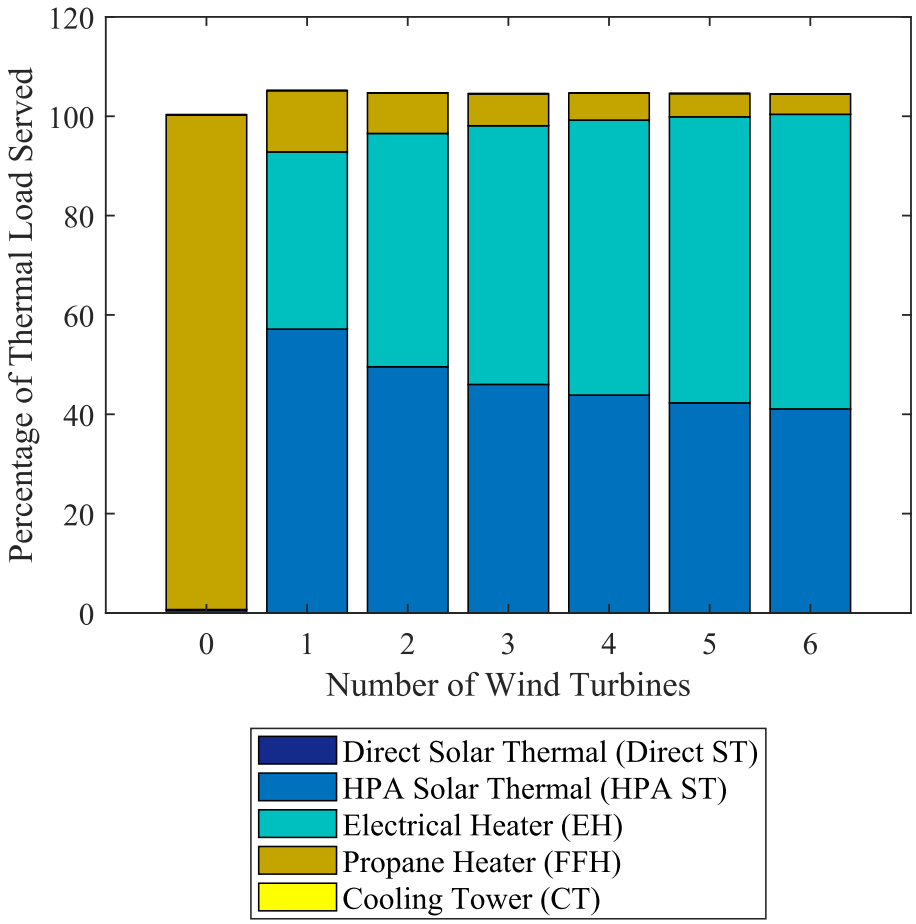

Figure 63: S2C2 50 ST thermal energy production results

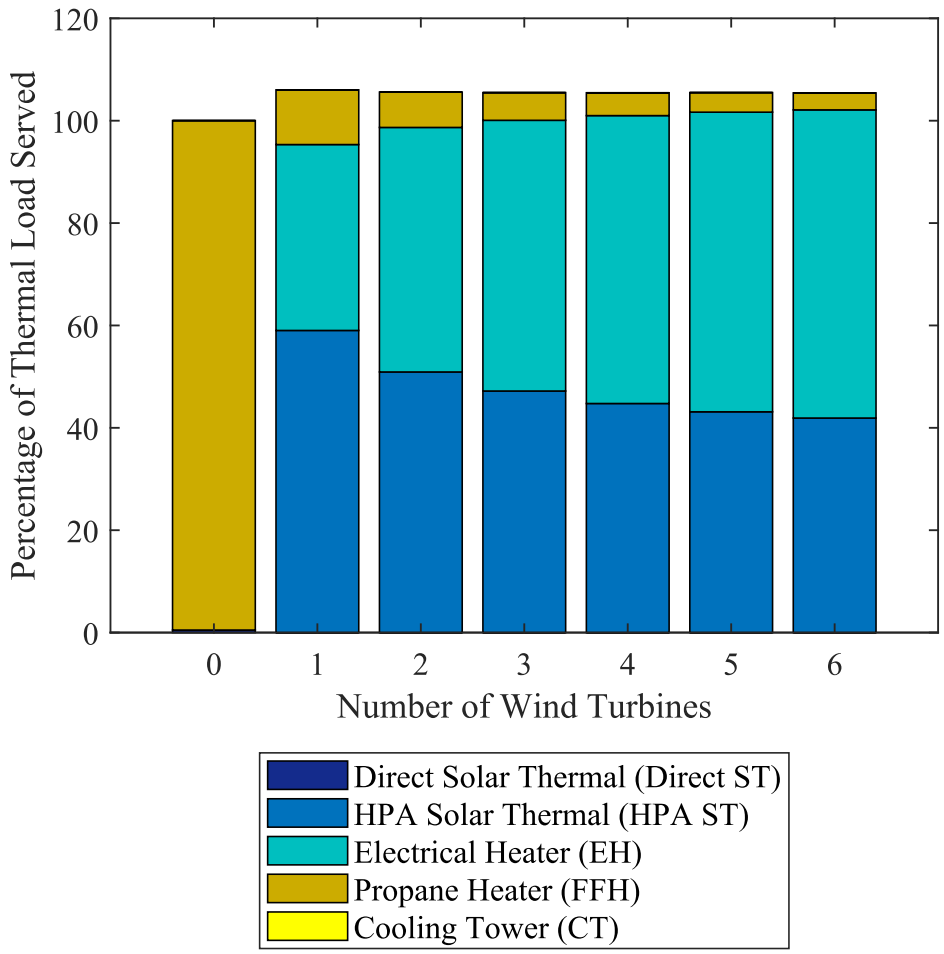

Figure 64: S2C2 75 ST thermal energy production results